UNIVERSITY OF ROME
"TOR VERGATA"

FACULTY OF MEDICINE

PHD PROGRAM in SCIENCE and BIOTECHNOLOGY of REPRODUCTION and DEVELOPMENT

XXI CYCLE

Effects of Culture Conditions on Proliferation and Self-renewal of Murine Embryonic Stem Cells: Growth Factors and 3D Substrates

ILANA MOSCATELLI

Advisor: Prof. Gregorio Siracusa

Coordinator: Prof. Raffaele Geremia

Ringrazio il Prof. Gregorio Siracusa per avermi dato la possibilità di lavorare nel suo laboratorio e per avermi sempre incoraggiata ad esplorare nuove vie in piena indipendenza.
Ringrazio la Prof.ssa Antonella Camaioni e la Dott.ssa Luisa Campagnolo per essermi state sempre vicine, sia scientificamente che personalmente, pronte ad ascoltare e consigliare. È stato un piacere lavorare con voi.
Ringrazio tutta "Istologia" e "Anatomia" per gli anni passati insieme. In particolare le mie vicine di laboratorio Marianna e Dona per la disponibilità, le risate e le merende.
Ringrazio tutti i miei Amici, soprattutto Filippo per l'aiuto prezioso.

INDEX

AIMS

The aim of this project is to study the effects of culture conditions on proliferation and self-renewal of murine embryonic stem (ES) cells. The regulation of ES cell fate is controlled by the interplay of signalling networks that either promote self-renewal or induce differentiation. We focused on two different aspects of culture conditions: the addition of growth factors to the culture medium, and the utilization of a three-dimensional substrate to mimic the extracellular matrix (ECM) produced by the feeder-layer of mitotically inactivated embryonic fibroblasts (MEFs), usually present in ES cell culture.

Data in the literature suggest that neurotrophins have an effect on survival of a variety of cell populations, including human embryonic stem cells. In this work we have studied the expression pattern of neurotrophin receptors and the effect of neurotrophins on murine ES cells. A MEF feeder-layer promotes ES cell renewal by producing leukemia inhibitory factor (LIF), a cytokine required to maintain ES cells in the undifferentiated state, and other factors. MEFs provide also an ECM to which the cells can anchor. We cultured ES cells on three-dimensional electrospun poly(ε-caprolactone) (PCL) scaffolds as a MEF substitute and compared them to cells grown on tissue culture plates (TCPs).

One of the rationals for studying cell growth on artificial scaffolds is their possible use in tissue engineering and regenerative medicine. Before it becomes clear what role stem cells will play in such fields, many scientific issues must be faced. A wider comprehension of the mechanisms of self-renewal and proliferation of ES cells would be of substantial help in these studies.

INTRODUCTION

In the first part of this Introduction I will summarize the main features of ES cells and the factors that can influence their proliferation and self-renewal. In the second part the connections that exist between stemness and neurotrophin receptors will be outlined, to clarify the reasons that prompted us to investigate the effect of specific growth factors on ES cell culture. Finally, in the third part I will introduce the rational for using a three-dimensional support in ES cell culture, to study pluripotency maintenance and for possible future applications in tissue engineering.

1. STEM CELLS

Stem cells are endowed with two important features that distinguish them from other types of cells. First, they are unspecialized cells that are able to renew themselves for long periods through cell division. Second, under physiologic or experimental conditions, they can be induced to become cells with differentiated functions.

Thus, a stem cell is a cell that is specialized to provide an indefinite supply of differentiated cells while retaining the status of a non-differentiated cell. The ultimate stem cell, the totipotent fertilized egg, initially divides to give rise to similarly totipotent cells. Then, through a series of divisions and differentiations, daughter cells give rise to progenies of stem cells whose differentiation potential becomes progressively restricted (Fig.1): pluripotent inner cell mass cells (from which all the embryo tissues derive, but unable to form extra-embryonic tissues), then multipotent stem cells (such as the hemopoietic stem cell), and finally unipotent stem cells (e.g. the epidermal stem cell).

It is generally accepted that multipotent or unipotent cells, involved in the physiological turnover of the tissue, are present in most, if not all tissues of an adult organism. Recent studies suggest that some of these cells retain a surprising and previously unrecognized degree of plasticity in their commitment, being able to differentiate into many different, unrelated cell types, and that their differentiation may be influenced by environment rather than by lineage.

Stem cells derived from adult and embryonic sources have great therapeutic potential, but much research is still needed before their clinical use becomes commonplace. There is debate about whether adult stem cells can be used instead of those derived from embryos. Some

characteristics enter this debate. Accessibility is important: some adult cells, such as neural stem cells, are difficult to obtain, at least from living donors. Other factors include the frequency and abundance of adult stem cells and their number and potency, which might decline with age or be affected by disease. For embryonic stem cells, ethical concerns have been raised. For both adult and embryonic stem cells, stability, potential to transmit harmful pathogens or genetic mutations, and risk of forming unwanted tissues or even teratocarcinomas have yet to be fully assessed (Vats et al., 2005).

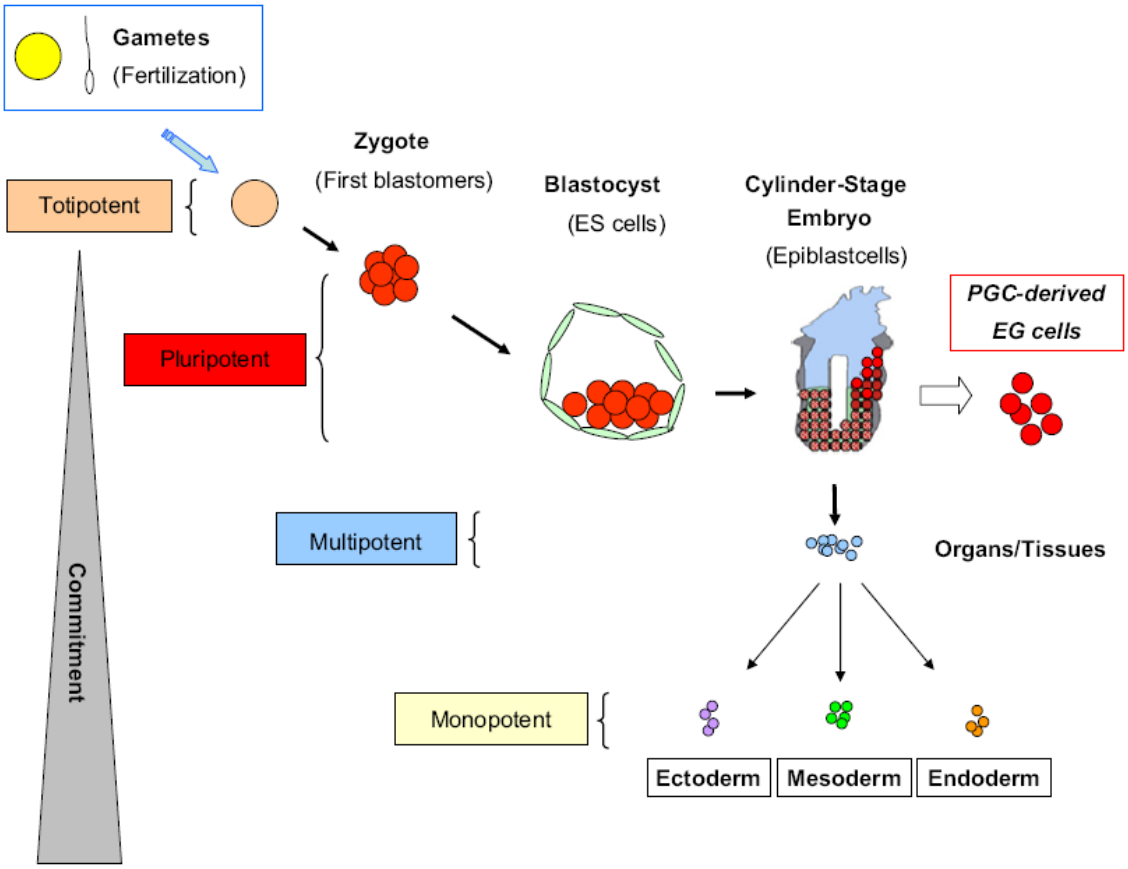

Fig.1 Developmental hierarchy of the stem cell compartment. The most primitive stem cell is a totipotent zygote or first blastomers that derives from the first division of the zygote. A totipotent stem cell divides to give cells that will form both the embryo and placenta. Pluripotent stem cells (PSC) that contribute only to embryo development are cells isolated from the inner cell mass (ICM) of a blastocyst, from the epiblast of cylinder-stage embryo (EPSC) or could be derived in ex vivo cultures from epiblast-derived primordial germ cells (PGC) e as a population of so-called embryonic germ cells (EGC). PSC contribute to all three germ layers in the developing embryo (ectoderm, mesoderm and endoderm). Multipotent stem cells give rise to monopotent stem cells that are committed to particular organs/tissues (Ratajczak et al., 2008).

1.1. *Embryonic Stem Cells*

Embryonic stem (ES) cells are pluripotent cells derived from the inner cell mass of the early embryo, able to differentiate into the three germ layer lineages from which all tissues derive (Thomson et al., 1998; Wobus et al., 1984). For this reason, there has been a surge of interest for ES cells as a potential source for tissue engineering and regeneration. Under defined culture conditions, ES cells can be either maintained in an undifferentiated state or stimulated to differentiate to various cell types (Odorico et al., 2001; Reubinoff et al., 2000).

1.2. *Transcription Factors That Regulate Pluripotency*

Several transcription factors are currently known to play essential roles in both early development and maintenance of pluripotency of ES cells.

Oct4 is a POU homeodomain transcription factor encoded by the *Pou5f1* gene. The lack of *Oct4* in early embryos results in the failure to develop the inner cell mass (ICM) and the embryos contain only trophectoderm cells (Nichols et al., 1998). Suppression of *Oct4* expression in mouse ES cells gives rise to differentiation along the trophoblast lineage (Niwa et al., 2000).

Sox2 is a member of the Sox (SRY-related HMG box) gene family that encodes transcription factors with a single HMG DNA-binding domain. *Sox2* loss-of-function in the embryo and ES cells results in defective epiblasts and differentiation into trophectoderm lineages (Avilion et al., 2003).

Nanog was first functionally identified through its ability to maintain mouse ES cells in the absence of LIF and feeder layer (Chambers et al., 2003; Mitsui et al., 2003). In contrast to the induction of differentiation by overexpression of *Oct4* (Niwa et al., 2000), overexpression of *Nanog* enhances self-renewal and maintenance of the undifferentiated state (Chambers et al., 2003; Mitsui et al., 2003). Mouse embryos deleted of *Nanog* fail to develop an epiblast whilst *Nanog*-depleted ES cells are driven towards extra-embryonic endoderm lineages (Ivanova et al., 2006; Loh et al., 2006; Mitsui et al., 2003). Therefore, unlike Oct4 and Sox2, Nanog plays a pivotal role in the maintenance of the epiblast and ES cells by repressing differentiation along the primitive endoderm lineage. Sox2 is capable of heterodimerizing with Oct4 to regulate the transcription activities of several ES cell specific genes including *Nanog* (Rodda

et al., 2005). Interestingly, Oct4 and Sox2 are also involved in reciprocal regulation of each other's expression (Chew et al., 2005).

Together, these studies suggest that Oct4, Sox2 and Nanog may function in distinct pathways but operate inter-dependently to coordinate the specification of the ES cell stemness.

1.3. *Culture of ES Cells*

Mouse ES cells and human ES cells were both originally derived and grown on a feeder layer of mitotically inactivated mouse fibroblasts in the presence of bovine serum. However, the factors that sustain the growth of these two cell types in a pluripotent condition appear to be distinct. The addition of the cytokine, leukaemia inhibitory factor (LIF), to serum containing medium allows mouse ES cells to proliferate in the absence of feeder cells. LIF modulates mouse ES cells through the activation of STAT3 protein. In serum-free culture, however, LIF alone is insufficient to prevent mouse ES cells from differentiating into neural cells.

Recently, Ying *et al.* reported that the combination of bone morphogenetic proteins (BMPs) and LIF is sufficient to support the self-renewal of mouse ES cells (Ying et al., 2003). The effects of BMPs on mouse ES cells involve induction of inhibitor of differentiation (Id) proteins, and inhibition of extracellular receptor kinase (ERK) and of p38 mitogen-activated protein kinases (MAPK) (Qi et al., 2004; Ying et al., 2003). However, LIF in the presence of serum is not sufficient to promote the self-renewal of human ES cells (Thomson et al., 1998), and the LIF/STAT3 pathway appears to be inactive in undifferentiated human ES cells (Daheron et al., 2004; Humphrey et al., 2004). Also, the addition of BMPs to human ES cells, differently from what has been described for murine ES cells leads to their rapid differentiation (Pera et al., 2004; Xu et al., 2002).

Several groups have attempted to define growth factors that sustain human ES cell growth and to identify culture conditions that reduce the exposure of human ES cells to non-human animal products. Basic fibroblast growth factor (bFGF) allows the use of a serum-free medium to sustain the clonal growth of human ES cells in the presence of fibroblasts (Amit et al., 2000). A "feeder-free" human ES cell culture system has been developed, in which human ES cells are grown on a protein matrix (mouse Matrigel or Laminin) in a bFGF-containing medium that has been previously "conditioned" through the culture of mouse fibroblasts (Xu

et al., 2001). Although this culture system eliminates direct contact of human ES cells with the fibroblasts, it does not remove the potential for mouse pathogens being introduced into the culture by the fibroblasts. Several different sources of human feeder cells have been found to support the culture of human ES cells, thus removing the possibility of pathogen transfer from mice to humans (Amit et al., 2003; Lee et al., 2005; Richards et al., 2002; Richards et al., 2003). However, the possibility of pathogen transfer from human to human in these culture systems still remains. More work is needed to develop a culture system that would completely eliminate the use of fibroblasts, decreasing much of the variability associated with the current culture conditions of human ES cells.

Sato *et al.* reported that activation of the Wnt pathway by 6-bromoindirubin-3'-oxime (BIO) promotes the self-renewal of human ES cells in the presence of bFGF, Matrigel, and a proprietary serum replacement product (Sato et al., 2004). Amit *et al.* reported that bFGF, TGFβ, and LIF could support some human ES cell lines in the absence of feeders (Amit et al., 2004). Although there are some questions about how well these new culture conditions will work for different human ES cell lines, there is now reason to believe that defined culture conditions for human ES cells, which could reduce the potential for contamination by pathogens, will soon be achieved (Lu et al., 2006; Ludwig et al., 2006). Once a set of defined culture conditions is established for the derivation and culture of human ES cells, challenges to improve the medium will still remain. For example, the cloning efficiency of human ES cells is very low (typically less than 1%) compared with that of mouse ES cells. Another difficulty is the possible accumulation of genetic and epigenetic changes over prolonged periods of culture. For example, karyotypic changes have been observed in several human ES cell lines after prolonged culture, and the rate at which these changes occur may depend on the culture method (Draper et al., 2004; Inzunza et al., 2004).

2. NEUROTROPHINS AND STEMNESS

Growth of ES cells as a pluripotent population requires a balance between survival, proliferation and self-renewal signals. A recent work by Pyle *et al.* demonstrated that hES cells express receptors of the tropomyosin-related kinase (Trk) family, which mediate antiapoptotic signals, and also that three Trk ligands, brain-derived neurotrophic factor, neurotrophin-3 and neurotrophin-4 are survival factors for hES cells. This work concluded that neurotrophins improve hES cell survival and may facilitate their manipulation and the development of high-throughput screens to identify factors responsible for hES cell differentiation (Pyle et al., 2006).

In our lab we have observed that murine ES cells have a different expression pattern for neurotrophin receptors as compared with human ES cells. RT-PCR and Western blotting analysis show the expression of $p75^{NTR}$ and TrkA, whereas TrkB and TrkC are undetectable. This is not surprising considering the species-specific differences between the two stem cell types described in the previous paragraph. The presence of such receptors led us to investigate the effect of neurotrophins on murine ES cell growth, with particular focus on nerve growth factor.

2.1. *Neurotrophins*

Nerve growth factor (NGF) is the prototype of a family of related neurotrophic factors known as neurotrophins (NTs), which also includes brain-derived neurotrophic factor (BDNF), neurotrophin-3 (NT-3), and neurotrophin-4 (NT-4). NTs are trophic factors for the growth, differentiation, and survival of specific subsets of neurons in the developing and mature nervous system. NTs are homodimers that target two classes of transmembrane receptors, the receptor tyrosine kinases (Trk)-A, -B, and -C, and the $p75^{NTR}$ neurotrophin receptor ($p75^{NTR}$), a member of the tumor necrosis factor (TNF) receptor superfamily. Whereas $p75^{NTR}$ binds all NTs equally well, TrkA preferentially interacts with NGF, TrkB with BDNF and NT-4, and TrkC with NT-3. Each NT can simultaneously engage two Trk receptors in a high-affinity complex that mediates receptor transphosphorylation and activation of well defined signalling pathways (Fig.2). Trks are often termed high-affinity NGF receptors, but their neurotrophin binding affinity is actually similar to that of $p75^{NTR}$, with a Kd of about 1-10 nM. However

when the receptors are coexpressed, $p75^{NTR}$ enhances the ability of Trk receptors to bind and respond to neurotrophins and sharpens the discrimination of Trks for their preferred neurotrophin ligands.

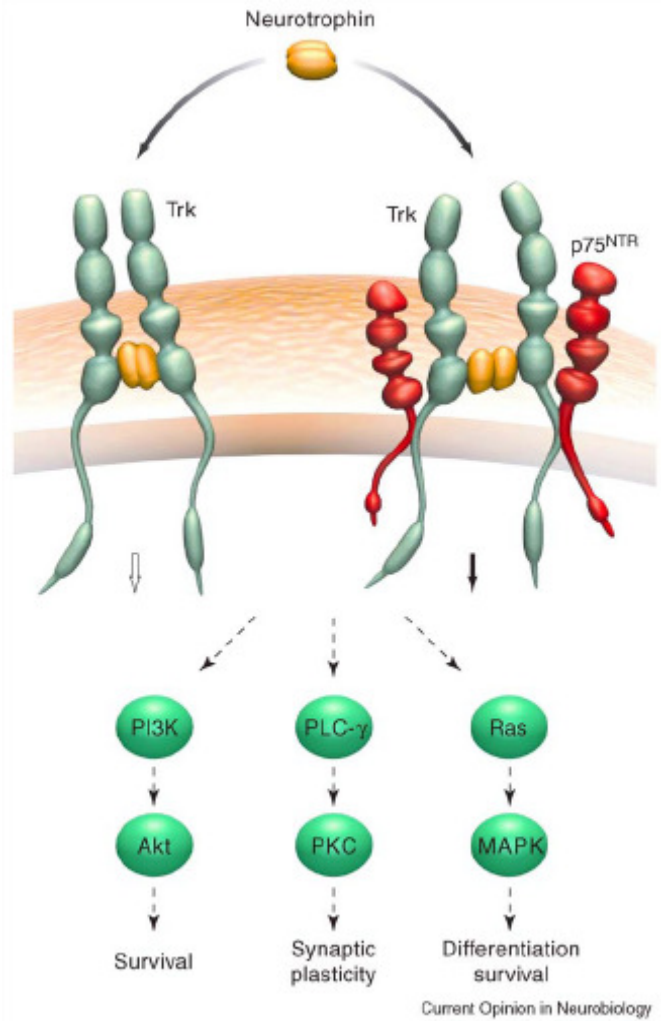

Fig.2 Neurotrophin binding to Trk dimers results *in trans* phosphorylation and activation of well-defined signaling pathways. Coexpression of $p75^{NTR}$ with Trk refines ligand specificity and affinity, and modifies the association with cytosolic adaptor proteins. As a consequence, $p75^{NTR}$–Trk dimer complexes might possess signaling activities that are different from those of a Trk dimer. Abbreviations: Akt, protein kinase B; MAPK, mitogen-activated protein kinase; PI3K, phosphatidylinositol 3-kinase; PKC, protein kinase C; PLC-γ, phospholipase Cγ (Nykjaer et al., 2004).

NGF, synthesized by and secreted from target tissues of sympathetic, sensory, and cholinergic basal forebrain neurons, binds to both its receptors, transduces appropriate signals in nerve terminals, is internalized in membrane-bound vesicles of peripheral nerves and transported along microtubules up the axon to the cell body, where it exerts its biological activity.

In addition to its well-described action on survival and differentiation of neurons, there is evidence that NGF is able to exert a wide spectrum of effects on immune cells as well (Aloe et al., 1997; Auffray et al., 1996; Labouyrie et al., 1997). NGF potently affects several functions of the monocyte/macrophage lineage, such as differentiation, cytokine production, phagocytosis, and antimicrobial activity (Ehrhard et al., 1993; Susaki et al., 1996). Also, the ability of NGF to act as an autocrine survival factor for memory B lymphocytes is well recognized (Torcia et al., 1996), as its capacity to promote the survival of mast cells (Aloe and Levi-Montalcini, 1977).

2.2. *$p75^{NTR}$ Expression in Non-Neuronal Tissues*

In addition to modulating Trk-mediated functions, $p75^{NTR}$ also controls and conveys Trk-independent activities. Numerous studies have demonstrated that $p75^{NTR}$, depending on the cellular context, can activate signalling cascades regulating apoptosis, Schwann cell migration, myelination, axonal growth and regeneration (Chao, 2003). Indeed, the $p75^{NTR}$ cytoplasmatic tail contains several potential motifs for interactions with downstream signalling molecules, and similar to other members of the TNF receptor superfamily, it comprises a “death” domain.

The role of $p75^{NTR}$ does not appear to be limited to the nervous tissue, however, as it may have various biological functions in non-neuronal tissues, during tissue morphogenesis and in the adult (Dechant and Barde, 2002). Studies have indeed shown unexpected functional complexity for $p75^{NTR}$ (Hempstead, 2002), in connection with the recent identification of $p75^{NTR}$-selective ligands (Lee et al., 2001), new co-receptors (Nykjaer et al., 2004) and new intracellular signalling mechanisms (Sofroniew et al., 2001). Thus the available data suggest that the neurotrophin receptor plays more complex roles than it had been until recently assigned.

2.3. *p75* ^{NTR} *and Stemness*

Various experimental observations show that cells bearing the $p75^{NTR}$ neurotrophin receptor frequently play a primary role in morphogenetic processes in many embryonic and adult tissues, and are endowed with a pluripotency or stem cell role.

A particularly evident and early example of the association $p75^{NTR}$/stem quality is given by neural crest cells, that are $p75^{NTR}$ immunoreactive and undergo extensive migration in the embryo to generate a prodigious variety of different cell phenotypes (Chao, 1992). At later developmental stages, in the rat and mouse embryo, the $p75^{NTR}$ receptor is expressed by mesenchymal cells that are essential for the morphogenesis of seminiferous tubules of the testis (Campagnolo et al., 2001; Russo et al., 1999; Russo et al., 1994), of kidney tubules (Huber et al., 1996), of the tooth (Luukko et al., 1996), of the inner ear (von Bartheld et al., 1991), of the respiratory tree (Wheeler et al., 1998).

Embryo myoblasts express $p75^{NTR}$, but the receptor is downregulated when myoblasts differentiate into myotubes (Wheeler et al., 1998); the $p75^{NTR}$ neurotrophin receptor is also present in satellite cells (Mousavi and Jasmin, 2006), that are adult muscle stem cells. It should be emphasized that in all cases, expression of the receptor begins well before such embryonal structures become innervated.

In the adult, the presence of $p75^{NTR}$ characterizes various types of epithelial progenitor cells: liver stem cells (stellate cells) (Suzuki et al., 2008), keratinocytes of the basal layer of the epidermis and of the corneal limbal epithelium (Di Marco et al., 1993; Qi et al., 2008), stem cells of the oral and oesophageal mucosae (Nakamura et al., 2007; Okumura et al., 2003). Likewise, $p75^{NTR}$ is considered as the most specific marker of bone marrow-derived mesenchymal stem cells (Buhring et al., 2007), and microvascular pericytes (Covas et al., 2008), both of which can differentiate into osteoblasts, chondroblasts, adipocytes.

3. MIMICKING STEM CELL NICHES

Niches regulate lineage-specific stem cell self-renewal versus differentiation in vivo and are composed of supportive cells and extracellular matrix components arranged in a three-dimensional topography of controlled stiffness in the presence of oxygen and growth factor gradients. ECM is a complex structure essentially based on fibrous collagens embedded in proteoglycans. Collagen is organized in a 3D fibrous network forming hierarchical structures from nanometre scale fibrils to macroscopic tissue architecture. The topology of ECM has been found to affect cell morphology, functionality, and physiological response (Causa et al., 2007). Recently, several studies have provided evidence that components of the extracellular matrix such as fibronectin and laminin-1 may substitute for feeder-layers to promote the self-renewal pathway in stem cells (Amit et al., 2004; Matsubara et al., 2004; Philp et al., 2005; Xu et al., 2001). These investigations have highlighted the role of ECM as a factor potentially important in regulating the balance between self-renewal and differentiation.

It has been suggested that presentation of ECM/basement membrane proteins and their conformational flexibility within a three-dimensional matrix may be critical parameters for promoting in vivo-like functional and structural changes between and within cells (Cukierman et al., 2001; Cukierman et al., 2002; Grinnell et al., 2003; Wozniak et al., 2003). A synthetic polyamide matrix has also been used to study self-renewal of ES cells (Nur et al., 2006).

To provide a topologically accurate representation of the geometry and porosity of the ECM for cell culture we used electrospun poly(ε-caprolactone) (PCL) scaffolds to investigate the role of three-dimensionality in ES cell growth.

3.1. *Stem cells for tissue engineering*

Tissue engineering (TE) is an interdisciplinary field that applies the principles of engineering to develop biological substitutes for regenerative medicine, aimed to restore, maintain or improve tissue function. One of the most critical issues in TE is the fabrication of scaffolds with tailored physical, mechanical and biological properties that act as substrates for cellular ingrowth and proliferation, and support new tissue formation (Causa et al., 2007). Scaffolds able to mimic the architecture and biological functions of ECM are very promising substitutes

since they might provide mechanical support, carry inductive molecules or cells, and supply signals to control structure and function of newly formed tissue (Table 1).

Niche properties	System details	Species	Cell type
Ligand presentation	Immobilized Delta1–Fc	Human	HSPC
	Jagged1 immobilized on Sepharose beads	Mouse	HSPC
	Multifunctional chimeric proteins immobilized by Ni chelating with decahistidine tag	Rat	NSC
	Immobilized IKVAV peptide in lipid bilayer surfaces	Rat	AHP
	Array of 500 μm × 500 μm LN-derived peptides	Human	ESC
	Heparin on PEG hydrogel	Human	MSC
	Ormosil-immobilized adhesion peptides	Rat	ESC
	Immobilized LN, FN, or Col w/EGF, NGF, NT-3, or CNTF	Rat	NSC
	BMP-2 islands on fibrin gel	Mouse	MDSC
Matrix stiffness	RGD-modified alginate gels	Human	MSC
	Collagen-coated polyacrylamide gels	Human	MSC
Topography	FN-coated PET nanofiber mesh	Human	HSPC
	Polyamide nanofiber mesh	Mouse	ESC
	Aminated PES nanofiber mesh	Human	HSPC

Table 1: Mimicking stem cell niches to alter the regulation of stem cell expansion and controlled differentiation. HSPC: hematopoietic stem and progenitor cell; NSC: neural stem cell; MSC: mesenchymal stem cell; AHP: adult hippocampal progenitor cell; ESC: embryonic stem cell; MDSC: muscle-derived stem cell; NOD/SCID: nonobese diabetic severe combined immunodeficient mice; NOG: NOD/SCID mice intercrossed with IL-2 receptor γ chain-knockout; BDF1: (C57B1/6 × DBA/2)F_1; PEG: polyethylene glycol; Ormosil: organically modified silica; LN: laminin; FN: fibronectin; EGF: epidermal growth factor; NGF: nerve growth factor; NT-3: neutrophin-3; CNTF: ciliary neurotrophic factor; BMP-2: bone morphogenic protein-2; IKVAV: laminin-derived peptide; RGD: fibronectin-derived peptide; PET: polyethylene terephthalate; PES: polyethersulfone (Dellatore et al., 2008).

Mimicking stem cell niches should facilitate production of the large numbers of cells needed to realize the promise of regenerative medicine.

There are at least three different ways to utilize scaffolds in tissue engineering: first, a resorbable scaffold can be used to temporarily substitute a damaged tissue until the endogenous stem cells with the appropriate signals replace it; second, stem cells can be loaded on the scaffold and after transplantation be induced to differentiate in a specific direction;

third, stem cells can be loaded on a scaffold, differentiated *in vitro*, and then transplanted in the damaged tissue.

Several reports (Gerecht-Nir et al., 2004; Levenberg et al., 2003; Liu and Roy, 2005) have described culturing embryonic stem cells within 3D scaffolds, with the general aim of inducing stem cell differentiation. Stem cells have been recognized as a promising alternative to somatic cells for cell therapy owing to their potential to renew themselves through cell division and to differentiate into a wide range of specialized cell types. In order to maintain the phenotypic expression of differentiated stem cells, the simulated environment of the biomimetic support must provide the appropriate signals, indispensable to mimic natural tissue growth.

Progress in the understanding of the molecular mechanisms of self-renewal and of directed differentiation of stem cells growing on biomimetic materials will lead to the possibility of cell-based therapies, and the possible use of stem cells in tissue engineering (Liao et al., 2008).

3.2. *Polymers as Biomaterials for Tissue Engineering*

A number of novel approaches have been developed for the fabrication of biomaterial-based 3D scaffolds. More recently, nanofiber-based scaffolding systems are being explored as scaffolds for tissue engineering (Li et al., 2002). The development of nanofibers has enhanced the scope for fabricating scaffolds that can potentially mimic the architecture of natural human tissue at the nanometer scale. Currently there are three techniques available for the synthesis of nanofibers: electrospinning, self-assembly, and phase separation. Of these, electrospinning is the most widely studied technique and also seems to exhibit the most promising results for tissue engineering applications. In the electrospinning process, fibers ranging from 50 nm to 1000 nm or greater can be produced by applying an electric potential to a polymeric solution. The solution is held at the tip of a capillary tube by virtue of its surface tension. The electric potential applied provides a charge to the polymer solution. An increase causes the electric potential to reach a critical value, at which it overcomes the

surface tension forces to cause the formation of a jet. The charged jet eventually forms randomly oriented nanofibers that can be collected on a stationary or rotating grounded metallic collector. Along with the advantage of producing nanofiber meshes with high porosity and surface area, the electrospinning technique can be applied to a wide variety of natural and synthetic polymers, making it a very versatile technique (Vasita and Katti, 2006). Owing to their functional properties and design flexibility, polymers are the primary choice of materials for making scaffolds. Polymers used for making scaffolds are classified as either naturally derived polymers or synthetic polymers (Murugan and Ramakrishna, 2006). The former includes collagen, gelatin, chitosan, chitin, cellulose, and starch. The later includes biodegradable synthetic polymers such as poly(lactic acid) (PLA), poly(glycolic acid) (PGA), poly(lactic-coglycolic acid) (PLGA) and poly(ε-caprolactone)(PCL).

The biodegradation rate is one of most important considerations (Table 2) and it is highly desirable to ensure that the degradation rate matches the speed of new tissue regeneration at the defect site.

Biodegradable polymer	Typical applications	Polymer degradation rate (months)
Polyorthoester	Bone ingrowth applications, drug delivery	Half life of 4 h
Poly(DL-lactic acid) (PDLA)	Drug delivery, tissue regeneration	12–16
Poly(L-lactic acid) (PLLA)	Sutures, orthopedic devices, tissue regeneration	>24
Poly(glycolic acid) (PGA)	Drug delivery, sutures.	6–12
Poly(lactide-co-glycolide) (PLGA) (50:50)	Sutures, films for retinal pigment epithelium transplantation and guided tissue regeneration, fracture fixation, oral implant, drug delivery.	Half life of 1.5 months
Polycaprolactone (PCL)	Long-term implantable drug delivery system, tissue regeneration.	>24
Polyanhydrides	Orthopedic prosthesis, drug delivery.	Half life of 1 h
Tyrosine-derived polycarbonates	Orthopedic applications.	Very slow degradation

Table 2: Biodegradable synthetic polymers and their degradation rates (Liao et al., 2008)

If the degradation is more rapid than the tissue regeneration, the scaffold will lose its carrier function for cell growth; on the other hand, if the degradation is too slow compared to the tissue regeneration, the scaffold will impede tissue regeneration.

Collagen, the primary structural protein of the native ECM, is the most widely used natural polymer for making scaffolds. Furthermore, it has desirable functional properties, making it favourable for cellular growth. Since collagen extracted from natural sources is known to elicit immunogenic responses upon implantation, the direct use of natural collagen has become limited. Instead, purified collagen or reconstituted collagen, which causes relatively low immunogenic responses, can be produced by biochemical processing and is commercially available. The main disadvantage of using collagen in scaffold is the rapid degradation rate and weak mechanical property. To overcome this deficiency, collagen fibres have been cross-linked to retard the degradation rate (Zhang et al., 2006).

Among synthetic polymers, PCL (a semi-crystalline aliphatic polyester) is one of the most used materials to fabricate biodegradable scaffolds. For example, it has been shown to be a good candidate for bone (Ciapetti et al., 2003; Swieszkowski et al., 2007) and cartilage scaffolding (Wise et al., 2008). Moreover, it has been used to mimic a 3D environment to support embryonic and mesenchymal stem cell differentiation (Kang et al., 2007; Fecek et al., 2008; Li et al., 2005). PCL degradation products are either metabolized via tricarboxylic acid cycle or directly eliminated by renal secretion (Woodward et al., 1985).

3.3. *Tissue Engineered Heart Valve using PCL Scaffolds*

Although we have focused mainly on the utilization of PCL scaffolds to study ES cell growth, we also investigated one of the possible applications of PCL scaffolds in tissue engineering.

End-stage failing heart valves are generally replaced by prosthetic substitutes, both mechanical and biological ones. However, these medical devices can be affected by thrombus formation or hemolysis (common risks associated with mechanical valves) and calcification, leading to formation of holes and tears in the cusps (biological valves). Thus, common heart valve prostheses have limited long-term efficacy, and no potential to grow, repair or remodel (Hoerstrup et al., 2000).

Tissue engineering might provide viable substitutes to overcome these limitations. Scaffolds fabricated by bioresorbable polymers might be used as prosthetic devices that can be

progressively replaced by novel autologous tissue and, therefore, be able to adapt to the modifications of the host. Thus, synchronization of polymer degradation with the replacement by novel tissue is a relevant feature for the long-term success of the tissue-engineered construct (Sung et al., 2004).

PCL was selected for electrospinning fabrication of prosthetic heart valves (Del Gaudio et al., 2008), being a bioresorbable polyester with a degradation period of about 2 years (Ciardelli et al., 2005), thus providing prolonged mechanical reliability with low inflammatory response within the surrounding tissue, due to the low concentration of acidic products released during the slow degradation (Sung et al., 2004). In the present work, we investigated the ability of ES cells to differentiate into endothelial cells when cultured on electrospun PCL scaffolds, by evaluating the expression of endothelial markers in VEGF-treated cultures.

MATERIALS AND METHODS

1. MOUSE ES CELL CULTURE

Mouse ES cell line R1 was a kind gift of Dr. Heidi Stuhlmann. ES cells were cultured following the standard procedure, on a feeder layer of mitotically-inactivated primary mouse embryonic fibroblasts (MEFs) from CD-1 mouse embryos in tissue culture polystyrene plates (TCPs) pre-coated with gelatin necessary to facilitate cell adhesion (a 0.7 % gelatin solution for 10 min at 37 °C). ES cells were expanded and maintained undifferentiated by culture in Dulbecco's Modified Eagle's Medium (DMEM with 4,5 g/L D-glucose) supplemented with 15 % heat-inactivated fetal calf serum (ES cell tested), 20 mM Hepes, 2 mM L-glutamine, 100 μM β-mercaptoethanol, 100 μM non-essential amino acids, 50 U/ml penicillin and 50 μg/ml streptomycin, and 10^3 U/ml Leukemia Inhibitory Factor. The cells were cultured at 37 °C in a humidified atmosphere of 5 % CO_2 in air. To obtain highly enriched ES cell populations, cultures reaching 80 % confluency were trypsinized and gently disaggregated by pipetting, cells were then suspended in culture medium and plated onto TCP for 20–40 min in the incubator. During this time, MEFs attach to the plate while ES cells remain suspended in the supernatant and can be harvested for subsequent use. The same procedure was used when testing experimental scaffolds. Those used in this work were fabricated in the Lab of Professor Alessandra Bianco, Dept. of Chemical Sciences and Technologies, Univ. of Rome Tor Vergata. The disks had a diameter of 13 mm and a thickness of approx. 0.3 mm). Before each experiment, scaffolds were sterilized in 70 % ethanol overnight, air dried, and secured by stainless steel rings to the bottom of the wells of 24-well plates. When necessary, MEFs were seeded on the scaffolds and on standard TCPs and incubated overnight. The next day, ES cells were seeded in each well. The medium was changed every 24 h until the ES colonies in the standard cultures were approximately 80 % confluent (about 3 days). For neurotrophin stimulation experiments, 50 ng/ml of BDNF, NT-3, NT-4 and 100 ng/ml NGF were used. Neurotrophins were added at the beginning of the culture and the medium was replaced every day.

Medium without LIF was used to initiate the differentiation of ES cells by the hanging drop method (Wobus et al., 1984). 25 μl droplets of an ES cell suspension ($3x10^4$ cells/ml) were placed in the inner side of the lid of a 10-cm Petri dish filled with 5 ml of PBS. After three days the embryoid bodies (EBs) formed were transferred into bacteriological dishes with 5 ml

medium and cultivated in suspension culture for two additional days. On day 5 EBs were either plated on scaffolds or on tissue culture plates. In order to enhance the differentiation into endothelial cells, EBs were treated with 50 ng/ml murine recombinant VEGF for 7 days.

2. PRE-IMPLANTATION EMBYOS AND PRIMORDIAL GERM CELLS

Outbred CD1 mice (Charles River, Calco, Italy) were housed and mated under standard laboratory conditions. Pre-implantation embryos at various developmental stages were collected according to standard procedures. Pregnant females were sacrificed at staged post-coital times, midday of the day on which the vaginal plug was found being considered as 0.5 post-coital day (dpc).

3.5 dpc blastocysts were cultured for 3-4 days on a gelatinized surface in DMEM, 10% FCS in order to obtain outgrowth of the inner cell mass.

Primordial germ cells (PGC) were immunomagnetically isolated from 11.5 dpc urogenital ridges (Pesce and De Felici, 1995). Briefly, urogenital ridges were dissociated in 0.5% trypsin -EDTA and cells were incubated with anti-SSEA1 antibody in M_2 at 4°C. After 45 min of rotation, 10 µl magnetic microbead-conjugated anti-mouse IgM (Miltenyi Biotec GmbH) were added to the cell suspension and incubated for a further 20 min at 4°C. Cells were sorted out by a magnetic field device (MiniMACS System; Miltenyi Biotec) according to the manufacturer's specifications. EG cells (a kind gift of Dr. Azim Surani) were cultured on a MEF feeder layer, in the same medium as ES cells.

3. RT-PCR ANALYSIS

ES cells were harvested and re-plated in a gelatinized dish for 30 min at 37°C in 5% CO2 in order to remove MEFs. Total RNA was isolated from non adhering cells using Trizol (Invitrogen) and DNaseI (Invitrogen) according to the manufacturer’s specifications. For EBs, RNA was isolated using the RNeasy Micro Kit (Qiagen). Total RNA (1 µg) was reverse transcribed using oligodT with the Superscript First Strand Synthesis System (Invitrogen) according to the manufacturer’s protocol. PCR was performed using 1 or 2 µl of the reverse transcriptase reaction in a volume of 25 µl using Platinum Taq polymerase (Invitrogen). PCR conditions were as follows: initial denaturation at 95°C (5 min) followed by up to 35 cycles of denaturation at 95°C (1 min), annealing at a temperature depending on the primer pair (1

min), and extension at 72°C (1 min). Amplified PCR products were analyzed by electrophoresis on a 1% agarose gel. PCR primer pairs were as follows:

p75NTR (T_A 60°C):	5'-CCTGCCTGGACAGTGTTACG -3'
	5'-GCCAAGATGGAGCAATAGACA -3'
TrkA (T_A 55°C):	5'-TCACCTGAATCTCTCCTCCAAT -3'
	5'-CCCGTTGTTGACATGCGTG -3'
TrkB (T_A 59°C):	5'-CGAGGTTGGAACCTAACAGC -3'
	5'-GAAATTTATGTGCCGCAGGT-3'
TrkC (T_A 59°C):	5'-CCCACCAGACCAATCTGAAC -3'
	5'-GTAGGGCTCGCATCAGACTC -3'
Pecam-1 (T_A 58°C):	5'-GCAAAGTGGAATCAAACCGTA-3'
	5'-ATCTGTGAATGTTGCTGGGTC-3'

4. STAINING PROCEDURES

For morphological analysis, at the end of the culture cells were washed with PBS and fixed with methanol for 5 min at -20 °C. To stain nuclei, a solution of 0.5 µg/ml Hoechst 33258 in PBS was added for 30 min. After three PBS washes, cells were mounted with Möwiol and fluorescent images were taken with Axioplan 2 microscope.

Pluripotency of the ES cell colonies was evaluated by alkaline phosphatase assay. Enzyme activity was detected by incubating the fixed cells for 15 min in a solution made by mixing 960 µl Fast Red TR salt (1 mg/ml) with 40 µl Naphthol AS-BI (4 mg/ml). Cells were washed with PBS and observed using a Leitz Diavert microscope. Pluripotent colonies expressing alkaline phosphatase appeared red, while the differentiated ones were colourless. Cell viability was determined by staining with a 0.4 % trypan blue solution. The dead/blue cells were counted with a hemocytometer and the data were expressed as percentages of the total cell number (±SD).

5. IMMUNOFLUORESCENCE ANALYSIS

ES cells were cultured on glass round coverslips in 4 well NUNC plates as described above. Five thousand cells per well were seeded and grown for up to five days. Medium and growth factors were replaced every day. Coverslips were then fixed in methanol for 10 min at -20°C, incubated for 30 min with 10% NGS and immunostained with anti- p75NTR and anti-Oct4 (Santa Cruz, Sc 5279) in 0.1% BSA in PBS overnight at 4°C. ES cell colonies were also

immunostained with anti-Nanog, anti-TrkA, -TrkB and –TrkC antibodies. Control sections were incubated with rabbit and mouse immunoglobulins in the same conditions as the primary antibodies. Primary antibodies were revealed by incubating the cells with the appropriate secondary antibody.

6. WESTERN BLOT ANALYSIS

For protein immunodetection by Western blot, at the end of the culture cells were homogenized in lysis buffer (50 mM HEPES, pH 7.4, 15 mM $MgCl_2$, 150 mM NaCl, 15 mM EGTA, 20 mM β-glycerophosphate, 1 % Triton X-100, 10 % glycerol, 0.5 mM sodium orthovanadate, 1 mM dithiothreitol) with Protease Inhibitor Cocktail. Homogenates were sonicated, centrifuged at 4 °C for 15 min at 15000 g, supernatants were collected and protein concentration was determined. Extracts were solubilized in NuPAGE LDS sample buffer with the addition of 50 mM dithiothreitol, separated by electrophoresis on a 4–12 % NuPAGE Bis–Tris Gel System, and transferred to PVDF Transfer Membrane Hybond™-P. Membranes were saturated with 5 % nonfat dry milk in PBS containing 0.1 % Tween 20 (PBS/T), for 1 h at room temperature and incubated overnight at 4 °C with the following primary antibodies, diluted 1:1000 in PBS/T with 5 % BSA: rabbit anti-Nanog (Cosmo Bio, Japan), mouse anti-Oct4 (Santa Cruz sc-5279), rabbit anti-$p75^{NTR}$ (Abcam 8875), rabbit anti-TrkA developed by Dr Reichardt (1:500; a kind gift of Dr Roberta Possenti), rabbit anti-pAKT (Biosource), mouse anti-CRM1 (BD-Biosciences) and mouse anti-αTubulin (Sigma, USA). Secondary anti-rabbit or anti-mouse antibodies conjugated to horseradish peroxidase (Amersham, UK) were incubated with the membranes for 1 h at room temperature at 1:10000 dilution in PBS/T with 5 % nonfat dry milk. Immunoreactive bands were detected by SuperSignal West Pico chemiluminescent reagent and densitometric analysis of the bands was performed using ImageQuant 5.0.

7. ALKALINE PHOSPHATASE ASSAY

ES cells were seeded in 96-well plates and cultured in different conditions for up to 5 days. 50 µl of 10 mM diethanolamine pH 9.0 (DEA) were added to each well and incubated for 3 min. The DEA solution was then replaced by 50 µl of a colorimetric substrate for alkaline phosphatase (1mg/ml p-nitrophenyl phosphate in DEA). The reaction was monitored until a

clear yellow colour appeared in the wells, and the OD at 405 nm was measured in an ELISA plate reader.

8. NGF IMMUNOASSAY

The NGF Elisa kit is designed to measure the amount of NGF in cell culture supernatants. Sheep polyclonal antibodies generated against mouse NGF are coated onto a microplate and are used to capture NGF from a 100 µl sample incubated for 3 hours at room temperature. After washing 4 times, NGF specific mouse monoclonal antibody (diluted as suggested by the manufacturer's protocol) is added and incubated for 2 hours to detect the captured NGF. After another 4 washes, mouse specific, peroxidase labelled, donkey polyclonal antibody is added and incubated for 2 hours. After washing, the substrate is added for 15 minutes until a blue colour appears and the stop solution is added to turn the blue solution yellow. The plate is read at 450 nm and, as the standard curve demonstrates a direct relationship between Optical Density (OD) and NGF concentration, it is possible to quantify the NGF in the culture medium.

9. CELL VIABILITY ASSAYS

Cell adhesion and proliferation were evaluated using three different methods, this was necessary due to the different kinds of scaffolds tested.

9.1. *MTT Assay*

We used a modification of the methylthiazolyldiphenyl-tetrazolium bromide (MTT) assay (Mosmann, 1983). Parallel cultures without ES cells (MEFs only) were analyzed in order to subtract the background due to the feeder layer. Briefly, each sample was rinsed with PBS to remove unattached cells and then incubated at 37 °C for 1 h with 250 µl/well MTT solution at 0.5 mg/ml. The MTT solution was then removed and dimethylsulfoxide (900 µl/well) and glycine buffer (pH 10.5, 125 µl/well) were added to each well. After 10 min of agitation, the absorbance at 540 nm was measured with a SmartSpec 3000 spectrophotometer and recorded as optical density (OD).

9.2. *MTS assay*

The MTS tetrazolium compound is bioreduced by cells into a coloured formazan product that is soluble in tissue culture medium. The assay is performed adding CellTiter 96® AQ_{ueous} One Solution Reagent (Promega) directly to culture wells, 1:5 with the culture medium, incubating for 2 hours and reading the absorbance at 490nm.

9.3. *[^{3}H]thymidine Incorporation*

Cell proliferation was evaluated by measuring incorporation in the acid-insoluble fraction of the radioactive DNA precursor [^{3}H]thymidine. Parallel MEF-only cultures were also run. For radiolabeling, cells were washed with PBS and incubated with fresh serum-free DMEM containing all the supplements and 1 µCi/well of [methyl-^{3}H]thymidine for 2 h at 37 °C. After incubation, cells were treated with 5 % trichloroacetic acid (TCA) on ice for 20 min, and then washed twice with ice-cold distilled water. The acid-insoluble material was dissolved with 1N NaOH for 20 min at room temperature, and an equal volume of 1N HCl was added. Each sample was mixed 1:10 with scintillation liquid and the radioactivity, expressed as counts per minute, was measured by a scintillation counter.

10. STATISTICAL ANALYSIS

Data from the MTT, MTS and [^{3}H]thymidine incorporation assays are shown as means ± standard error of three replicates from three independent experiments. Radioactivity counts were normalized to take into account the differences in the number of cells after the 6 h adhesion time. Statistical analysis was performed by one-way analysis of variance (ANOVA) and Tukey test for pairwise multiple comparisons.

RESULTS

1. EFFECT OF GROWTH FACTORS ON ES CELL CULTURES

1.1. *p75^{NTR} in pluripotent cells*

Data in the literature (see Section 2 of Introduction) suggesting a close relationship between pluripotency and p75^{NTR} expression, prompted us to study when p75^{NTR} and its cognate receptors first appear during mouse development and to look for its possible presence in embryo-derived cell lines (ES and EG cells) that are characterized by wide pluripotency. RT-PCR experiments show that p75^{NTR} RNA first appears in the mouse embryo at the early blastocyst stage; the signal becomes stronger in the late blastocyst. Whole-mount immunolocalization analysis (Fig.3) showed that at such stage p75^{NTR} expression was confined to the inner cell mass (ICM).

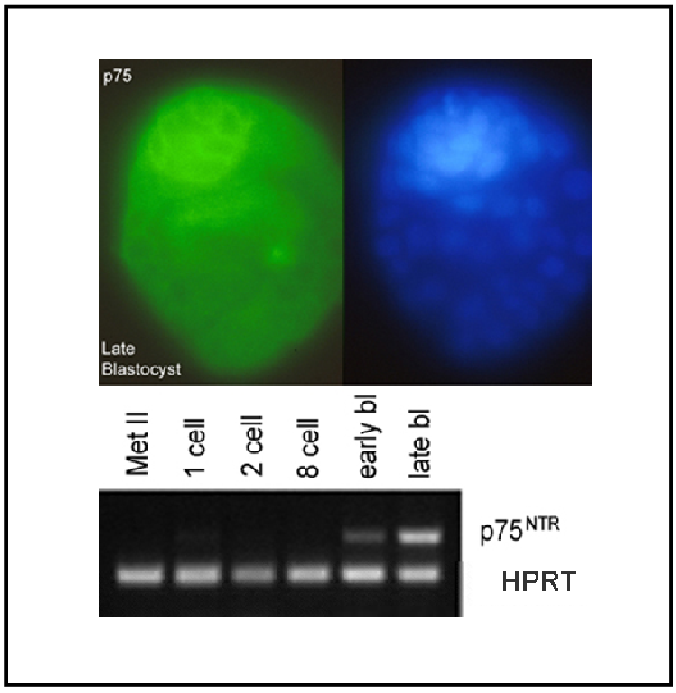

Fig.3 Whole mount immunolocalization of p75NTR in the mouse embryo at the late blastocyst stage (upper panel). RT-PCR analysis during early developmental stages of the mouse embryo (lower panel).

We then tested whether ES cells, known to be derived from the blastocyst ICM, continue to express the receptor (Fig.4). RT-PCR analysis on three ES cell lines (R1, D3, W4) shows that

p75^{NTR} mRNA is present. Western blot analysis has confirmed the presence of a band at about 70 kDa, consistent with the molecular weight of the receptor. ES cell clones appear to be highly immunoreactive to the anti-p75^{NTR} antibody, but as the ES cell clones differentiate p75^{NTR} positivity is lost, as it occurs for Oct4.

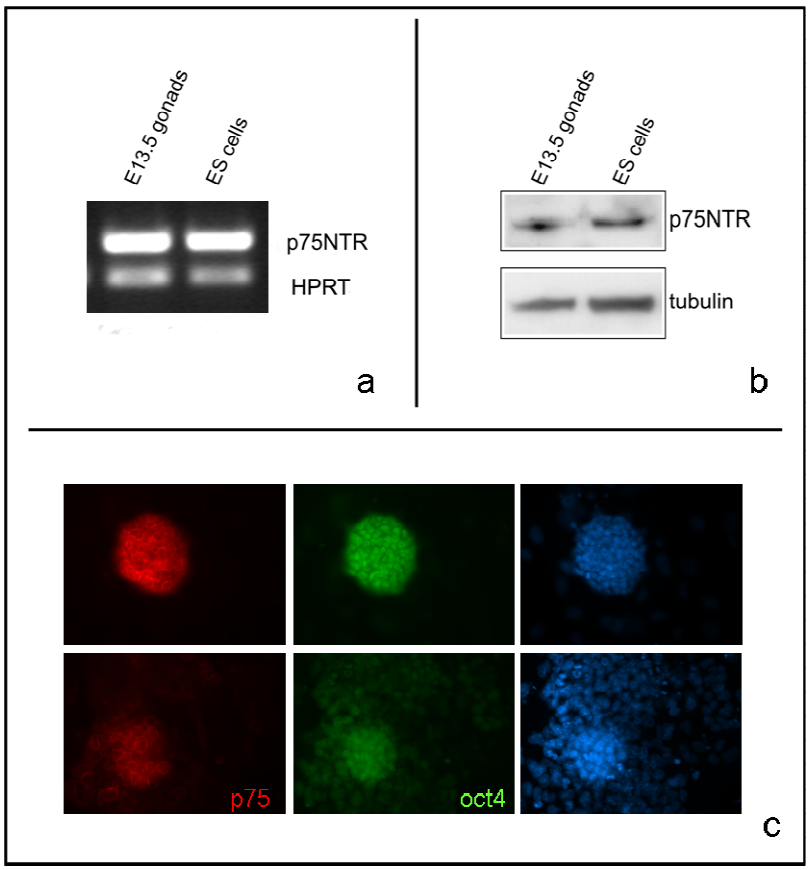

Fig.4 Expression of p75^{NTR} in ES cells. RT-PCR analysis (a) of p75^{NTR} expression in ES cells and embryonic gonads. Western blot analysis (b) of p75^{NTR} expression in ES cells and embryonic gonads, α-tubulin was used as a loading control. Immunofluorescence analysis (c) of p75^{NTR} and Oct4 expression by ES cells in an undifferentiated state (upper panel) and while differentiating (lower panel).

We also tested ES cells for expression of the other neurotrophin receptors, belonging to the trk family (Fig.5). RT-PCR analysis shows that only TrkA is expressed by ES cells, whereas TrkB and TrkC are not. The expression of TrkA is confirmed by Western blotting analysis.

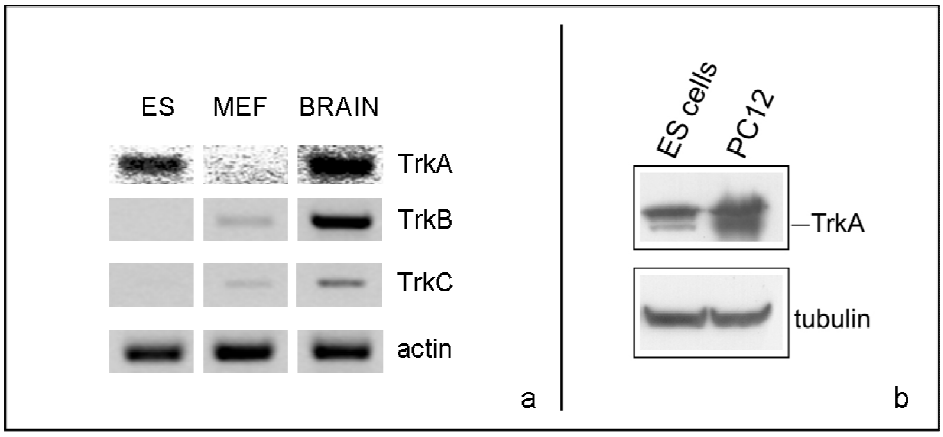

Fig.5 RT-PCR analysis (a) of TrkA, TrkB, and TrkC expression in ES cells. Western blot analysis (b) of TrkA expression in ES cells and PC12 cell line, α-tubulin was used as a loading control.

EG cells are pluripotent cells, very similar to ES cells but obtained through de-differentiation of primordial germ cells (PGCs), the embryonic lineage committed to differentiate into gametes. As with ES, EG cells are capable of self-replicating and of differentiating into all tissues types and, when injected into a blastocyst, of generating mouse mosaics by extensively colonizing all tissues of the animal. We have observed by immunofluorescence analysis that PGCs do not express $p75^{NTR}$, whereas EG cells, identified by the presence of Oct-4 (not shown), become strongly immunoreactive for $p75^{NTR}$. The results clearly show that the recovery of pluripotency that occurs when PGCs are made to revert to an ES-like phenotype (through de-differentiation into EG cells) is associated with resumption of $p75^{NTR}$ expression (Fig.6).

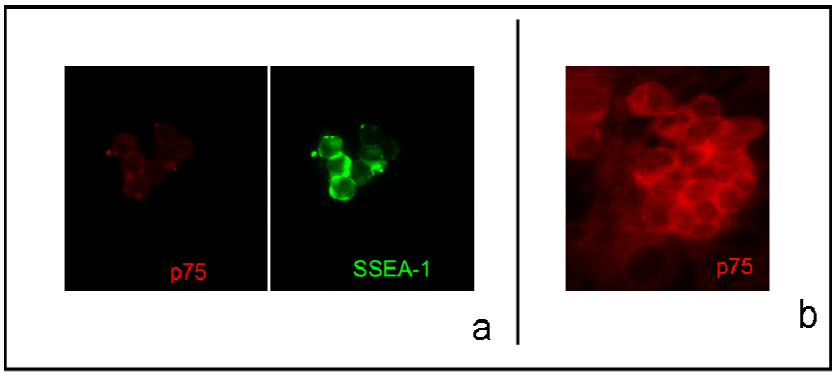

Fig.6 Immunofluorescence analyses of PGCs (a) and EGs (b).

1.2. *NGF Stimulates ES cell Colony Growth*

Based on the result reported above, we then tested whether NGF, the ligand for $p75^{NTR}$ and TrkA, was involved in the proliferation or pluripotency of ES cells.

ES cells were cultured at low density in the presence of 100 ng/ml NGF (concentration generally used in the literature to elicit an effect from NGF responding cell types). After 4 days the cultures were fixed and stained with Hoechst, and the number of ES cell colonies and their area measured. In three independent experiments a total of 347 ctrl colonies and 388 NGF-treated colonies were counted and measured. The average number of colonies per five microscopic fields was not significantly different (ctrl 20±3, NGF 19±3).

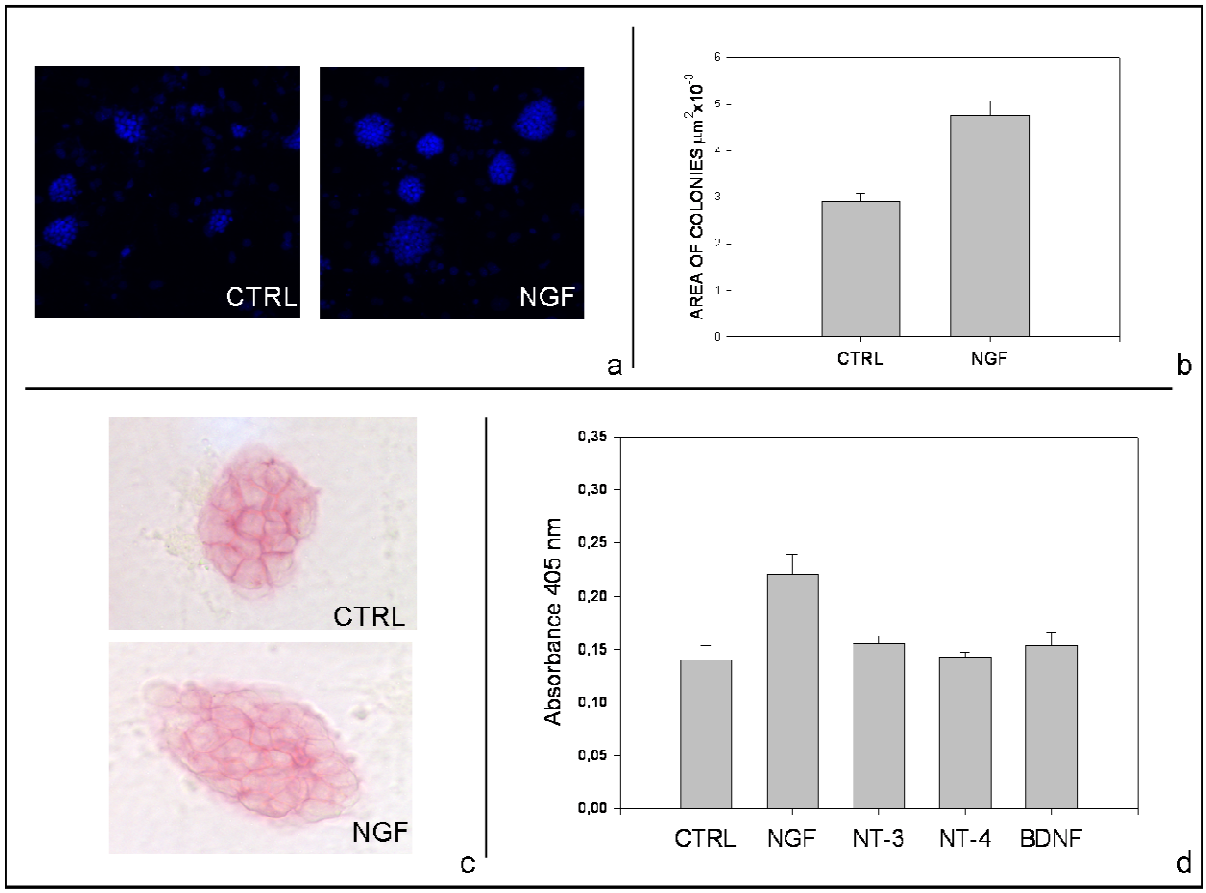

Fig.7 Effect of NGF on ES cell cultures. The average area of the colonies is higher, as can be appreciated from the Hoechst staining images (a) and the measures show a 1,6 fold increase (b). AP staining is positive in both conditions (c) so the 1,6 fold increase in the OD at 405 nm indicates a higher number of AP positive cells (d) after addition of NGF to the culture medium

On the contrary, the average area of colonies grown in the presence of NGF was significantly larger (Fig.7a-b) than the area of colonies grown in standard conditions (ctrl $2,9x10^3 \pm 0,2\ \mu m^2$, NGF $4,7 \pm 0,3\ \mu m^2$) reflecting a 1,6 fold increase. Altogether, these data suggest that the growth factor does not act on the adhesion and/or survival of the cells, but on their proliferation rate.

The colonies grown in the presence of NGF remain positive for all the stem cell markers we examined, including alkaline phosphatase (AP) (Fig.7c), Oct-4 and Nanog (Fig.8).

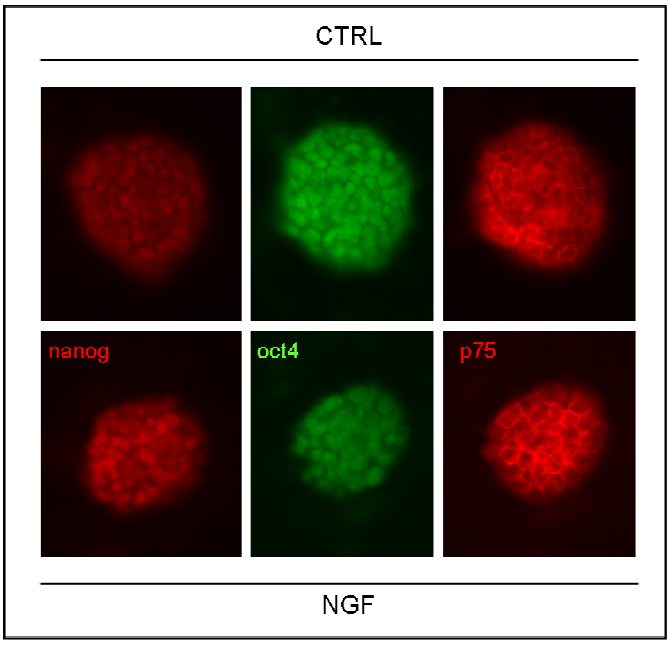

Fig.8 Immunofluorescence analyses of pluripotency markers nanog and oct4 on ES cell colonies grown with or without NGF. Colonies in both conditions are positive for $p75^{NTR}$.

To validate the colony area data, suggesting an increase in ES cell numbers, we used a colorimetric assay that measures alkaline phosphatase activity. A preliminary experiment had shown a linear relation between number of undifferentiated ES cells and AP activity (Fig.9). While the presence of 100 ng/ml BDNF, NT-3 and NT-4 had no effect on AP activity, ES cells grown in the presence of NGF showed a 1,6 fold higher alkaline phosphatase activity than cells grown in standard cultures (Fig.7d), thus confirming that NGF stimulates ES cell proliferation, without affecting the expression of pluripotency markers.

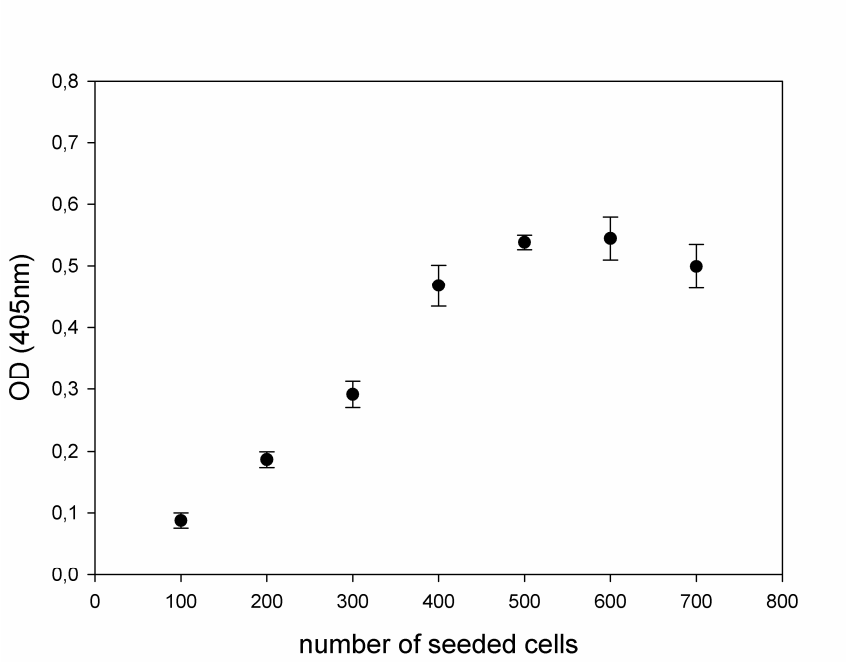

Fig.9 Graph showing relation between number of cells and alkaline phosphatase activity.

In order to assess if the NGF/neurotrophin receptor system might be working in basal culture conditions, as NGF might be produced by MEFs and/or ES cells, we dosed by ELISA kit endogenous NGF released in culture medium. Fig.10 shows that the amount of NGF produced by the cells in culture is in the order of 100 pg/ml.

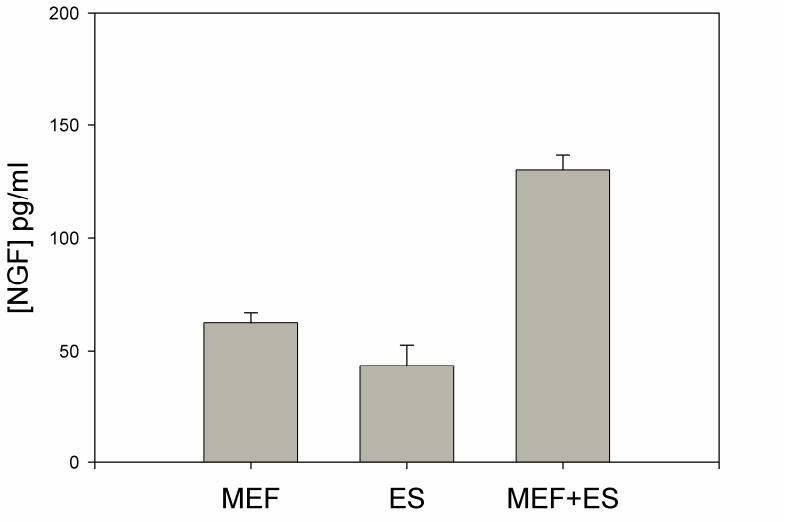

Fig.10 Endogenous NGF produced by MEFs and ES cells, measured by ELISA kit.

1.3. *Involvement of $p75^{NTR}$ and TrkA in NGF response*

The extracellular domain of $p75^{NTR}$ comprises four tandemly arranged cystein–rich domains required for NT binding. Although it is known as the "low-affinity" receptor, $p75^{NTR}$ actually binds NTs with about the same affinity as monomeric Trks (Chao, 2003). However, recent structural analysis of $p75^{NTR}$ with NGF suggests the formation of an asymmetric complex of one dimeric NT bound to a single $p75^{NTR}$.

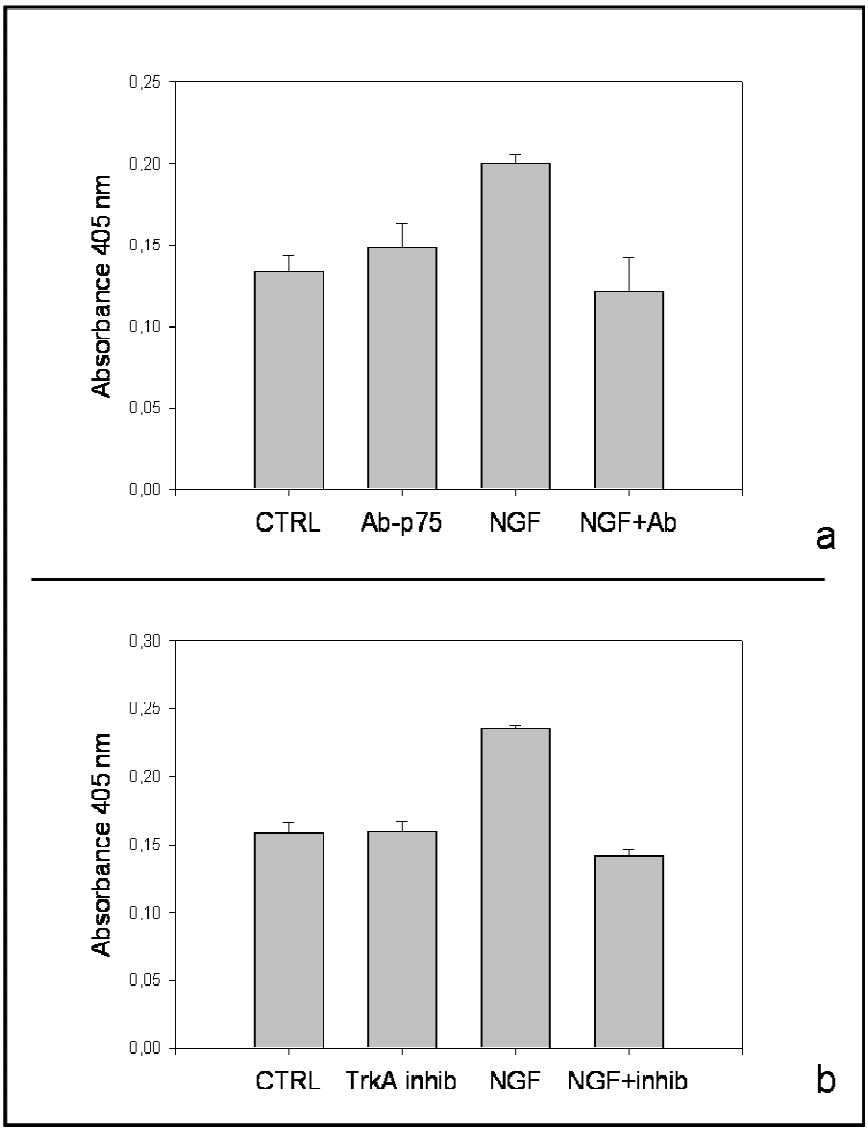

Fig.11 Inhibition of NGF effect on ES cells, evaluated by AP activity quantification. Both the $p75^{NTR}$ blocking antibody and the specific TrkA inhibitor, GW441756 prevent the effect of NGF in this system.

Thus, the conformation of the $p75^{NTR}$ –NT complex is such that it cannot recruit more than one receptor and therefore cannot form high-affinity two-chain sites, as Trk dimers do (He and Garcia, 2004). However when they are coexpressed, $p75^{NTR}$ enhances the ability of Trk receptors to bind and respond to neurotrophins and sharpens the discrimination of Trks for their preferred neurotrophin ligands.

We investigated whether the observed NGF effect on ES cell proliferation was mediated by its binding to TrkA, $p75^{NTR}$, or both. To such end we have evaluated the effect of an antibody that binds $p75^{NTR}$ and blocks the function of nerve growth factor (Abcam 8874). The addition of 20 μg/ml of the antibody to the ES culture was able to prevent the effect mediated by NGF (Fig.11a). TrkA was equally involved in mediating the response to NGF: treatment of the cells with specific TrkA inhibitor GW441756 blocks the effect of NGF on the ES cell growth (Fig.11b). Taken together, the data indicate that both receptors are involved in the response of ES cells to NGF.

2. EFFECT OF A 3D SUPPORT ON ES CELL GROWTH

In standard cultures, ES cells are grown in the presence of LIF and on a feeder layer of mitotically inactivated murine embryonic fibroblasts, that not only secrete factors necessary to prevent ES cell differentiation but also provide a three dimensional matrix to which ES cells may anchor. We evaluated the importance of a three dimensional support for ES cell growth by monitoring the behaviour of ES cells seeded on electrospun PCL scaffolds (Fig.12).

The cells have been grown on tissue culture plates and on scaffolds under different conditions:

- with the support of a feeder layer of MEFs and in the presence of leukemia inhibitory factor (LIF), a condition that promotes proliferation with self-renewal;
- without the support of MEFs, with or without LIF, conditions that should cause differences in the levels of cell differentiation.

The aim of the experiments was to evaluate: first, the possibility of ES cell self-renewal and amplification on scaffolds, a point that might be an asset in tissue engineering, and second, the behaviour of ES cells after withdrawal of support cells and/or LIF, to study the importance of a 3D support in maintaining pluripotency and also with the perspective of inducing a differentiation pathway using specific factor/s.

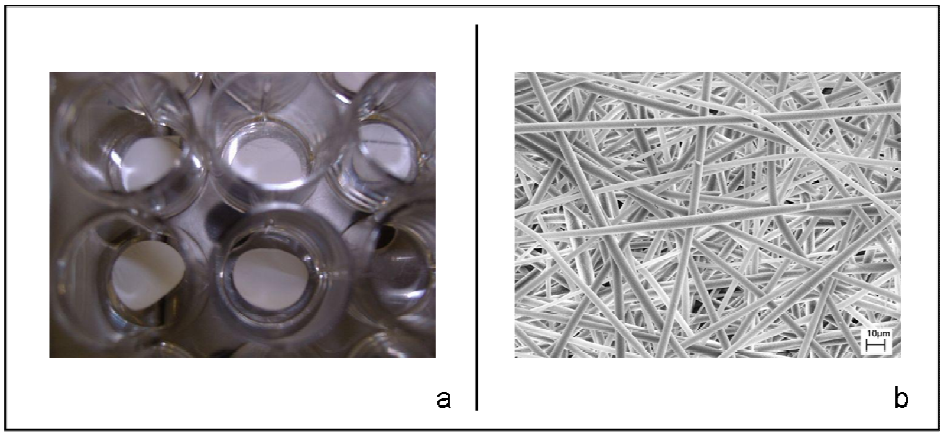

Fig.12 PCL scaffolds in 24-well culture plate (a). SEM micrograph of electrospun PCL mat (b). Average fibre diameter 3.6 ± 0.8 µm.

2.1. CULTURES IN CONDITIONS AIMED TO MAINTAIN PLURIPOTENCY

2.1.1. *Effect on adhesion, viability and proliferation*

In order to assess PCL scaffolds suitability for ES cell culture, we evaluated cell adhesion and proliferation on such substrate. For cell adhesion studies, we performed MTT assays after 6h of culture, when ES cells should have adhered but proliferation would still be minimal or absent. As shown in Fig.13a, the OD values generated by cells present on the PCL scaffolds were about 45 % those by cells seeded on standard culture plates. Since the OD values measured by the MTT assay are proportional to the cell number, our results indicate that PCL mats allow the adhesion of approximately one half of the cells that are found in standard cultures.

To rule out the possibility that the lower cell adhesion rates on scaffolds was due to scaffold cytotoxicity, the unattached cells was stained with live-dead cell stain trypan blue. The percentage of blue/dead cells found in the supernatant of PCL cultures (60±8 %) were not significantly different from that found in culture plates (60±9%), indicating that the presence of electrospun PCL does not affect cell viability.

We then evaluated ES cell proliferation, by measuring ^{3}H-thymidine (^{3}HTdR) incorporation after 3 days of culture. Our results show that on PCL scaffolds the cells incorporate about one half the counts as cells growing on culture plates. However, if the incorporation data are normalized for the percentage of cell adhesion at 6 h, essentially no difference in ^{3}HTdR incorporation can be detected between ES colonies grown on culture plates or on scaffolds (Fig.13b).

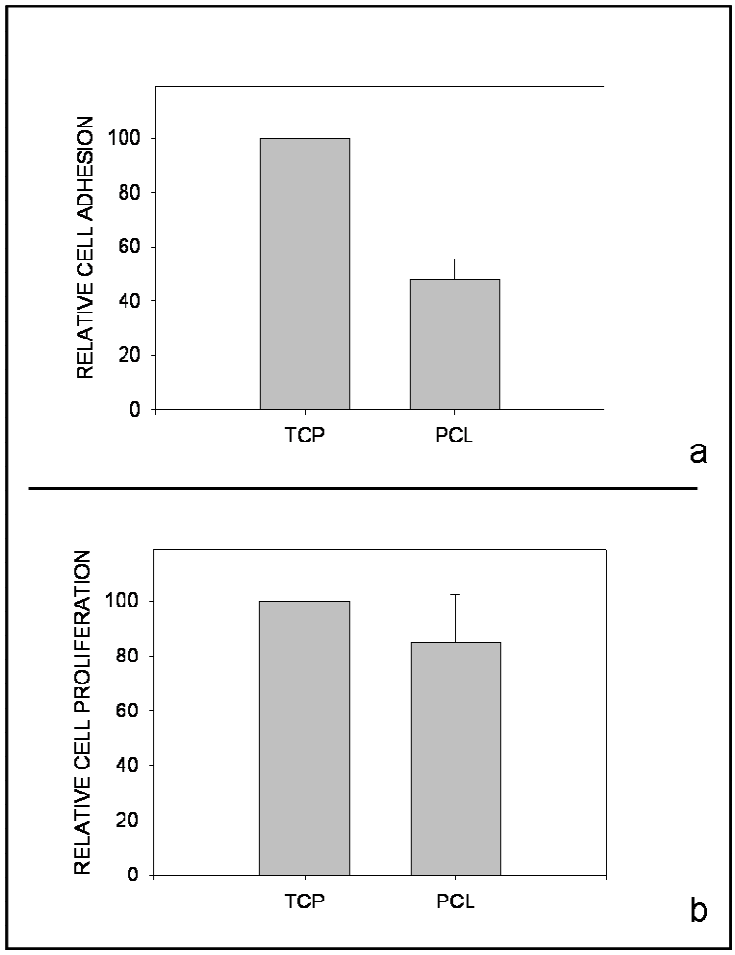

Fig.13 ES cell adhesion (a), measured by MTT assay 6 h after seeding the cells in standard cultures (TCP), and in cultures on PCL scaffolds (PCL) in the presence of MEF and LIF. ES cell proliferation (b), measured by ^{3}H-thymidine (^{3}HTdR) incorporation after 3 days of growth in standard cultures (TCP), and in cultures on PCL scaffolds (PCL). Results are expressed as percentage of the standard culture (TCP = 100%).

2.1.2. *Effect on colony morphology*

We then assessed to what extent PCL scaffolds may influence ES cell growth. Morphological features of ES cell colonies were evaluated after 3 days of culture in the presence of MEFs and LIF, conditions aimed to maintain pluripotency.

The size and shape of ES colonies, as analyzed by Hoechst nuclear staining, were similar in all experimental conditions, as shown in Fig.14a-c. In addition, nuclear morphology did not show any appreciable sign of apoptosis, such as nuclear condensation, in any of the cultures examined.

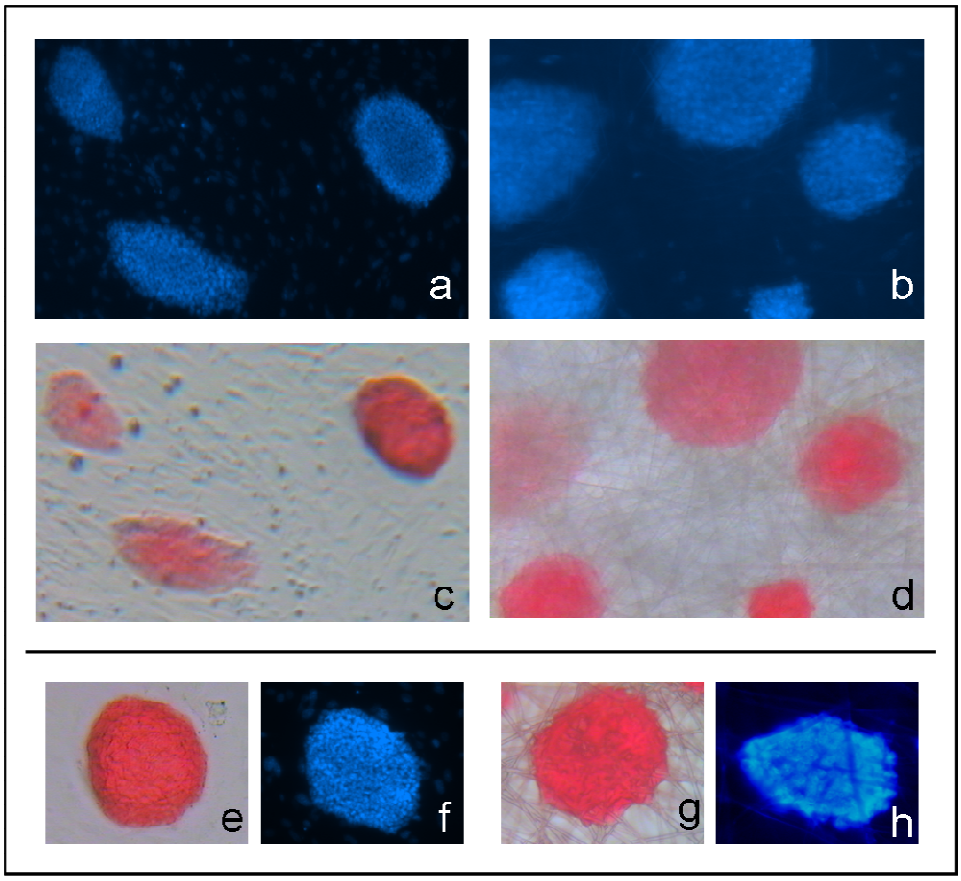

Fig.14 Micrographs of ES cell colonies in standard cultures conditions (a,c,e,f), and in cultures on PCL scaffolds (b,d,g,h) grown in the presence of MEF and LIF for 3 days: fluorescence analysis of ES cell colonies after nuclear staining with Hoechst 33258; cytochemical analysis of the same colonies for alkaline phosphatase (red), a marker of ES cell pluripotency.

2.1.3. *Effect on the expression of pluripotency markers*

Cell colonies grown on PCL scaffolds and on culture plates were cytochemically stained for alkaline phosphatase (AP). As shown in Fig.14d-f, all colonies grown on the scaffolds were AP positive, as they were in standard cultures.

In addition, the colonies were analyzed by Western blot for the presence of Nanog, a transcription factor that plays a crucial role in maintaining the pluripotent state of ES cells. Fig.15 shows the immunodetection of Nanog and α-Tubulin (upper panel). The densitometric analysis of the bands (lower panel) showed similar levels of Nanog in standard and in PCL cultures, indicating that, the presence of the scaffold does not hinder the maintenance of cell pluripotency, thus confirming at a molecular level the AP data.

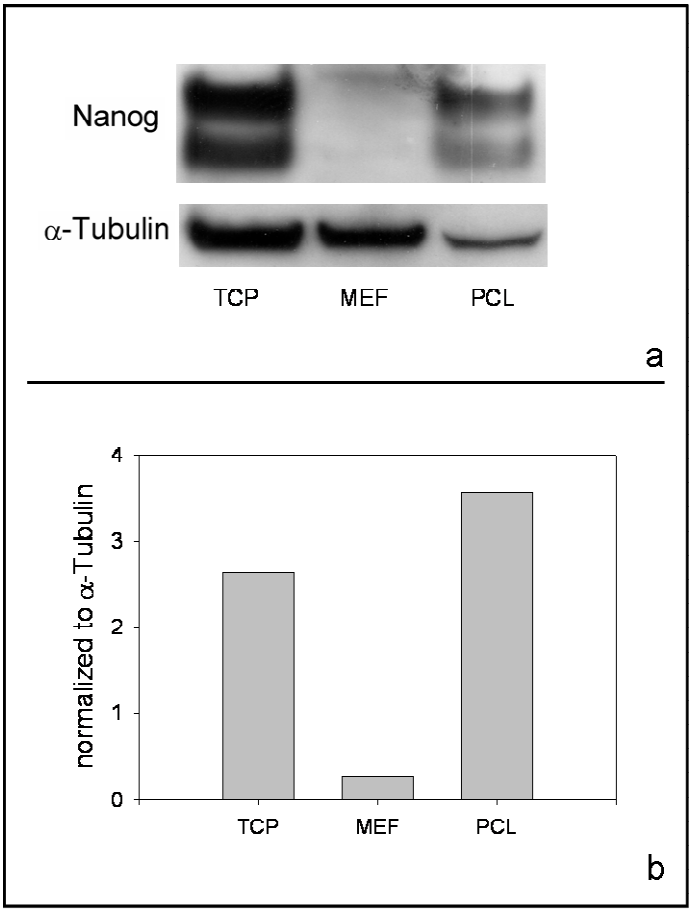

Fig.15 Immunodetection of Nanog and α-Tubulin proteins by Western blot (a) and densitometric analysis of the bands (b). Protein extracts were obtained from ES cells grown in standard cultures (TCP), and in cultures on PCL scaffolds (PCL) in the presence of MEF and LIF for 3 days. The second lane contains the protein extract of a control culture without ES cells (MEF only). Representative immunodetection from three independent experiments.

2.2. CULTURES IN DIFFERENTIATING CONDITIONS

2.2.1. *Adhesion and proliferation*

We first verified if the absence of a feeder layer and of LIF would have affected the adhesion and proliferation of ES cells on the scaffolds.

The number of ES cells adhering to the substrate was measured by MTS assay 6 h after seeding the cells in standard culture plates and on PCL scaffolds. The results showed that the adhesion on the scaffolds was 50% that on culture plates (Fig.16a). ES cell proliferation was measured by MTS assay after 2, 4 and 6 days of growth (Fig.16b). Taking into account the

adhesion results, in order to obtain comparable starting cell numbers to measure cell growth, twice as many cells were seeded on PCL than on culture plates. The growth curves in the two conditions were very similar, with no statistically significant differences.

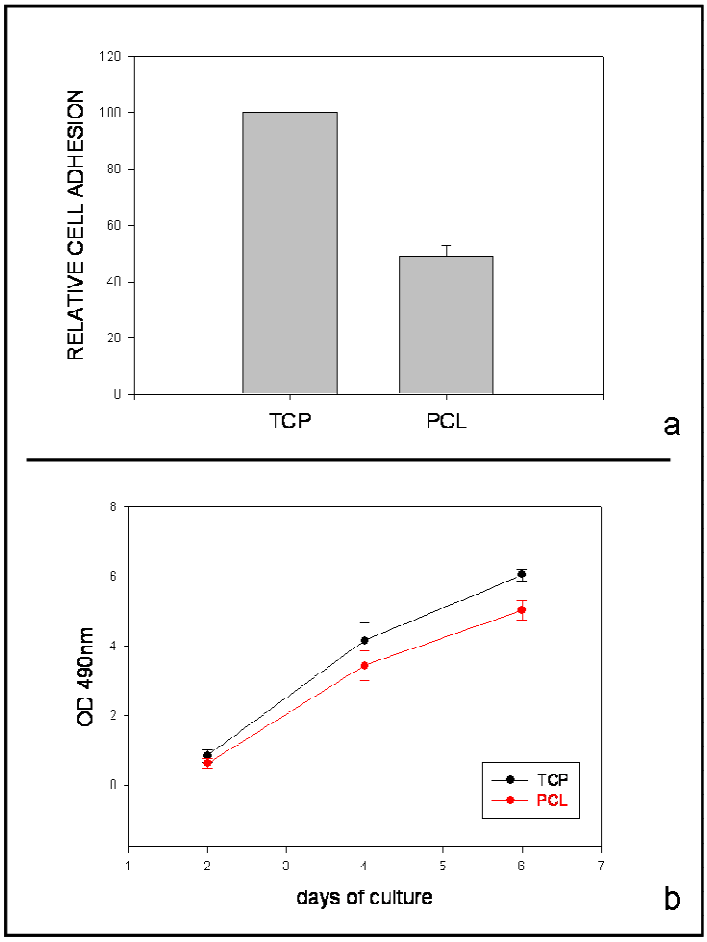

Fig.16 ES cell adhesion (a), measured by MTS assay 6 h after seeding the cells in standard cultures (TCP) and in cultures on PCL scaffolds (PCL) without MEF and LIF. Results are expressed as percentage of the standard culture (TCP = 100%). ES cell proliferation (b), measured by MTS assay after 2, 4 and 6 days of growth in standard cultures (TCP), and in cultures on PCL scaffolds (PCL). Taking account of the adhesion results, the number of cells seeded on the PCL mats was double that seeded on TCPs.

2.2.2. *Morphological analysis*

We studied the morphology of ES cells grown on PCL mats and on culture plates, without MEF at three different time points, to verify if the presence of the PCL support causes differences in colony shape or size.

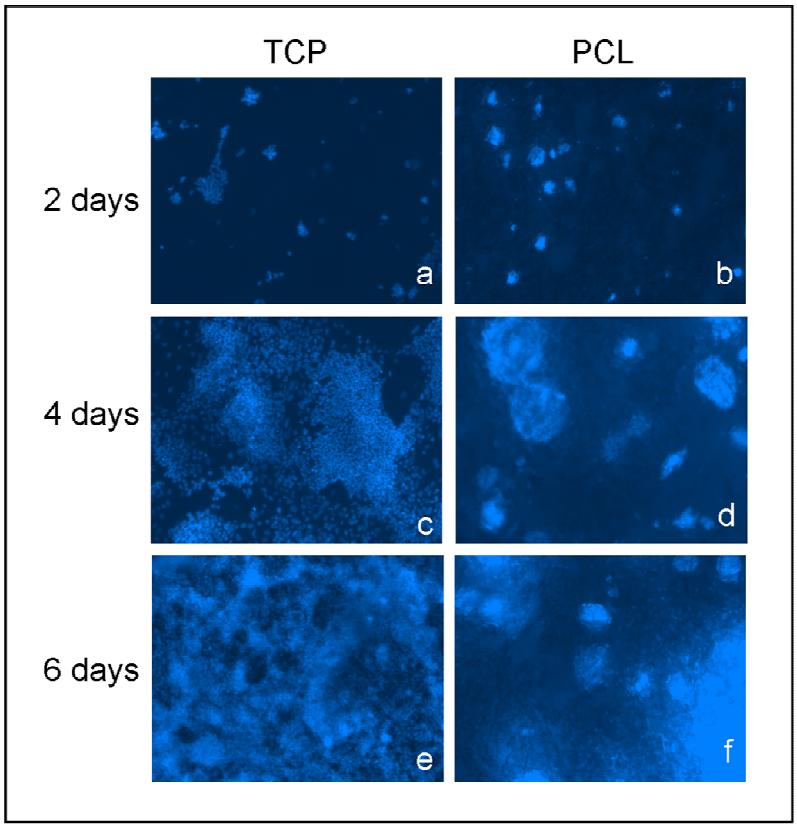

Fig.17 Micrographs of ES cell colonies stained with Hoechst 33258 on tissue culture plates (a, c, e), and on PCL scaffolds (b, d, f) after 2, 4 and 6 days of culture without MEF and without LIF.

Microscopic examination of ES cell colonies (Fig.17) grown without a feeder-layer for 2, 4 and 6 days on culture plates and on PCL scaffolds and then stained with Hoechst 33258, showed that in general the colonies growing on the scaffolds appeared to retain in a higher percentage a spherical shape, typical of undifferentiated ES cells. The different morphology between cells grown on scaffolds and on culture plates is particularly evident at 4 days of culture.

2.2.3. *Pluripotency markers in feeder cell free cultures*

On the basis of the above observations we hypothesized that, in the presence of LIF, a feeder cell free PCL scaffold might provide sufficient signals to replace the feeder cells, and to maintain the cells in the undifferentiated state, at least for 4 days. To confirm this hypothesis, we compared the expression of pluripotency markers and of a signalling

molecule involved in stemness, by cells grown in feeder-free conditions for 4 days, with and without LIF

We first analyze cytochemically the presence of AP. As shown in Fig.18, the intensity was higher in cultures with LIF than without LIF. Interestingly, the level of AP activity was greatly increased in colonies grown on PCL scaffolds.

To quantitatively support this observation, the colonies were analyzed by Western blot for the presence of two additional stem cell markers, Oct4 and Nanog (Fig.19) .

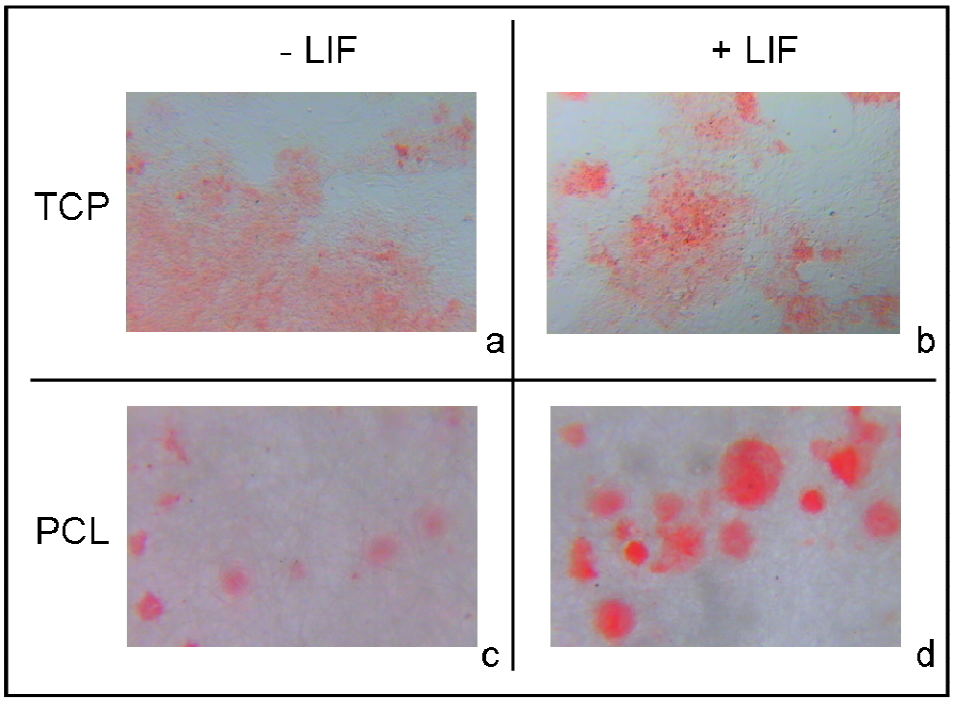

Fig.18 Alkaline phosphatase staining of ES cell colonies grown without MEF on tissue culture plates (a,b), and on PCL scaffolds (c,d) for 4 days. ES cells grown with LIF (b,d), and without LIF (a,c) in the culture medium were analysed on both supports.

Densitometric analysis of the immunoblots showed that Oct4 and Nanog were still present after 4 days of culture in differentiating conditions, and, when normalized to the housekeeping gene CRM1, the ES colonies grown on PCL scaffolds with LIF showed the higher level of both proteins.

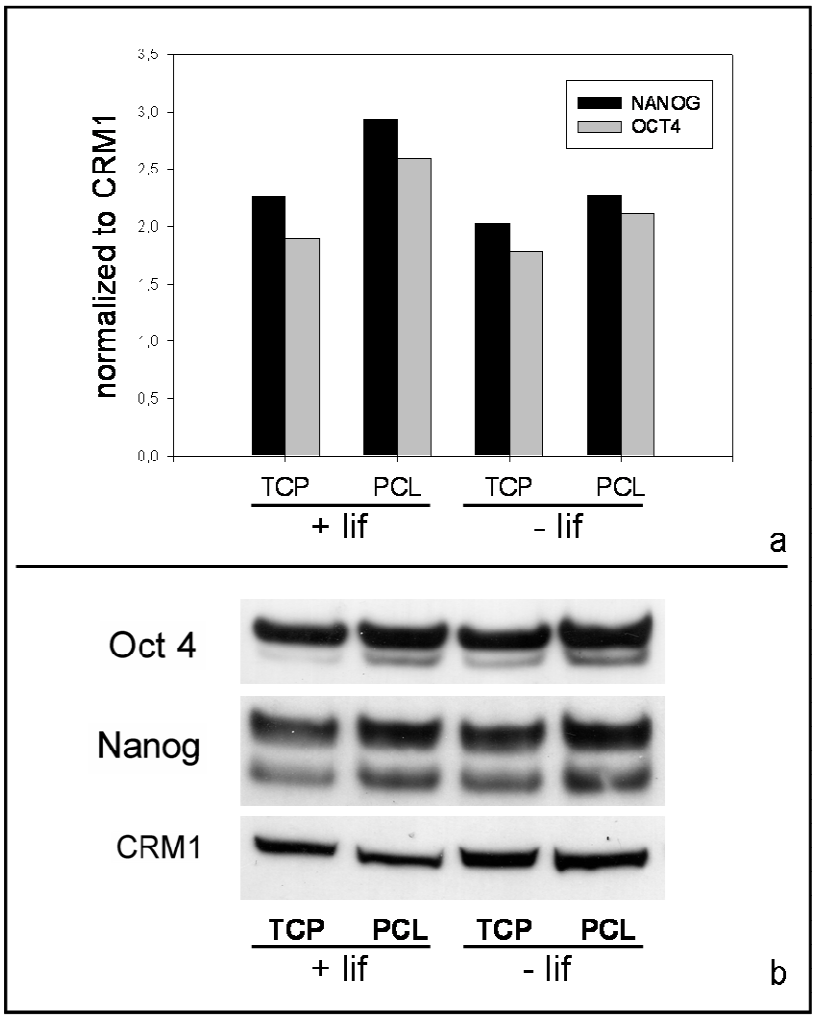

Fig.19 Immunodetection of stem cell markers Oct4 and Nanog and of the housekeeping CRM1 by Western blot (a). Protein extracts were obtained from ES cells grown on tissue culture plates (TCP) and on PCL scaffolds (PCL) for 4 days in the absence of MEF, with or without LIF. Densitometric analysis of the bands (b).

Finally, as Nanog expression in ES cells involves signaling through phosphoinositide 3-kinase (PI3K), we examined whether the 3D PCL surface helps to maintain AKT in a phosphorilated form (p-AKT), a condition indispensable for the activation of the PI3K pathway. The densitometric analysis showed an increase of p-AKT in ES cells cultured on feeder-free PCL scaffolds for 4 days independently of the presence of LIF (Fig.20).

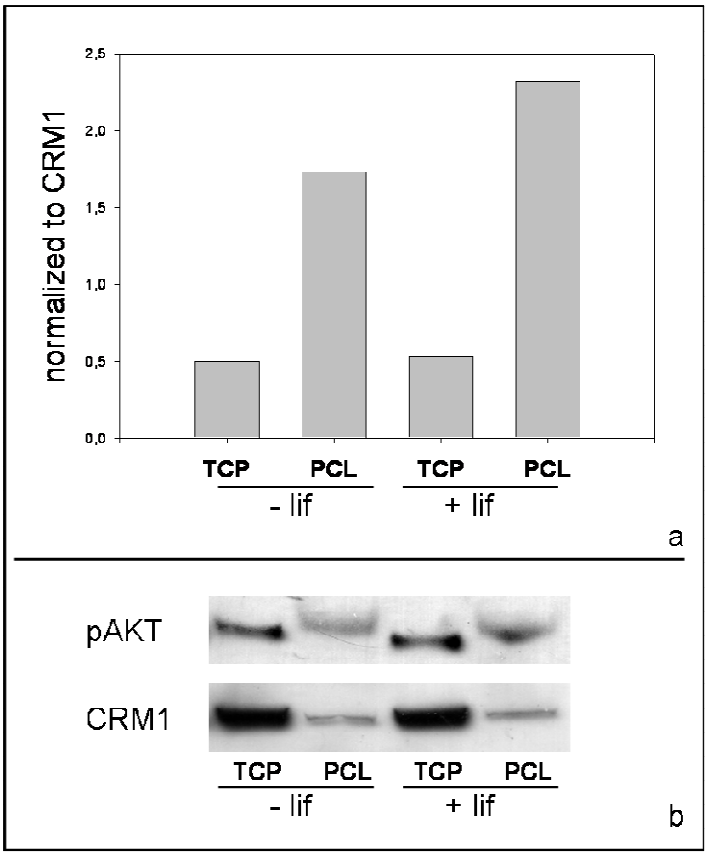

Fig.20 Immunodetection of pAKT and CRM1 proteins by Western blot (b) and densitometric analysis of the bands (a). Protein extracts were obtained from ES cells grown in standard cultures (TCP), and in culture on PCL scaffolds (PCL), in the absence of MEF, with or without LIF, for 4 days.

3. ENDOTHELIAL DIFFERENTIATION OF ES CELLS ON PCL SCAFFOLDS

The results reported above, regarding cell adhesion and proliferation, clearly show that PCL scaffolds are ES cell-biocompatible and can sustain cell growth. Such scaffolds have been recently electrospun in the shape of a trileaflet heart valve prototype (Del Gaudio et al., 2008), in the perspective of a possible use in regenerative medicine (Fig.21).

To this end, we tested if endothelial cell differentiation could be obtained on PCL scaffolds. Festag *et al.* have shown that when embryoid bodies (EBs), generated after 3 days of ES cells cultured in hanging drops, were kept for two additional days in suspension culture and allowed to attach on plastic in the presence of VEGF, they were able to produce cells expressing endothelial markers such as Pecam1 and flk1 (Festag et al., 2007). Following this

protocol, we compared the expression of Pecam1 in EBs attached on culture plates and on PCL scaffolds.

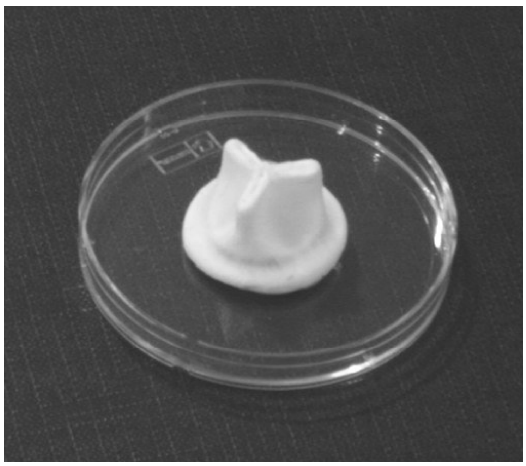

Fig.21 PCL electrospun heart valve (Del Gaudio et al., 2008).

RT-PCR analysis showed comparable increases in Pecam1 expression in the two experimental conditions (Fig.22). The results clearly indicate that the presence of a PCL scaffold does not perturb endothelial differentiation of mouse ES cells through EB formation.

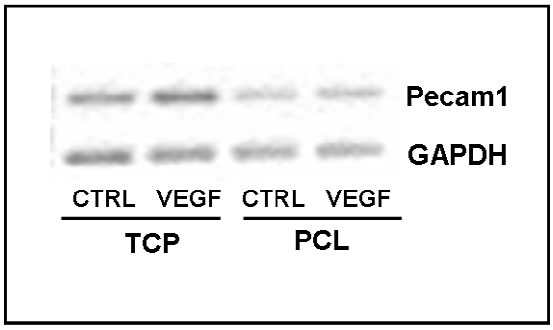

Fig.22 Gene expression for the endothelial marker Pecam1 and the housekeeping GAPDH by RT-PCR. EBs obtained by the hanging drop method were plated on TCP or PCL on day 5 of differentiation and were treated with 50 ng/ml VEGF for 7 days.

DISCUSSION

ES cells are pluripotent stem cells that have the dual ability to self-renew and to differentiate into all cell types of the embryo proper. Growth of pluripotent ES cells requires a balance between survival, proliferation and self-renewal signals. Although some of the growth factors involved in ES cell self-renewal are known, many have yet to be identified. Based on the accumulating evidence for a connection between the p75 neurotrophin receptor and stemness, we hypothesized that neurotrophins might be involved in ES cell proliferation and self-renewal. In our laboratory we had observed that multipotent mesenchymal cells of mesonephric origin that migrate into the fetal testis and that give rise to the somatic population of the interstitial compartment (i.e., Leydig, myoid and endothelial cells) are $p75^{NTR}$ positive (Campagnolo et al., 2001). Other authors had demonstrated that populations of stem cells bearing $p75^{NTR}$ are involved in the morphogenesis of kidney tubules (Huber et al., 1996), of the tooth (Luukko et al., 1996), of the inner ear (von Bartheld et al., 1991), and of the respiratory tree (Wheeler et al., 1998).

In the adult $p75^{NTR}$ can be considered as a marker for mesenchymal stem cells from bone marrow (Buhring et al., 2007), microvascular pericytes (Covas et al., 2008), subcutaneous adipose tissue (Yamamoto et al., 2007) and for a variety of epithelial progenitor cell types, as detailed in the Introduction. Finally, the presence of the p75 receptor has been exploited to immunoselect stem cells from most such tissues.

We studied further the connection between $p75^{NTR}$ and pluripotent stem populations and demonstrated that $p75^{NTR}$ is expressed in the late blastocyst stage of the developing mouse embryo. Interestingly, the cells immunoreactive to the $p75^{NTR}$ antibody are confined to the inner cell mass of the blastocyst, from which ES cells are derived. The hypothesis that $p75^{NTR}$ might be a fairly general marker of stem cells was also supported by our observations on EG cells. EG have the same potentialities as ES cells, but a different origin, as they derive – through a de-differentiation process – from germ-line committed primordial germ cells. It should be noticed that while primordial germ cells are not immunoreactive to anti-$p75^{NTR}$ antibodies, EG cells express $p75^{NTR}$. Likewise, parallel changes in $p75^{NTR}$ expression and stem quality have been reported in the literature for a variety of stem cells (see, Introduction).

Altogether, these observations prompted us to study the expression of $p75^{NTR}$ and other neurotrophin receptors in ES cells, with the aim to understand the role played by such receptors and their ligands in pluripotency and self-renewal.

Using RT-PCR analysis we have found that transcripts for both TrkA and $p75^{NTR}$ are present in ES cells, whereas TrkB and TrkC are undetectable. Western blotting analyses of ES cell lysates have shown the presence of immunoreactive bands with molecular weights consistent with those of TrkA and $p75^{NTR}$, confirming the presence of the proteins. Immunofluorescence experiments have shown that both TrkA and $p75^{NTR}$ receptors are localized on ES cell surface.

It has been recently shown by Pyle *et al.* that human ES cells have a pattern of neurotrophin receptor expression that differs from what we have shown for murine ES cells, as they express TrkB and TrkC but not TrkA and $p75^{NTR}$ (Pyle et al., 2006). Such a difference is not surprising, as mouse and human ES cells show several differences in the gene expression pattern and in the factors that are required to sustain their growth. The cytokine, leukaemia inhibitory factor (LIF) modulates mouse ES cell growth through activation of STAT3. The presence of LIF in the culture medium allows mouse ES cells to proliferate and maintain pluripotency even in the absence of feeder cells (Nichols et al., 1990). On the contrary, LIF is not sufficient to promote the self-renewal of human ES cells (Thomson et al., 1998); moreover in human cells cultured under non-differentiating conditions, the LIF/STAT3 pathway appears to be inactive (Daheron et al., 2004; Humphrey et al., 2004).

As mouse ES cells express both TrkA and $p75^{NTR}$, we tested whether NGF, the ligand for both receptors, affects proliferation or self-renewal of ES cells. We have found that the number of colonies formed by ES cells cultured in clonal conditions in the presence of 100 ng/ml NGF is not significantly different from the number present in control cultures. However, the addition of NGF determines an average 1,6 fold increase in colony size. Based on these results it can be concluded that NGF affects ES cell proliferation, but not survival. It should be mentioned here that, in contrast with our observations, by a clonal survival assay Pyle *et al*. found that neurotrophins act as survival rather than proliferation factors for human ES cells (Pyle et al., 2006).

The experiments reported above do not provide information as to whether the increase in colony size was due to an increased number of undifferentiated cells per colony, or to an increased cell size, consequent to a possible NGF-induced differentiation.

In order to clarify this point we performed experiments to evaluate the expression of pluripotency markers in the colonies cultured with or without NGF. Immunofluorescence analysis for Oct4 and Nanog and alkaline phosphatase (AP) staining showed that there was no decrease in the expression of the markers in NGF-exposed cells, suggesting that NGF was not inducing ES cell differentiation.

Data in the literature described an AP assay that can be used to quantify the number of AP-positive cells in a culture (Garcia-Castro et al., 1997); such assay has the dual advantage that it may at the same time provide information on cell number and on stemness. . After assessing that a linear relationship between AP activity and cell number was occurring in our system, we decided to exploit the expression of AP by undifferentiated ES cells to quantify the increase of cell number in the NGF-treated cultures. The results we obtained were consistent with the observed increase of colony size, as we registered a 1,6 fold increase in AP activity of ES cells cultured with NGF.

The other neurotrophins, NT-3, NT-4, and BDNF, did not have any effect on the level of AP activity as to be expected from the RT-PCR results showing that their receptors, TrkB and TrkC, are not expressed in ES cells.

Overall, our results clearly demonstrate that NGF stimulates proliferation of self-renewing ES cells, with no loss of stem cell markers.

We next investigated if the effect of NGF on ES cell proliferation was requiring the combined activation of TrkA and $p75^{NTR}$, or only one of the two receptors, as it occurs in other cell systems. To this purpose we tested AP activity of ES cell cultures in conditions in which one of the two receptors was blocked. When we added to the cell culture a blocking antibody for $p75^{NTR}$ or a specific TrkA inhibitor (GW441756), no response to NGF was observed. These results suggest that activation of both receptors is required for NGF to stimulate ES cell proliferation.

In order to preserve their pluripotency, mouse ES cells are typically grown on a feeder layer of mitotically inactivated MEFs or in the presence of medium conditioned by MEFs. As it is known that MEFs produce and release LIF and other factors, fundamental for ES cell growth, we hypothesized that these cells might as well produce NGF, and the factor might be endogenously present in standard ES cell cultures. We measured whether pure MEF and ES/MEF cultures produced NGF, and in both instances we did find that low amounts of NGF (approx 70 pg/ml and 130 pg/ml, respectively) are released in the medium. Such values are

much lower (approx 1000 times) than the NGF concentrations we used, and are normally used to obtain reproducible effects by NGF-responsive cultured cells. It should be noticed that a very similar situation occurs with LIF, which is produced by MEFs, but at low concentration. For this reason, in order to prevent ES cell differentiation, exogenous LIF has to be added to the culture medium (Wobus et al., 1984). Based on these considerations, it can be hypothesized that, in vivo, in the stem cell niche, factors like LIF and NGF might be locally present at appropriately high concentrations in order to elicit a cell response in terms of growth and proliferation with self renewal.

MEFs are not only responsible for secreting growth factors or cytokines required to sustain ES cell renewal, they also secrete extracellular matrix components which provides ES cells with a three-dimensional support. Man-made ECM-like substrates, by their chemical and physical properties, might be able to free ES cells from MEF support, by playing a niche-like role favouring self-renewal of the cells. It has recently been shown, in a MEF-free culture system, that a three-dimensional nanofibillar surface greatly enhances proliferation and self-renewal of mouse ES cells, correlated with activation of the PI3K pathway, and sustained Nanog expression (Nur et al., 2006).

In the light of this, we have studied if 3D electrospun PCL mats might be of advantage for culturing ES cells. PCL has been shown to be a promising material for regenerative medicine, and its possible use to support stem cell growth might open new interesting avenues. To detect possible toxic effects of the PCL scaffold, we first studied growth rate and maintenance of stem markers by ES cells growing in non-differentiating conditions (i.e., in LIF-containing medium, on MEF-seeded PCL scaffolds). We then investigated if the pure scaffold by itself (i.e. not seeded with MEFs), would be sufficient to sustain self-renewal: a positive finding might be exploited to expand ES cell populations on a 3D substrate without the need for a feeder layer, possibly with addition of a defined cocktail of growth factors. In this direction, the ultimate goal would be the fabrication of a 3D scaffold serving both as a cell support and a growth factor delivery system (Boontheekul and Mooney, 2003).

When we cultured the ES cells under non-differentiating conditions, adhesion to the scaffolds was found to be about 45 % that to culture plates. Such lower adhesion was not caused by a toxic effect of the scaffold, since non-adhering cells, collected from scaffold or plate supernatants, did not show significant differences in cell viability. As it is known from the

literature, a crucial step when testing synthetic scaffolds is cell adhesion, that can be improved by immobilizing adhesive proteins or peptides on the material (Hersel et al., 2003).
Despite the lower adhesion rate, the ES cells that had attached to the mats proliferated, formed colonies and expressed pluripotency markers at levels comparable with ES cells grown on culture plates. It should be underlined that, since ES cells are highly susceptible to a suboptimal culture environment, to have succeeded in expanding them on scaffolds at the same rate as on standard culture plates is an important feat, that might be of advantage for regenerative medicine studies in which cultures in a three-dimensional substrate may be required.
We have finally evaluated if three-dimensional PCL scaffolds might replace the MEF feeder-layer. After normalizing for differences in initial cell adhesion, in the absence of MEF and LIF the cells showed the same proliferation rate on PCL as on MEF-free culture plates, and the morphological analysis of ES cells grown on the different supports revealed interesting differences: the colonies growing on the scaffolds appeared to retain in a higher percentage a spherical shape, typical of undifferentiated ES cells. Furthermore, we found that, in feeder-free cultures, with the addition of LIF, the expression of AP and pAKT was clearly higher in cells cultured on PCL than on culture plates. Moreover, pAKT was increased on PCL scaffolds also in the absence of LIF. Oct4 and Nanog expression, however, was only slightly higher in scaffold-growing cells, possibly due to a greater stability of these two proteins.
These data provide evidence that topographic, 3D cues play a role in maintaining stemness in proliferating ES cells and also suggests that electrospun PCL scaffolds may become an important tool for stem cell use in regenerative medicine. Interestingly, in a recent work, Ouyang *et al*. suggested the use of a feederlayer-free 3D fibrous matrix, with conditioned media, for long-term cultures of ES cells in an undifferentiated state (Ouyang et al., 2007). Mimicking stem cell niches is an important issue for tissue engineering applications, not only to favour stem cell expansion but also to direct stem cell differentiation towards specific lineages.
Since electrospun PCL has been used to fabricate a bioresorbable heart valve (Del Gaudio et al., 2008), as a further development of such study we have evaluated the capability of electrospun PCL scaffolds to support endothelial differentiation from ES cells in vitro.
Our results indicate that the scaffold allows embryoid bodies to differentiate and express Pecam-1, an endothelial lineage marker, indicating that the presence of a PCL scaffold does

not interfere with endothelial differentiation. This preliminary observation supports the possible use of this scaffold in tissue engineering.

In conclusion, in this thesis various issues concerning ES cell proliferation and self-renewal have been addressed, and the importance of two different aspects of culture conditions have been demonstrated. NGF addition to the culture medium stimulates ES cells proliferation with self-renewal and, similarly, a 3D PCL scaffold, in the absence of MEFs, helps preventing differentiation in ES cells. These observations, while describing only a part of the interplay of signalling networks that either promote self-renewal or induce differentiation in ES cells, may provide useful information for a better comprehension of the multiple components of the stem cell niche.

BIBLIOGRAPHY

Aloe, L., Bracci-Laudiero, L., Bonini, S., and Manni, L. (1997). The expanding role of nerve growth factor: from neurotrophic activity to immunologic diseases. Allergy *52*, 883-894.

Aloe, L., and Levi-Montalcini, R. (1977). Mast cells increase in tissues of neonatal rats injected with the nerve growth factor. Brain Res *133*, 358-366.

Amit, M., Carpenter, M.K., Inokuma, M.S., Chiu, C.P., Harris, C.P., Waknitz, M.A., Itskovitz-Eldor, J., and Thomson, J.A. (2000). Clonally derived human embryonic stem cell lines maintain pluripotency and proliferative potential for prolonged periods of culture. Dev Biol *227*, 271-278.

Amit, M., Margulets, V., Segev, H., Shariki, K., Laevsky, I., Coleman, R., and Itskovitz-Eldor, J. (2003). Human feeder layers for human embryonic stem cells. Biol Reprod *68*, 2150-2156.

Amit, M., Shariki, C., Margulets, V., and Itskovitz-Eldor, J. (2004). Feeder layer- and serum-free culture of human embryonic stem cells. Biol Reprod *70*, 837-845.

Auffray, I., Chevalier, S., Froger, J., Izac, B., Vainchenker, W., Gascan, H., and Coulombel, L. (1996). Nerve growth factor is involved in the supportive effect by bone marrow--derived stromal cells of the factor-dependent human cell line UT-7. Blood *88*, 1608-1618.

Avilion, A.A., Nicolis, S.K., Pevny, L.H., Perez, L., Vivian, N., and Lovell-Badge, R. (2003). Multipotent cell lineages in early mouse development depend on SOX2 function. Genes Dev *17*, 126-140.

Boontheekul, T., and Mooney, D.J. (2003). Protein-based signaling systems in tissue engineering. Curr Opin Biotechnol *14*, 559-565.

Buhring, H.J., Battula, V.L., Treml, S., Schewe, B., Kanz, L., and Vogel, W. (2007). Novel markers for the prospective isolation of human MSC. Ann N Y Acad Sci *1106*, 262-271.

Campagnolo, L., Russo, M.A., Puglianiello, A., Favale, A., and Siracusa, G. (2001). Mesenchymal cell precursors of peritubular smooth muscle cells of the mouse testis can be identified by the presence of the p75 neurotrophin receptor. Biol Reprod *64*, 464-472.

Causa, F., Netti, P.A., and Ambrosio, L. (2007). A multi-functional scaffold for tissue regeneration: the need to engineer a tissue analogue. Biomaterials *28*, 5093-5099.

Chambers, I., Colby, D., Robertson, M., Nichols, J., Lee, S., Tweedie, S., and Smith, A. (2003). Functional expression cloning of Nanog, a pluripotency sustaining factor in embryonic stem cells. Cell *113*, 643-655.

Chao, M.V. (1992). Neurotrophin receptors: a window into neuronal differentiation. Neuron *9*, 583-593.

Chao, M.V. (2003). Neurotrophins and their receptors: a convergence point for many signalling pathways. Nat Rev Neurosci *4*, 299-309.

Chew, J.L., Loh, Y.H., Zhang, W., Chen, X., Tam, W.L., Yeap, L.S., Li, P., Ang, Y.S., Lim, B., Robson, P.*, et al.* (2005). Reciprocal transcriptional regulation of Pou5f1 and Sox2 via the Oct4/Sox2 complex in embryonic stem cells. Mol Cell Biol *25*, 6031-6046.

Ciapetti, G., Ambrosio, L., Savarino, L., Granchi, D., Cenni, E., Baldini, N., Pagani, S., Guizzardi, S., Causa, F., and Giunti, A. (2003). Osteoblast growth and function in porous poly epsilon -caprolactone matrices for bone repair: a preliminary study. Biomaterials *24*, 3815-3824.

Ciardelli, G., Chiono, V., Vozzi, G., Pracella, M., Ahluwalia, A., Barbani, N., Cristallini, C., and Giusti, P. (2005). Blends of poly-(epsilon-caprolactone) and polysaccharides in tissue engineering applications. Biomacromolecules *6*, 1961-1976.

Covas, D.T., Panepucci, R.A., Fontes, A.M., Silva, W.A., Jr., Orellana, M.D., Freitas, M.C., Neder, L., Santos, A.R., Peres, L.C., Jamur, M.C.*, et al.* (2008). Multipotent mesenchymal stromal cells obtained from diverse human tissues share functional properties and gene-expression profile with CD146+ perivascular cells and fibroblasts. Exp Hematol *36*, 642-654.

Cukierman, E., Pankov, R., Stevens, D.R., and Yamada, K.M. (2001). Taking cell-matrix adhesions to the third dimension. Science *294*, 1708-1712.

Cukierman, E., Pankov, R., and Yamada, K.M. (2002). Cell interactions with three-dimensional matrices. Curr Opin Cell Biol *14*, 633-639.

Daheron, L., Opitz, S.L., Zaehres, H., Lensch, M.W., Andrews, P.W., Itskovitz-Eldor, J., and Daley, G.Q. (2004). LIF/STAT3 signaling fails to maintain self-renewal of human embryonic stem cells. Stem Cells *22*, 770-778.

Dechant, G., and Barde, Y.A. (2002). The neurotrophin receptor p75(NTR): novel functions and implications for diseases of the nervous system. Nat Neurosci *5*, 1131-1136.

Del Gaudio, C., Grigioni, M., Bianco, A., and De Angelis, G. (2008). Electrospun bioresorbable heart valve scaffold for tissue engineering. Int J Artif Organs *31*, 68-75.

Dellatore, S.M., Garcia, A.S., and Miller, W.M. (2008). Mimicking stem cell niches to increase stem cell expansion. Curr Opin Biotechnol *19*, 534-540.

Di Marco, E., Mathor, M., Bondanza, S., Cutuli, N., Marchisio, P.C., Cancedda, R., and De Luca, M. (1993). Nerve growth factor binds to normal human keratinocytes through high and low affinity receptors and stimulates their growth by a novel autocrine loop. J Biol Chem *268*, 22838-22846.

Draper, J.S., Smith, K., Gokhale, P., Moore, H.D., Maltby, E., Johnson, J., Meisner, L., Zwaka, T.P., Thomson, J.A., and Andrews, P.W. (2004). Recurrent gain of chromosomes 17q and 12 in cultured human embryonic stem cells. Nat Biotechnol *22*, 53-54.

Ehrhard, P.B., Ganter, U., Stalder, A., Bauer, J., and Otten, U. (1993). Expression of functional trk protooncogene in human monocytes. Proc Natl Acad Sci U S A *90*, 5423-5427.

Fecek, C., Yao, D., Kacorri, A., Vasquez, A., Iqbal, S., Sheikh, H., Svinarich, D.M., Perez-Cruet, M., and Chaudhry, G.R. (2008). Chondrogenic derivatives of embryonic stem cells seeded into 3D polycaprolactone scaffolds generated cartilage tissue in vivo. Tissue Eng Part A *14*, 1403-1413.

Festag, M., Sehner, C., Steinberg, P., and Viertel, B. (2007). An in vitro embryotoxicity assay based on the disturbance of the differentiation of murine embryonic stem cells into endothelial cells. I: Establishment of the differentiation protocol. Toxicol In Vitro *21*, 1619-1630.

Garcia-Castro, M.I., Anderson, R., Heasman, J., and Wylie, C. (1997). Interactions between germ cells and extracellular matrix glycoproteins during migration and gonad assembly in the mouse embryo. J Cell Biol *138*, 471-480.

Gerecht-Nir, S., Cohen, S., Ziskind, A., and Itskovitz-Eldor, J. (2004). Three-dimensional porous alginate scaffolds provide a conducive environment for generation of well-vascularized embryoid bodies from human embryonic stem cells. Biotechnol Bioeng *88*, 313-320.

Grinnell, F., Ho, C.H., Tamariz, E., Lee, D.J., and Skuta, G. (2003). Dendritic fibroblasts in three-dimensional collagen matrices. Mol Biol Cell *14*, 384-395.

He, X.L., and Garcia, K.C. (2004). Structure of nerve growth factor complexed with the shared neurotrophin receptor p75. Science *304*, 870-875.

Hempstead, B.L. (2002). The many faces of p75NTR. Curr Opin Neurobiol *12*, 260-267.

Hersel, U., Dahmen, C., and Kessler, H. (2003). RGD modified polymers: biomaterials for stimulated cell adhesion and beyond. Biomaterials *24*, 4385-4415.

Hoerstrup, S.P., Sodian, R., Daebritz, S., Wang, J., Bacha, E.A., Martin, D.P., Moran, A.M., Guleserian, K.J., Sperling, J.S., Kaushal, S.*, et al.* (2000). Functional living trileaflet heart valves grown in vitro. Circulation *102*, III44-49.

Huber, L.J., Hempstead, B., and Donovan, M.J. (1996). Neurotrophin and neurotrophin receptors in human fetal kidney. Dev Biol *179*, 369-381.

Humphrey, R.K., Beattie, G.M., Lopez, A.D., Bucay, N., King, C.C., Firpo, M.T., Rose-John, S., and Hayek, A. (2004). Maintenance of pluripotency in human embryonic stem cells is STAT3 independent. Stem Cells *22*, 522-530.

Inzunza, J., Sahlen, S., Holmberg, K., Stromberg, A.M., Teerijoki, H., Blennow, E., Hovatta, O., and Malmgren, H. (2004). Comparative genomic hybridization and karyotyping of human embryonic stem cells reveals the occurrence of an isodicentric X chromosome after long-term cultivation. Mol Hum Reprod *10*, 461-466.

Ivanova, N., Dobrin, R., Lu, R., Kotenko, I., Levorse, J., DeCoste, C., Schafer, X., Lun, Y., and Lemischka, I.R. (2006). Dissecting self-renewal in stem cells with RNA interference. Nature *442*, 533-538.

Kang, X., Xie, Y., Powell, H.M., James Lee, L., Belury, M.A., Lannutti, J.J., and Kniss, D.A. (2007). Adipogenesis of murine embryonic stem cells in a three-dimensional culture system using electrospun polymer scaffolds. Biomaterials *28*, 450-458.

Labouyrie, E., Parrens, M., de Mascarel, A., Bloch, B., and Merlio, J.P. (1997). Distribution of NGF receptors in normal and pathologic human lymphoid tissues. J Neuroimmunol *77*, 161-173.

Lee, J.B., Lee, J.E., Park, J.H., Kim, S.J., Kim, M.K., Roh, S.I., and Yoon, H.S. (2005). Establishment and maintenance of human embryonic stem cell lines on human feeder cells derived from uterine endometrium under serum-free condition. Biol Reprod *72*, 42-49.

Lee, R., Kermani, P., Teng, K.K., and Hempstead, B.L. (2001). Regulation of cell survival by secreted proneurotrophins. Science *294*, 1945-1948.

Levenberg, S., Huang, N.F., Lavik, E., Rogers, A.B., Itskovitz-Eldor, J., and Langer, R. (2003). Differentiation of human embryonic stem cells on three-dimensional polymer scaffolds. Proc Natl Acad Sci U S A *100*, 12741-12746.

Li, W.J., Laurencin, C.T., Caterson, E.J., Tuan, R.S., and Ko, F.K. (2002). Electrospun nanofibrous structure: a novel scaffold for tissue engineering. J Biomed Mater Res *60*, 613-621.

Liao, S., Chan, C.K., and Ramakrishna, S. (2008). Stem cells and biomimetic materials strategies for tissue engineering. Materials Science and Engineering: C *28*, 1189-1202.

Liu, H., and Roy, K. (2005). Biomimetic three-dimensional cultures significantly increase hematopoietic differentiation efficacy of embryonic stem cells. Tissue Eng *11*, 319-330.

Loh, Y.H., Wu, Q., Chew, J.L., Vega, V.B., Zhang, W., Chen, X., Bourque, G., George, J., Leong, B., Liu, J.*, et al.* (2006). The Oct4 and Nanog transcription network regulates pluripotency in mouse embryonic stem cells. Nat Genet *38*, 431-440.

Lu, J., Hou, R., Booth, C.J., Yang, S.H., and Snyder, M. (2006). Defined culture conditions of human embryonic stem cells. Proc Natl Acad Sci U S A *103*, 5688-5693.

Ludwig, T.E., Levenstein, M.E., Jones, J.M., Berggren, W.T., Mitchen, E.R., Frane, J.L., Crandall, L.J., Daigh, C.A., Conard, K.R., Piekarczyk, M.S.*, et al.* (2006). Derivation of human embryonic stem cells in defined conditions. Nat Biotechnol *24*, 185-187.

Luukko, K., Moshnyakov, M., Sainio, K., Saarma, M., Sariola, H., and Thesleff, I. (1996). Expression of neurotrophin receptors during rat tooth development is developmentally regulated, independent of innervation, and suggests functions in the regulation of morphogenesis and innervation. Dev Dyn *206*, 87-99.

Matsubara, T., Tsutsumi, S., Pan, H., Hiraoka, H., Oda, R., Nishimura, M., Kawaguchi, H., Nakamura, K., and Kato, Y. (2004). A new technique to expand human mesenchymal stem cells using basement membrane extracellular matrix. Biochem Biophys Res Commun *313*, 503-508.

Mitsui, K., Tokuzawa, Y., Itoh, H., Segawa, K., Murakami, M., Takahashi, K., Maruyama, M., Maeda, M., and Yamanaka, S. (2003). The homeoprotein Nanog is required for maintenance of pluripotency in mouse epiblast and ES cells. Cell *113*, 631-642.

Mosmann, T. (1983). Rapid colorimetric assay for cellular growth and survival: application to proliferation and cytotoxicity assays. J Immunol Methods *65*, 55-63.

Mousavi, K., and Jasmin, B.J. (2006). BDNF is expressed in skeletal muscle satellite cells and inhibits myogenic differentiation. J Neurosci *26*, 5739-5749.

Murugan, R., and Ramakrishna, S. (2006). Nano-featured scaffolds for tissue engineering: a review of spinning methodologies. Tissue Eng *12*, 435-447.

Nakamura, T., Endo, K., and Kinoshita, S. (2007). Identification of human oral keratinocyte stem/progenitor cells by neurotrophin receptor p75 and the role of neurotrophin/p75 signaling. Stem Cells *25*, 628-638.

Nichols, J., Evans, E.P., and Smith, A.G. (1990). Establishment of germ-line-competent embryonic stem (ES) cells using differentiation inhibiting activity. Development *110*, 1341-1348.

Nichols, J., Zevnik, B., Anastassiadis, K., Niwa, H., Klewe-Nebenius, D., Chambers, I., Scholer, H., and Smith, A. (1998). Formation of pluripotent stem cells in the mammalian embryo depends on the POU transcription factor Oct4. Cell *95*, 379-391.

Niwa, H., Miyazaki, J., and Smith, A.G. (2000). Quantitative expression of Oct-3/4 defines differentiation, dedifferentiation or self-renewal of ES cells. Nat Genet *24*, 372-376.

Nur, E.K.A., Ahmed, I., Kamal, J., Schindler, M., and Meiners, S. (2006). Three-dimensional nanofibrillar surfaces promote self-renewal in mouse embryonic stem cells. Stem Cells *24*, 426-433.

Nykjaer, A., Lee, R., Teng, K.K., Jansen, P., Madsen, P., Nielsen, M.S., Jacobsen, C., Kliemannel, M., Schwarz, E., Willnow, T.E*., et al.* (2004). Sortilin is essential for proNGF-induced neuronal cell death. Nature *427*, 843-848.

Odorico, J.S., Kaufman, D.S., and Thomson, J.A. (2001). Multilineage differentiation from human embryonic stem cell lines. Stem Cells *19*, 193-204.

Okumura, T., Shimada, Y., Imamura, M., and Yasumoto, S. (2003). Neurotrophin receptor p75(NTR) characterizes human esophageal keratinocyte stem cells in vitro. Oncogene *22*, 4017-4026.

Ouyang, A., Ng, R., and Yang, S.T. (2007). Long-term culturing of undifferentiated embryonic stem cells in conditioned media and three-dimensional fibrous matrices without extracellular matrix coating. Stem Cells *25*, 447-454.

Pera, M.F., Andrade, J., Houssami, S., Reubinoff, B., Trounson, A., Stanley, E.G., Ward-van Oostwaard, D., and Mummery, C. (2004). Regulation of human embryonic stem cell differentiation by BMP-2 and its antagonist noggin. J Cell Sci *117*, 1269-1280.

Pesce, M., and De Felici, M. (1995). Purification of mouse primordial germ cells by MiniMACS magnetic separation system. Dev Biol *170*, 722-725.

Philp, D., Chen, S.S., Fitzgerald, W., Orenstein, J., Margolis, L., and Kleinman, H.K. (2005). Complex extracellular matrices promote tissue-specific stem cell differentiation. Stem Cells *23*, 288-296.

Pyle, A.D., Lock, L.F., and Donovan, P.J. (2006). Neurotrophins mediate human embryonic stem cell survival. Nat Biotechnol *24*, 344-350.

Qi, H., Li, D.Q., Shine, H.D., Chen, Z., Yoon, K.C., Jones, D.B., and Pflugfelder, S.C. (2008). Nerve growth factor and its receptor TrkA serve as potential markers for human corneal epithelial progenitor cells. Exp Eye Res *86*, 34-40.

Qi, X., Li, T.G., Hao, J., Hu, J., Wang, J., Simmons, H., Miura, S., Mishina, Y., and Zhao, G.Q. (2004). BMP4 supports self-renewal of embryonic stem cells by inhibiting mitogen-activated protein kinase pathways. Proc Natl Acad Sci U S A *101*, 6027-6032.

Ratajczak, M.Z., Zuba-Surma, E.K., Wysoczynski, M., Wan, W., Ratajczak, J., Wojakowski, W., and Kucia, M. (2008). Hunt for pluripotent stem cell -- regenerative medicine search for almighty cell. J Autoimmun *30*, 151-162.

Reubinoff, B.E., Pera, M.F., Fong, C.Y., Trounson, A., and Bongso, A. (2000). Embryonic stem cell lines from human blastocysts: somatic differentiation in vitro. Nat Biotechnol *18*, 399-404.

Richards, M., Fong, C.Y., Chan, W.K., Wong, P.C., and Bongso, A. (2002). Human feeders support prolonged undifferentiated growth of human inner cell masses and embryonic stem cells. Nat Biotechnol *20*, 933-936.

Richards, M., Tan, S., Fong, C.Y., Biswas, A., Chan, W.K., and Bongso, A. (2003). Comparative evaluation of various human feeders for prolonged undifferentiated growth of human embryonic stem cells. Stem Cells *21*, 546-556.

Rodda, D.J., Chew, J.L., Lim, L.H., Loh, Y.H., Wang, B., Ng, H.H., and Robson, P. (2005). Transcriptional regulation of nanog by OCT4 and SOX2. J Biol Chem *280*, 24731-24737.

Russo, M.A., Giustizieri, M.L., Favale, A., Fantini, M.C., Campagnolo, L., Konda, D., Germano, F., Farini, D., Manna, C., and Siracusa, G. (1999). Spatiotemporal patterns of expression of neurotrophins and neurotrophin receptors in mice suggest functional roles in testicular and epididymal morphogenesis. Biol Reprod *61*, 1123-1132.

Russo, M.A., Odorisio, T., Fradeani, A., Rienzi, L., De Felici, M., Cattaneo, A., and Siracusa, G. (1994). Low-affinity nerve growth factor receptor is expressed during testicular morphogenesis and in germ cells at specific stages of spermatogenesis. Mol Reprod Dev *37*, 157-166.

Sato, N., Meijer, L., Skaltsounis, L., Greengard, P., and Brivanlou, A.H. (2004). Maintenance of pluripotency in human and mouse embryonic stem cells through activation of Wnt signaling by a pharmacological GSK-3-specific inhibitor. Nat Med *10*, 55-63.

Sofroniew, M.V., Howe, C.L., and Mobley, W.C. (2001). Nerve growth factor signaling, neuroprotection, and neural repair. Annu Rev Neurosci *24*, 1217-1281.

Sung, H.J., Meredith, C., Johnson, C., and Galis, Z.S. (2004). The effect of scaffold degradation rate on three-dimensional cell growth and angiogenesis. Biomaterials *25*, 5735-5742.

Susaki, Y., Shimizu, S., Katakura, K., Watanabe, N., Kawamoto, K., Matsumoto, M., Tsudzuki, M., Furusaka, T., Kitamura, Y., and Matsuda, H. (1996). Functional properties of murine macrophages promoted by nerve growth factor. Blood *88*, 4630-4637.

Suzuki, K., Tanaka, M., Watanabe, N., Saito, S., Nonaka, H., and Miyajima, A. (2008). p75 Neurotrophin receptor is a marker for precursors of stellate cells and portal fibroblasts in mouse fetal liver. Gastroenterology *135*, 270-281 e273.

Swieszkowski, W., Tuan, B.H., Kurzydlowski, K.J., and Hutmacher, D.W. (2007). Repair and regeneration of osteochondral defects in the articular joints. Biomol Eng *24*, 489-495.

Thomson, J.A., Itskovitz-Eldor, J., Shapiro, S.S., Waknitz, M.A., Swiergiel, J.J., Marshall, V.S., and Jones, J.M. (1998). Embryonic stem cell lines derived from human blastocysts. Science *282*, 1145-1147.

Torcia, M., Bracci-Laudiero, L., Lucibello, M., Nencioni, L., Labardi, D., Rubartelli, A., Cozzolino, F., Aloe, L., and Garaci, E. (1996). Nerve growth factor is an autocrine survival factor for memory B lymphocytes. Cell *85*, 345-356.

Vasita, R., and Katti, D.S. (2006). Nanofibers and their applications in tissue engineering. Int J Nanomedicine *1*, 15-30.

Vats, A., Bielby, R.C., Tolley, N.S., Nerem, R., and Polak, J.M. (2005). Stem cells. lancet *366*, 592-602.

von Bartheld, C.S., Heuer, J.G., and Bothwell, M. (1991). Expression of nerve growth factor (NGF) receptors in the brain and retina of chick embryos: comparison with cholinergic development. J Comp Neurol *310*, 103-129.

Wheeler, E.F., Gong, H., Grimes, R., Benoit, D., and Vazquez, L. (1998). p75NTR and Trk receptors are expressed in reciprocal patterns in a wide variety of non-neural tissues during rat embryonic development, indicating independent receptor functions. J Comp Neurol *391*, 407-428.

Wobus, A.M., Holzhausen, H., Jakel, P., and Schoneich, J. (1984). Characterization of a pluripotent stem cell line derived from a mouse embryo. Exp Cell Res *152*, 212-219.

Woodward, S.C., Brewer, P.S., Moatamed, F., Schindler, A., and Pitt, C.G. (1985). The intracellular degradation of poly(epsilon-caprolactone). J Biomed Mater Res *19*, 437-444.

Wozniak, M.A., Desai, R., Solski, P.A., Der, C.J., and Keely, P.J. (2003). ROCK-generated contractility regulates breast epithelial cell differentiation in response to the physical properties of a three-dimensional collagen matrix. J Cell Biol *163*, 583-595.

Xu, C., Inokuma, M.S., Denham, J., Golds, K., Kundu, P., Gold, J.D., and Carpenter, M.K. (2001). Feeder-free growth of undifferentiated human embryonic stem cells. Nat Biotechnol *19*, 971-974.

Xu, R.H., Chen, X., Li, D.S., Li, R., Addicks, G.C., Glennon, C., Zwaka, T.P., and Thomson, J.A. (2002). BMP4 initiates human embryonic stem cell differentiation to trophoblast. Nat Biotechnol *20*, 1261-1264.

Yamamoto, N., Akamatsu, H., Hasegawa, S., Yamada, T., Nakata, S., Ohkuma, M., Miyachi, E., Marunouchi, T., and Matsunaga, K. (2007). Isolation of multipotent stem cells from mouse adipose tissue. J Dermatol Sci *48*, 43-52.

Ying, Q.L., Nichols, J., Chambers, I., and Smith, A. (2003). BMP induction of Id proteins suppresses differentiation and sustains embryonic stem cell self-renewal in collaboration with STAT3. Cell *115*, 281-292.

Zhang, Y.Z., Venugopal, J., Huang, Z.M., Lim, C.T., and Ramakrishna, S. (2006). Crosslinking of the electrospun gelatin nanofibers. Polymer *47*.

APPENDIX

The following original articles, although not directly pertinent to the main project I described, are included in the thesis as part of the work I have done during my PhD studies:

Campagnolo L., **Moscatelli I**., Pellegrini M., Siracusa G. and Stuhlmann H. Expression of EGFL7 in primordial germ cells and in adult ovaries and testes. *Gene Expression Patterns*, 8 (2008) 389-396.

Bianco A., Di Federico E.*, **Moscatelli I**.*, Camaioni A., Armentano I., Campagnolo L., Dottori M., Kenny J.M., Siracusa G. and Gusmano G. (2009). Electrospun Poly(ε-caprolactone)/Ca-deficient Hydroxyapatite Nanohybrids: Microstructure, Mechanical Properties and Cell Response by Murine Embryonic Stem Cells. *Materials, Science and Engineering C,* submitted in revised form.
*These authors contributed equally to this work

Gene Expression Patterns 8 (2008) 389–396

Contents lists available at ScienceDirect

Gene Expression Patterns

journal homepage: www.elsevier.com/locate/gep

Expression of EGFL7 in primordial germ cells and in adult ovaries and testes

Luisa Campagnolo [a,*], Ilana Moscatelli [a], Manuela Pellegrini [a], Gregorio Siracusa [a], Heidi Stuhlmann [b,1]

[a] Department of Public Health and Cell Biology, University of Rome "Tor Vergata", Via Montpellier 1, 00133 Rome, Italy
[b] Department of Cell Biology, The Scripps Research Institute, La Jolla, CA 92037, USA

ARTICLE INFO

Article history:
Received 9 June 2007
Received in revised form 29 April 2008
Accepted 1 May 2008
Available online 10 May 2008

Keywords:
Egf17 gene expression
Mouse embryonic development
Primordial germ cells
Spermatogenesis

ABSTRACT

We have previously reported the isolation and characterization of a novel endothelial-restricted gene, *Egfl7*, that encodes a secreted protein of about 30-kDa. We and others demonstrated that *Egfl7* is highly expressed by endothelial cells during embryonic development and becomes down-regulated in the adult vasculature. In the present paper, we show that during mouse embryonic development, *Egfl7* is also expressed by primordial germ cells (PGC). Expression is down-regulated when PGCs differentiate into pro-spermatogonia and oogonia, and by 15.5 dpc *Egfl7* can no longer be detected in the germ line of both sexes. Notably, *Egfl7* is again transiently up-regulated in germ cells of the adult testis. In contrast, expression in the ovary remains limited to the vascular endothelium. Our results provide the first evidence of a non-endothelial expression of EGFL7 and suggest distinctive roles for *Egfl7* in vascular development and germ cell differentiation.

1. Results and discussion

In a genetic screen for genes expressed in the cardiovascular system using a gene-trap approach in ES cells, we have identified a novel gene, EGF-like domain 7 (*Egfl7*) (Kuhnert and Stuhlmann, 2004; Fitch et al., 2004). The *Egfl7* gene spans 11.5-kb of chromosome 2 and encodes 278 amino acids secreted protein that is highly conserved in vertebrates. *Egfl7* was independently identified by two other laboratories (Parker et al., 2004; Soncin et al., 2003). The protein contains an N-terminal signal peptide required for secretion, a cysteine-rich EMI domain, and two centrally located EGF domains. A region with similarity to an extracellular domain that is conserved in ligands of Notch receptors (Delta-Serrate-LAG-2) and is required for ligand-receptor binding is located within the first EGF domain (Fitch et al., 2004). EGFL7 acts as a chemoattractant for endothelial cells and embryonic fibroblasts. EGFL7 alone has no effect on the migration of vascular smooth muscle cells (VSMC) (Soncin et al., 2003; Campagnolo et al., 2005), but blocks PDGF-induced VSMC migration (Soncin et al., 2003). In addition, a fraction of secreted EGFL7 binds efficiently to the extracellular matrix of endothelial cells (Schmidt et al., 2007; M. Fitch and H. Stuhlmann, unpublished).

We previously showed that embryonic expression of *Egfl7* is restricted to the vascular endothelium of the embryo proper and the yolk sac (Fitch et al., 2004). In the adult, expression is overall down-regulated in the quiescent vasculature, but remains detectable in highly vascularized adult organs, such as lung, heart, uterus, and ovary (Campagnolo et al., 2005). Moreover, *Egfl7* is transiently up-regulated during physiological angiogenesis in the pregnant uterus and upon vascular injury in the regenerating endothelium (Campagnolo et al., 2005). Together, these results show a correlation between *Egfl7* expression and an active, proliferative state of the endothelium. Studies in zebrafish embryos demonstrated that knock-down of *Egfl7* results in disruption of vascular tube formation, suggesting that *Egfl7* plays a crucial role during vascular development (Parker et al., 2004).

Here, we report that a second site of *Egfl7* expression is detected in a temporal window during embryogenesis in primordial germ cells, the precursors of the germ cells in both sexes. In addition, we demonstrate that in the adult, *Egfl7* expression is *de novo* up regulated in the male germ line, while in the ovaries its expression is restricted to endothelial cells. Importantly, analysis of the avascular cloche mutant indicated that *Egfl7* in zebrafish is not expressed outside the cardiovascular system (Parker et al., 2004). This suggests an important difference regarding a potential involvement of *Egfl7* in germ cell and gonad development between mammals and fish.

1.1. Egfl7 expression in pre-implantation embryos

In a previous study, we showed that *Egfl7* mRNA is already detectable at the blastocyst stage and in embryonic stem (ES) cells that are derived from the inner cell mass of the blastocyst. In early post-implantation embryos, its expression is localized to the extra-embryonic mesoderm and in the most anterior and posterior re-

* Corresponding author. Tel.: +39 06 72596154; fax: +39 06 72596172.
E-mail address: campagno@med.uniroma2.it (L. Campagnolo).
[1] Present address: Department of Cell and Developmental Biology, Weill Medical College of Cornell University, New York, NY 10021, USA.

1567-133X/$ - see front matter © 2008 Elsevier B.V. All rights reserved.
doi:10.1016/j.gep.2008.05.001

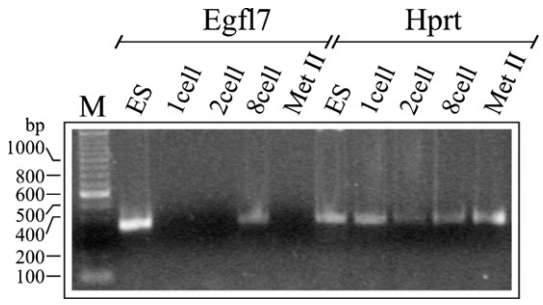

Fig. 1. RT-PCR analysis of *Egfl7* expression in pre-implantation mouse embryos. Using intron spanning primers for *Egfl7*, a band of 348 bp was amplified from RNA isolated from ES cells and 8-cell stage embryos, but not from 1- and 2-cell stage embryos, and ovulated oocytes. Hprt primers were used as an amplification control.

gions of the embryo proper (Fitch et al., 2004). To determine the developmental stage at which *Egfl7* is first expressed, RT-PCR analysis was performed on unfertilized oocytes and staged early pre-implantation embryos. Using primers that discriminate against genomic DNA, a 348-bp *Egfl7*-specific PCR product was amplified from 8-cell stage embryos, while no band was detected from 1-cell or 2-cell stage embryos or unfertilized ovulated oocytes (metaphase II oocytes) (Fig. 1). Undifferentiated embryonic stem cell (ES) mRNA was used as a positive control and yielded a strong RT-PCR band. By the 8-cell stage, mRNA of maternal origin is already degraded and synthesis of embryonic RNA has begun (Schultz 1993). We therefore conclude that the *Egfl7*-specific amplification product obtained from 8-cell morulas reflects the onset of *Egfl7* transcription during mouse embryonic development.

1.2. *Egfl7* expression in primordial germ cells

During post-implantation development, EGFL7 expression was found to be restricted to the developing vascular system and its progenitors in the yolk sac (Fitch et al., 2004; Soncin et al., 2003; Parker et al., 2004). RNA *in situ* hybridization studies also showed that in 7.5 dpc embryos, *Egfl7* mRNA can be detected in the extra-embryonic mesoderm close to the posterior end of the proximal epiblast (Fitch et al., 2004), at sites were primordial germ cells (PGCs) are located. This observation stimulated a thorough analysis of EGFL7 expression in PGCs using affinity-purified polyclonal anti-EGFL7 antibodies (Fitch et al., 2004; Campagnolo et al., 2005).

Between 8.5 and 10.5 dpc, PGCs are defined as migratory, since they move from the base of the allantois, migrate along the hindgut endoderm, and finally through the dorsal mesentery they reach the urogenital ridge. By 11 dpc, PGCs have entered the gonads and are defined as post-migratory cells. However, they are not yet organized in their definitive structures, cords, and follicles, thus rendering male and female gonads morphologically indistinguishable until 12.5 dpc. Double immunostaining using specific antibodies against EGFL7 and the germ cell marker SSEA1, respectively, shows that isolated PGCs from 8.5 dpc embryos (Fig. 2A, panels a and d), as well as 10.5 dpc migrating PGCs (Fig. 2A, panels b and e) do not express EGFL7 at significant levels. In contrast, PGCs immuno-magnetically sorted from 11.5 dpc gonads (De Felici, 1998) displayed co-immunolocalization of EGFL7 and SSEA1 (Fig. 2A, panels c and f). After each PGC purification, we routinely performed staining for alkaline phosphatase, another marker for PGCs, to assure purity of the PGC population (not shown). Expression of EGFL7 in 11.5 dpc PGCs was confirmed by Western blot analysis (Fig 2D). A 30–32-kDa EGFL7 immuno-reactive band was detected in PGC extracts, and its specificity was verified by comparing with total cell extracts from 293 cells transiently transfected with an EGFL7 expression vector (Fitch et al., 2004), the empty vector, and an unrelated control vector, respectively (Fig. 2D). However, the intensity of the band was low in 11.5 dpc PCGs when compared to cell extracts from EGFL7-transfected HEK293 cells. A band of low intensity was also detected in the somatic cell fraction of 11.5 dpc gonads, presumably due to the presence of endothelial cells lining the primitive vasculature of the gonads.

Next we investigated EGFL7 expression on cryostat sections of male and female gonads starting at 12.5 dpc, when sex specification becomes morphologically evident, and up to 15.5 dpc, when proliferation of germ cells has ceased, pro-spermatogonia have entered mitotic arrest, and oocytes are arrested at the prophase of the first meiotic division. Germ cells were identified by co-staining with anti-GCNA1 antibodies, which stains the nuclei of pro-spermatogonia and oocytes (Enders and May 1994). Starting around 13.5 dpc, we observed a progressive down-regulation of EGFL7 protein in the germ cells in both sexes (Fig. 2B and C), and by 15.5 dpc, EGFL7 expression was undetectable (Fig. 2B, panels c, g, and m, and C, panels c, g, and m).

We also investigated if expression of EGFL7 is altered in the gonads of White-spotting (W) mice. Mice homozygous for the W mutation contain very few PGCs that reach the gonads, and they die soon after birth as a result of severe anemia (Mintz and Russell, 1957). We performed double immuno-localization of GCNA1 and EGFL7 on sections of gonads from 13.5 dpc W−/− female embryos and wild type littermates. Clearly, EGFL7-positive germ cells were absent in W−/− gonads (compare Fig. 3D and F with C and E), while EGFL7 persisted in a vascular restricted expression that was comparable between mutant and control wild type mice (Fig 3B with A).

Together, these results show that EGFL7 expression in PGCs is regulated in a temporal manner and is only detectable in proliferating, post-migratory PGCs. Since EGFL7 interacts with extracellular matrix components (Schmidt et al., 2007; M. Fitch and H. Stuhlmann, unpublished), it is possible that EGFL7 is involved in homing of PGCs once they reach their new environment in the gonads, or in the organization of testis cords and follicles. The generation of mice with a conditional knock-out in PGCs will help to address this possibility. Recently knock-out mice for *Egfl7* have been generated (Schmidt et al., 2007), 50% of which die in utero be-

Fig. 2. Expression of EGFL7 in primordial germ cells (PGCs), gonocytes, and oogonia. (A) Immunofluorescence analysis of EGFL7 and SSEA1 expression in isolated PGCs at 8.5 dpc (a, d, and g) and 11.5 dpc (c, f, and i) and in sagittal sections of 10.5 dpc embryos (b, e, and h). Alkaline phosphatase staining was used to identify sections containing PGCs; adjacent sections were then incubated with antibodies. Arrows point to a migrating germ cell identified by the SSEA-1 antibody (e) that appears negative for EGFL7 (b); an EGFL7-positive and SSEA1-negative blood vessel is shown in (b) and (e), respectively (arrowheads). The inserts show migrating PGCs and the arrows identify the cell shown at a higher magnification in (b), (e), and (h). (a–c) EGFL7; (d–f) SSEA1; (g–i) Hoechst. Magnification 100×. (B) Immunofluorescence analysis of EGFL7 and GCNA1 on cryostat sections of embryonic mouse testis from 12.5, 13.5 (longitudinal sections), and 15.5 dpc (cross section). Arrows indicate location of testicular cords. (a–c) EGFL7; (e–g) GCNA1; (i, l, and m) merge of EGFL7 and GCNA1; (d and h) section of 15.5 dpc testis incubated with non-specific rabbit IgG and rat IgM, respectively. Magnification 40×. (C) Immunofluorescence analysis of EGFL7 and GCNA1 on cryostat sections of embryonic mouse ovaries from 12.5 dpc up to 15.5 dpc. (a–c) EGFL7; (e–g) GCNA1; (i, l, and m) merge of EGFL7 and GCNA1; (d and h) section of 15.5 dpc ovaries incubated with non-specific rabbit IgG and rat IgM, respectively. Magnification 40×. (D) Western blot analysis of EGFL7 expression in PGCs isolated from 11.5 dpc embryos. Somatic cells represent the flow through fraction of the immuno-magnetic purification and presumably contain endothelial cells. Cell extract from 293 cells transiently transfected with an Egfl7 expression vector, the empty vector and an unrelated vector (pEGFP-C1), were used as positive and negative controls, respectively. Anti-tubulin antibody was used as a loading control.

tween 13.5 and 15.5 dpc. Interestingly, although those mice that developed to term showed a delay in vascular development, fertility appeared not to be impaired; however, the development of PGCs and embryonic gonads was not examined in these mutants.

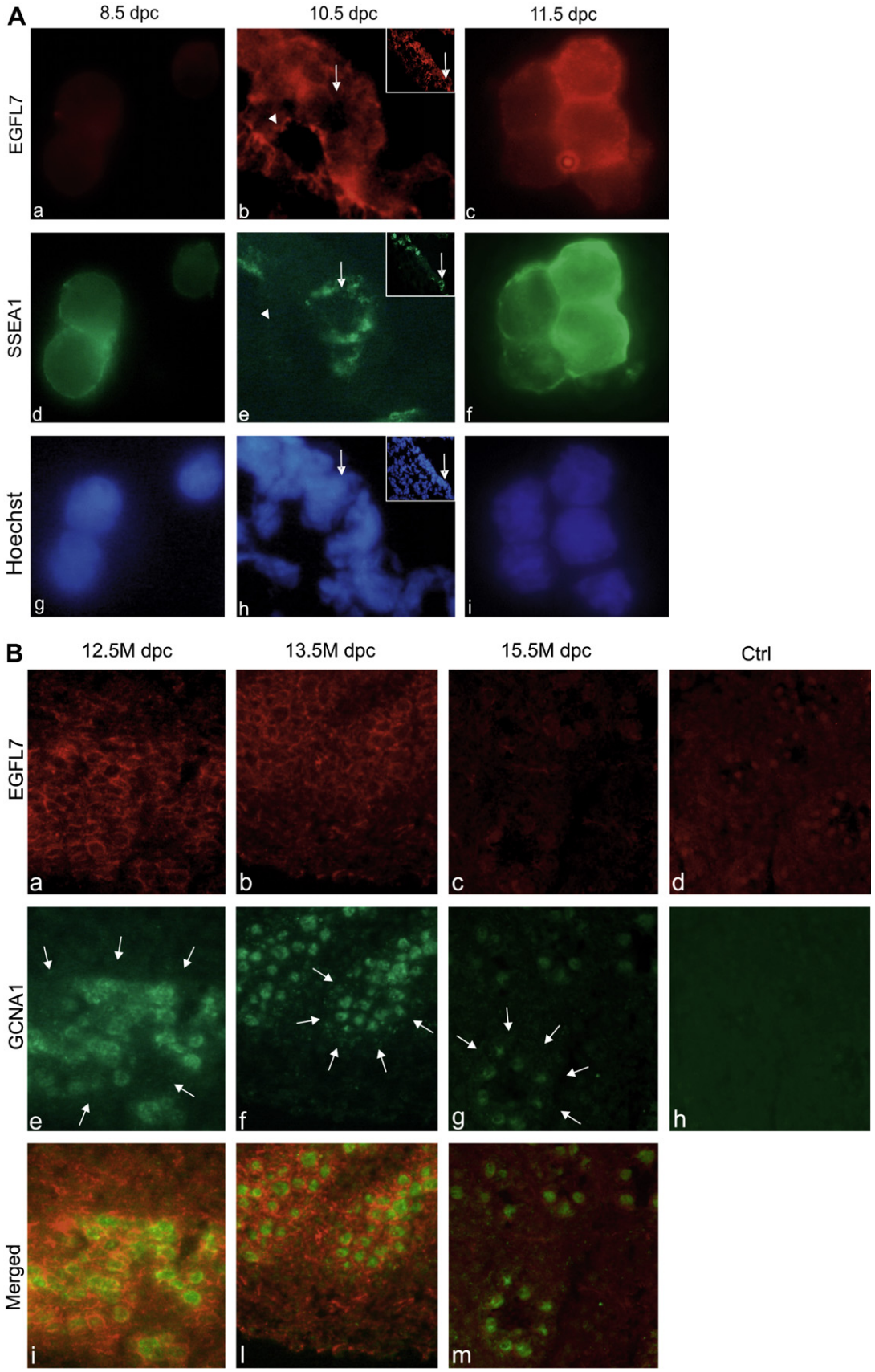

1.3. Egfl7 expression in adult male germ cells

The temporal expression of EGFL7 in PGCs prompted us to investigate if EGFL7 could be detected at later stages during germ cell differentiation and gonadal development. Using RNA *in situ* hybridization on postnatal testis, we found that *Egfl7* transcripts in the pre-pubertal testes (P19) were localized exclusively in the capillary network that surrounds seminiferous tubules (Fig. 4A and D, arrows). In contrast, in the testis of adult mice, *Egfl7* expression is also detected in germ cells. In the seminiferous tubules, germ cells are spatially organized in a pluristratified epithelium, and they are distributed, following their maturational stages, from the periphery to the center of the tubules. Spermatogonia, the stem cells of the testis, reside in the outer ring of the tubules adjacent to the basal membrane. Moving toward the lumen reside spermatocytes which enter meiosis to give rise to haploid spermatids that are located closer to the lumen of the tubules. During spermiogenesis, spermatids undergo profound morphological and functional modifications leading ultimately to the differentiation of spermatozoa, which become released into the lumen. *Egfl7* transcripts were specifically identified in a ring of cells surrounding the lumen of the seminiferous tubules (Fig. 4B and E, arrowhead), consistent with being expressed by post-meiotic spermatids, but not spermatocytes. Of interest, signal was detected only on some of the tubules, reflecting that they are at different stages of maturation, and consistent with *Egfl7* expression being restricted to specific stages of spermatid maturation (steps 1–8).

To confirm the expression of EGFL7 on post-meiotic cells, we performed immunostaining of testes sections using anti-EGFL7 antibodies. EGFL7 protein was detected in capillaries of the interstitial compartment (not shown), and in a subpopulation of cells within the tubules (Fig. 5A and B, arrows). This population can be identified as post-meiotic germ cells by the smaller size of their nuclei and the presence of a single nucleolus. In contrast, cells with larger, heterochromatic nuclei, located closer to the tubular basal membrane were negative for EGFL7 (Fig. 5A and B). Immunofluo-

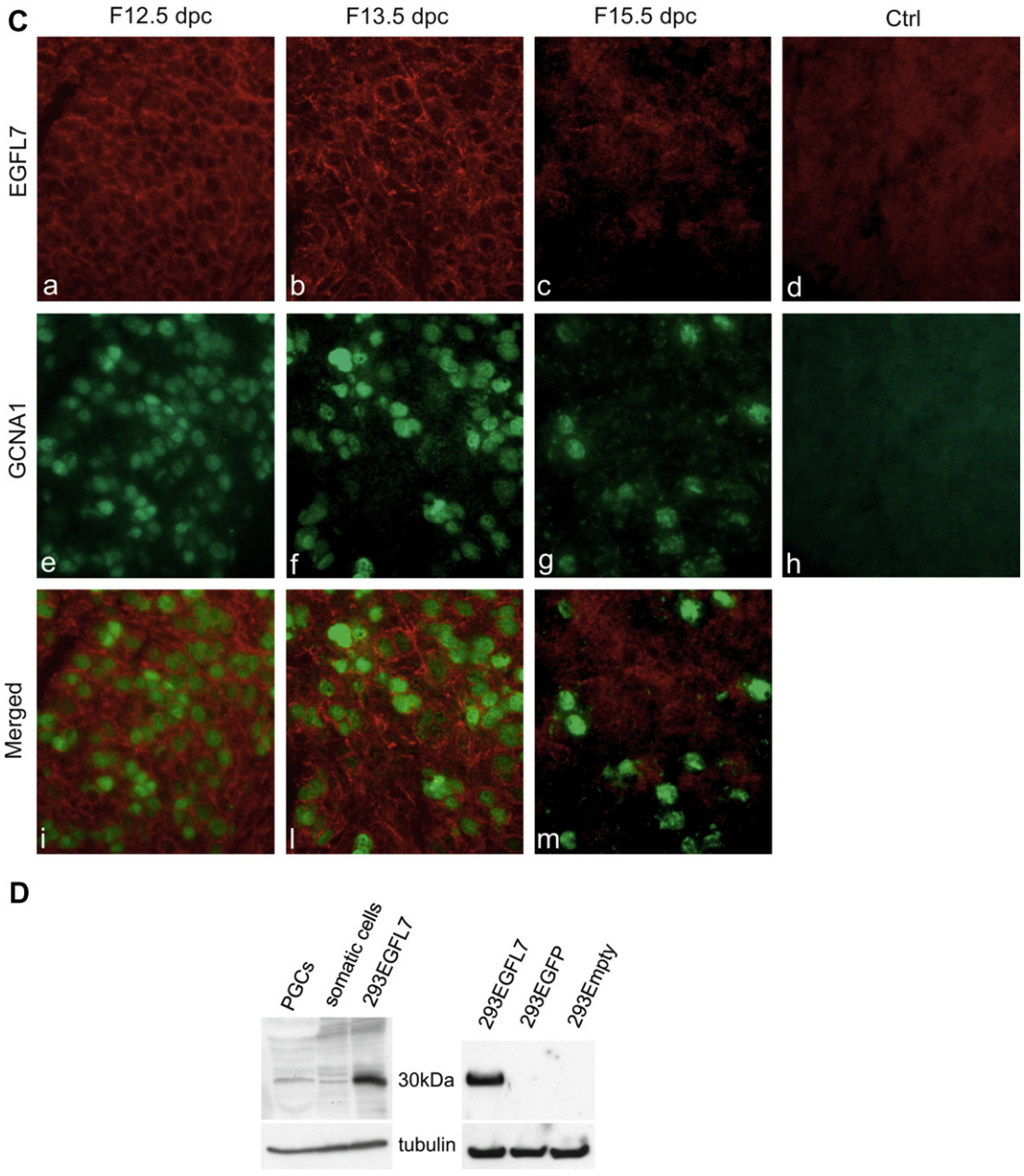

Fig. 2 (*continued*)

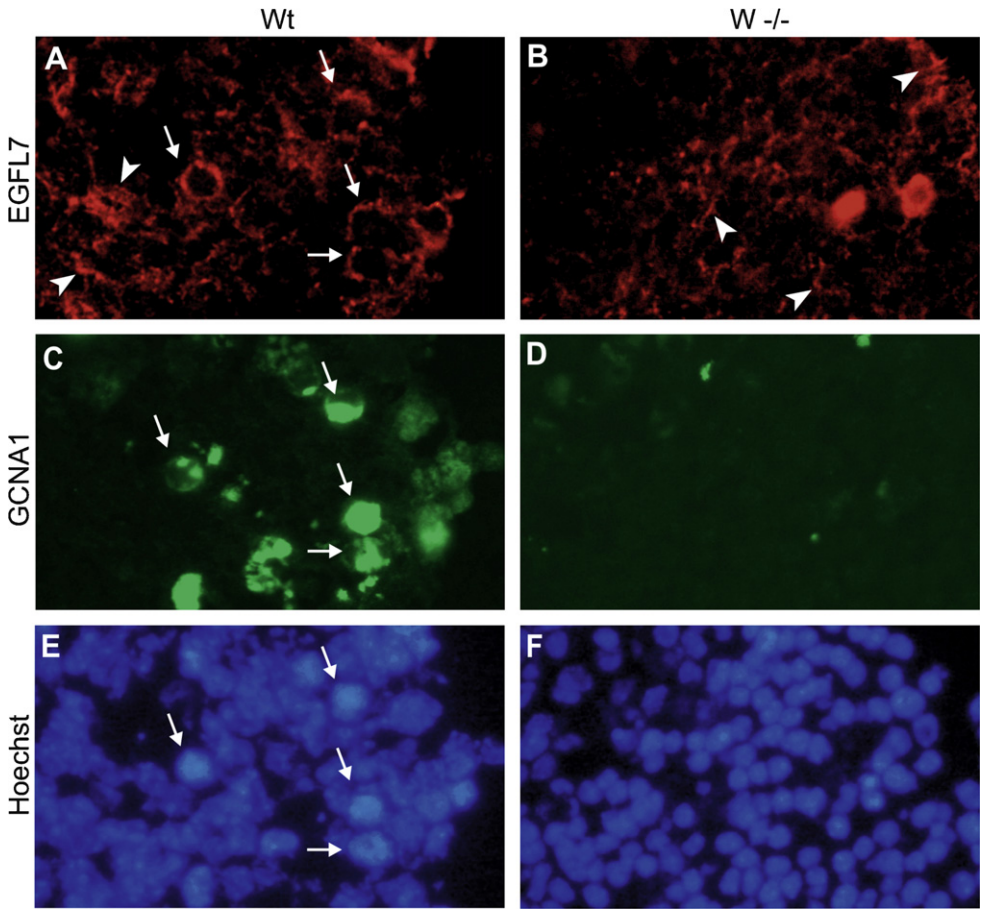

Fig. 3. Immunofluorescence analysis of EGFL7 in gonads from 13.5 dpc White-spotting (W) females. Germ cells, identified by using the anti-GCNA1 antibody, were present in the wild type but not in the W−/− homozygous mutants (C and D). Wild type germ cells were also positive for EGFL7 (compare A and B: some of the germ cells were indicated by arrows). No evident differences in the vascular EGFL7 were observed (arrowheads depict some of the capillaries). (A–B) EGFL7; (C–D) GCNA1; (E–F) Hoechst. Magnification 40×.

rescence analysis was also performed on stage-specific, enriched populations of adult male germ cells, obtained by cell elutriation (Sette et al, 1999; Meistrich 1977). These experiments revealed the presence of a strong signal associated with spermatids and spermatozoa (Fig. 5C and D, respectively). No staining was detected on spermatocytes (not shown), confirming the results from RNA *in situ* hybridization. Western blot analysis using cell extracts from germ cells populations confirmed the results obtained from immunostaining (not shown). Together, these data demonstrate restricted expression of EGFL7 during male germ cell differentiation, and they suggest a possible role in spermatid maturation and sperm cell release. In order to test this hypothesis, we are currently generating a conditional knock-out of *Egfl7*.

We also analyzed *Egfl7* expression in pre-pubertal (not shown) and mature ovaries. In contrast to the male gonads, *Egfl7* transcripts are exclusively located on the endothelium of the capillaries surrounding the follicles and in the corpus luteum, while no signal was detected on maturing oocytes (Fig. 4C and F, arrows; compare also Fig. 1). Thus, our results demonstrate that post-natal expression of *Egfl7* is restricted to the endothelium and the male germ line.

2. Experimental procedures

2.1. Isolation of pre-implantation embryos and primordial germ cells

Outbred CD1 mice (Charles River, Calco, Italy) were housed and mated under standard laboratory conditions. Six-week-old females were induced to superovulate by administration of pregnant mare's serum gonadotropin (PMSG, 5U.I./female) and human chorionic gonadotropin (hCG, 5U.I./female) with a 48 h interval, and then mated with CD-1 males. Pre-implantation embryos at various developmental stages were collected (Nagy et al, 2003). Pregnant females were sacrificed at staged post-coital times (midday of the day of the vaginal plug was considered 0.5 day post-coitum (dpc)). Metaphase II oocytes and embryos were collected in RLT buffer (Qiagen) and stored at −80 °C. To isolate primordial germ cells (PGCs) at 8.5 dpc, embryos were collected in enriched M2 medium (M2 supplemented with 1 mg/ml BSA, 0.2 mg/ml *N*-acetyl-cysteine and 0.036 μg/ml sodium pyruvate). The posterior half of the embryo, including the allantois, was dissected using fine needles, and digested for 5 min at RT in 0.5% trypsin. Digestion was blocked with FBS, and the suspension pipetted several times in order to completely dissociate the cells. After a short centrifugation step at 1000 rpm, cells were resuspended in M2 without BSA and spotted on poly-L-lysine coated slides for 10 min, followed by fixation in 2% paraformaldehyde. PGCs from 11.5 dpc embryos were isolated according to De Felici and McLaren, 1982 (De Felici, 1998; De Felici, 2000). Gonads were dissociated in 0.5% trypsin–EDTA and the resulting cell suspension incubated with anti-SSEA1 antibody, or EMA-1 (Hybridoma Bank), respectively, in enriched M2 at 4 °C. After 45 min of rotation, 10 μl magnetic microbead-conjugated anti-mouse IgM (Miltenyi Biotec GmbH) were added to the suspension and incubated for a further 20 min at 4 °C. PGCs were sorted by using the MiniMACS System according to the manufacturer's specifications (Miltenyi Biotec). Ten microliters of the sorted cell suspension was spotted on a slide and stained for alkaline phosphatase (De Felici, 2000) to evaluate the efficiency of purification. Sorted PGCs with at least 90–95% purity were spotted on slides for immunofluorescence analysis or pelleted and stored at −80 °C for Western blot analysis. Whole 10.5 dpc embryos were embedded in OCT and frozen on N2 vapor. Sections containing PGCs were identified by alkaline phosphatase staining, and the adjacent sections were stained for SSEA1 and EGFL7. Male and female urogenital ridges from 12.5, 13.5, and 15.5 dpc CD1 embryos, and 13.5 dpc White-spotting (W) embryos, were collected in M2, embedded in OCT and frozen on N2 vapor. Eight micron sections were fixed in methanol for 5 min at −20 °C, air dried and processed for immunofluorescence.

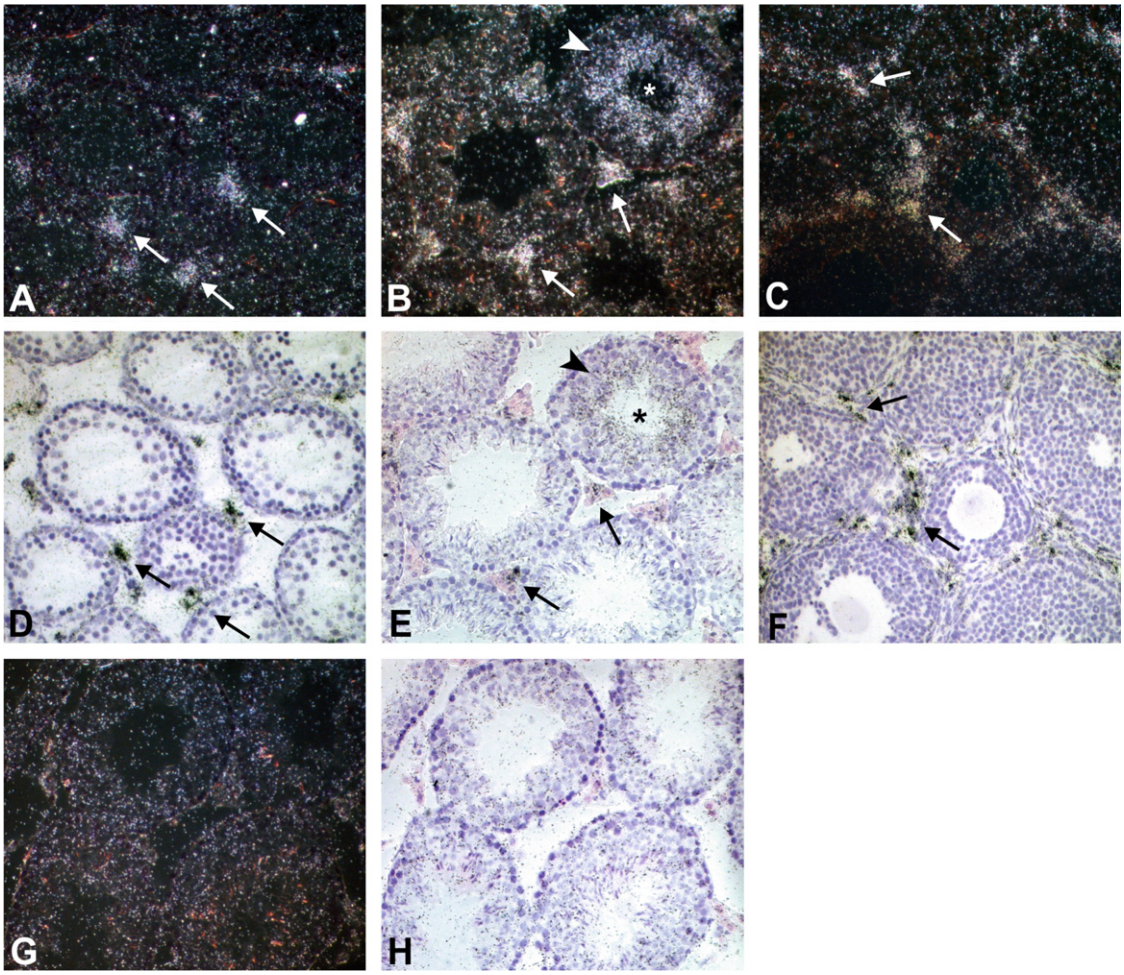

Fig. 4. *In situ* hybridization analysis of *Egfl7* in mouse testes and ovaries. (A) Dark field image of a pre-puberal mouse testis section hybridized with an *Egfl7* antisense probe showing expression of Egfl7 in the vasculature surrounding the tubules (arrows); (B) adult mouse testis section hybridized with an *Egfl7* antisense probe. The grains form a ring (arrowhead) surrounding the lumen of seminiferous tubules (*), a presumptive localization of post-meiotic germ cells; *in situ* signal is also present at low levels on the interstitial vasculature (arrows). (C) *Egfl7 in situ* hybridization analysis of adult mouse ovaries showing *Egfl7* expression limited to the vasculature surrounding the follicles (arrows). (D–F) Bright field images of (A–C), respectively. (G and H) Sections of adult testis hybridized with an *Egfl7* sense control probe. Magnification 20×.

2.2. Isolation of adult male germ cells

After removal of their albuginea membrane, testes from adult CD1 mice (Charles River Italia) were digested for 15 min in minimum essential medium (MEM, Invitrogen.), 2 mM lactate, 1 mM sodium pyruvate (Sigma), and 0.25% (w/v) collagenase (type IX, Sigma), at 30 °C under constant shaking. Tubules were sedimented and incubated in 0.5% trypsin–EDTA for 30 min at 30 °C. Undigested tissue debris were sedimented at unit gravity for 10 min and the supernatant containing the released germ cells was collected, pelleted at 1200 g and resuspended in elutriation medium (120.1 mM NaCl, 4.8 mM KCl, 25.2 mM $NaHCO_3$, 1.2 mM KH_2PO_4, 1.2 mM $MgSO_47$-H_2O, 1.3 mM $CaCl_2$, 11 mM glucose, 0.2% BSA). Spermatocytes, round spermatids, and elongated spermatids were enriched by elutriation of the single cell suspension as described previously (Meistrich, 1977; Sette et al., 1999). Homogeneity of cell populations, determined by morphological analysis, ranged between 80% and 85% (pachytene spermatocytes), and 95% (round spermatids). Spermatozoa from cauda were obtained from mature mice as described by Sette et al (1997).

2.3. RNA in situ hybridization

Procedures for RNA *in situ* hybridization were essentially as previously described (Campagnolo et al, 2005; Sassoon and Rosenthal, 1993). Paraffin embedded pre-pubertal and pubertal mouse testis and mature ovaries were sectioned, de-paraffinized and digested with Proteinase K, followed by 16 h. hybridization with a 35S-[UTP]radiolabeled full-length *Egfl7* riboprobes (final probe concentration was 35 dpm/ml in hybridization buffer). Sense control probes were synthesized for all experiments. After a 5-day exposure, slides were counter-stained with hematoxylin and eosin. Dark field and bright field photographs were taken using a Zeiss Axioplan2 microscope with an attached digital camera (Axiocam, Zeiss). For immunofluorescence analysis of testes sections, adult mouse testes were dissected, cut in half and OCT embedded.

2.4. Western blot analysis

PGCs and somatic cells collected and purified from one hundred 11.5 dpc gonads were homogenized in 2× Laemmle buffer. Denatured protein samples were resolved on 10% SDS–polyacrylamide gels and electro blotted onto polyvinylidene difluoride (PVDF) membranes (Millipore Corporation, Bedford, MA) using standard procedures. Adult germ cells were homogenized in lysis buffer (50 mM Hepes pH 7.4, 150 mM NaCl, 10% glycerol, 1% Triton X-100, 1 mg/ml SDS, 15 mM $MgCl_2$, 1 mM EGTA, 2 mM PMSF, 0.5 μg/ml leupeptin, 0.7 μg/ml pepstatin, 0.2 U/ml aprotinin, and 50 mM benzamidine), followed by centrifugation at 13,000*g* for 30 min to remove the insoluble material. Protein concentrations were evaluated by Bradford assay. Pre-stained molecular weight standards (Bench Mark Pre-stained, Invitrogen) and 15 μg of denatured proteins were resolved on 10% SDS gels and transferred to PVDF membranes. Filters were incubated with an affinity purified rabbit polyclonal anti-EGFL7 antibody (1:250 dilution) (Fitch et al., 2004). As a loading control, blots were stripped and re-probed with mouse anti-β-tubulin antibody (1:1000 dilution). Horseradish peroxidase conjugated anti-rabbit IgG and anti-mouse IgG (Amersham Biosciences, Piscataway, NJ) were used at a 1:10,000 and 1:5000 dilution, respectively. Specific bands were detected with SuperSignal West Pico Chemiluminescent Substrate (Pierce).

2.5. Immunofluorescence and histochemical analysis

For immunofluorescence analysis, anti-EGFL7 and anti-SSEA1 antibodies were used at 1:200 and 1:100 dilutions, respectively. Germ cells from 12.5, 13.5, and 15.5 dpc embryos were identified by anti-GCNA1 antibody (a kind gift from Dr. G.C. Enders, University of Kansas Medical Center, Kansas City, KS). Phalloidin FITC-labeled (Sigma) was used to stain spermatozoa tails. Secondary antibodies were Cy3-labelled goat anti-rabbit IgG, AlexaFluor 488-labeled anti-mouse IgM, and AlexaFluor 488-labeled anti-rat IgM, all used at a 1:500 dilution. Control slides

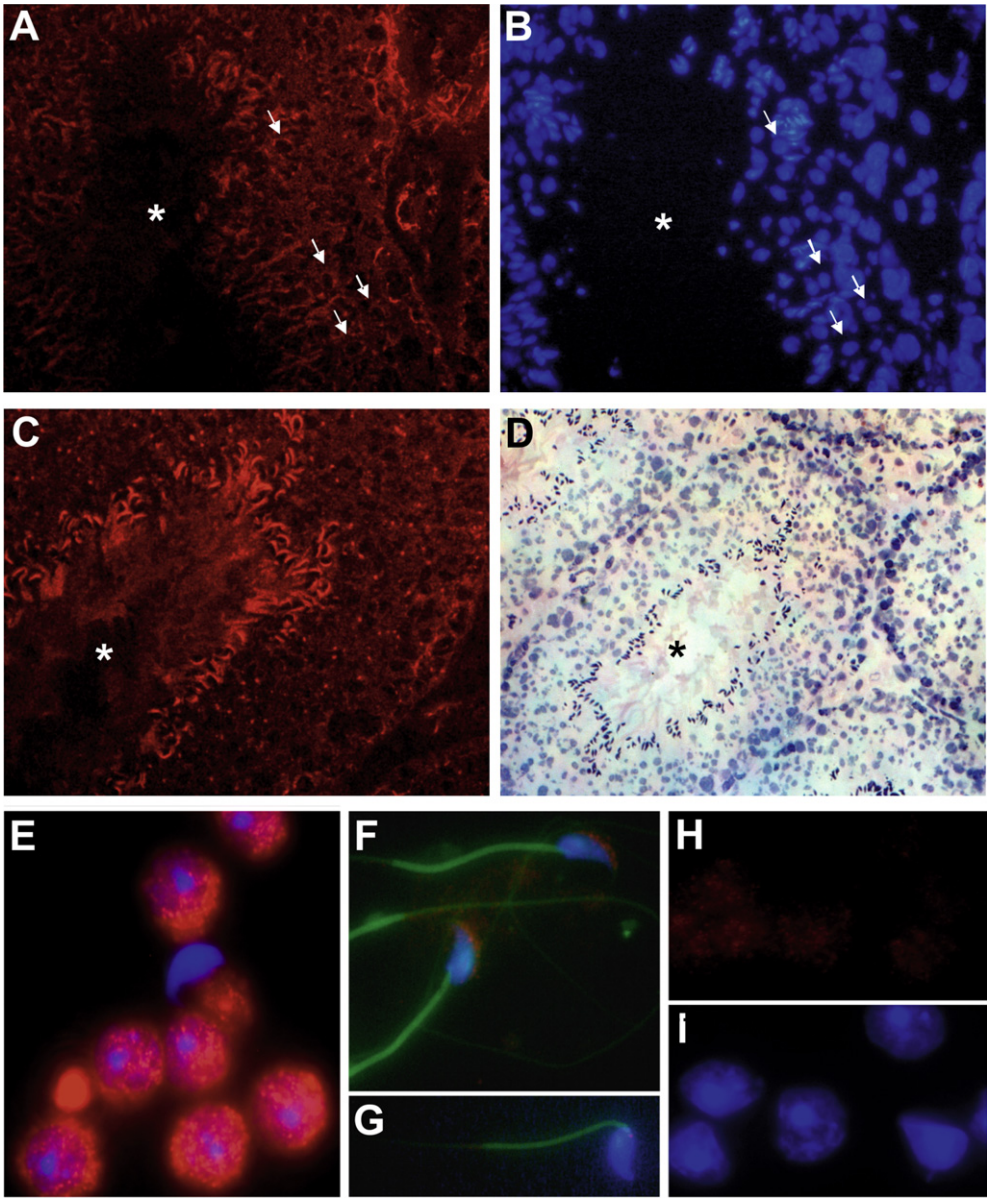

Fig. 5. Immuno-fluorescence analysis of EGFL7 expression in adult mouse testis and isolated adult germ cells. (A–D) Cross sections of adult mouse testis showing two seminiferous tubules (A, B and C, D, respectively); arrows in (A and B) indicate few of the EGFL7 positive spermatids. The tubule in (C) shows EGFL7 expression on spermatozoa; (A and C) anti-EGFL7 antibody; (B) Hoechst staining; (D) hematoxylin and eosin counterstaining of section shown in (C). Due to the H&E staining procedure, the tubule in (D) appears slightly shrunk compared to the corresponding image in (C). Asterisks indicate the lumen of the tubules. (E) Spermatids isolated from adult testes by elutriation show strong immuno-reactivity to the EGFL7 antibody. (F) EGFL7 was also detected on the head of caudal sperm cells, possibly associated with the acrosomal vesicle; sperm tails were stained using FITC-phalloidin. (G) Control slide of sperm cells incubated with non-specific rabbit IgG and stained with FITC-phalloidin. (H) Control slides of spermatids incubated with non-specific rabbit IgG. (I) Hoechst staining of (H). Magnification in (A–D) 40×. Magnification in (E–I) 100×.

were incubated with rabbit IgG and rat or mouse IgM in the same conditions as the primary antibodies. Fluorescent images were taken using a Zeiss Axioplan2 microscope. After immunofluorescence analysis, adult mouse testis sections were stained with hematoxilin and eosin (H&E) according to standard protocols. The procedure of H&E staining caused the specimen to shrink slightly in size.

2.6. RT-PCR analysis

RNA from pre-implantation embryos was isolated using the RNeasy Micro Kit (Qiagen). Total RNA was reverse transcribed using oligo dT with the Superscript First Strand Synthesis System (Invitrogen) according to the manufacturer's protocol. PCR was performed using 2 μl of the reverse transcriptase reaction in a volume of 25 μl with Platinum Taq polymerase (Invitrogen). PCR conditions were as follows: initial denaturation at 95 °C (5 min) followed by 38 cycles of denaturation at 95 °C (1 min), annealing at a temperature indicated below (1 min), and extension at 72 °C (1 min). Amplified PCR products were analyzed by electrophoresis on a 1% agarose gel. PCR primer pairs were designed to span introns in order to avoid amplification of genomic DNA. Sequences were as follows:

Egfl7 (T_A 59 °C):	5′-GAGCATGGGCTACAAGATCC-3′,
	5′-TGGAGACAATCCCCACCTTA-3′;
Hprt (T_A 58 °C):	5′-CTGCTGGATTACATTAAAGCACTG-3′,
	5′-CTGAAGTACTCATTATAGTCAAGG-3′.

Acknowledgements

We thank Professor Massimo De Felici and Professor Susanna Dolci for precious advises and critical reading of the manuscript, and Graziano Bonelli for graphic assistance. The monoclonal antibody SSEA1 (developed by B.B. Knowles and D. Solter) was obtained from the Developmental Studies Hybridoma Bank

developed under the auspices of the NICHD and maintained by the University of Iowa, Department of Biological Sciences, Iowa City, USA. Support for this study was provided by Public Health Service Grant NIH R21 HL072270 and NIH R01 HL082098 to H.S.

References

Campagnolo, L., Leahy, E., Chitnis, S., Koschnick, S., Fitch, M.J., Fallon, J.T., Loskutoff, D., Taubman, M.B., Stuhlmann, H., 2005. EGFL7 is a chemoattractant for endothelial cells and is up-regulated in angiogenesis and arterial injury. Am. J. Pathol. 167, 275–284.

De Felici, M., 1998. Isolation and culture of germ cells from the mouse embryo. In: Cell Biology: A Laboratory Handbook, vol. I, Academic Press, New York, pp. 73–85.

De Felici, M., 2000. Regulation of primordial germ cell development in the mouse. Int. J. Dev. Biol. 44, 575–580.

De Felici, M. McLaren, A., 1982. Isolation of mouse primordial germ cells. Exp. Cell Res. 142, 476–482.

Enders, G.C., May, J.J.2nd, 1994. Developmentally regulated expression of a mouse germ cell nuclear antigen examined from embryonic day 11 to adult in male and female mice. Dev. Biol. 63, 331–340.

Fitch, M.J., Campagnolo, L., Kuhnert, F., Stuhlmann, H., 2004. Egfl7 a novel epidermal growth factor-domain gene expressed in endothelial cells. Dev. Dyn. 230, 316–324.

Kuhnert, F., Stuhlmann, H., 2004 Identifying early vascular genes through gene trapping in mouse ES cells. Curr. Top. Dev. Biol. 62, 261–281 (Chapter 9).

Meistrich, M.L., 1977. Separation of spermatogenic cells and nuclei from rodent testes. Methods Cell Biol. 15, 15–54.

Mintz, B., Russell, E.S., 1957. Gene induced embryological modifications of primordial germ cells. J. Exp. Zool. 134, 207–239.

Nagy, A., Gertsenstein, M., Vintersten, K., Behringer, R., 2003. Manipulating the Mouse Embryo. A Laboratory Manual, third ed. Cold Spring Harbor Laboratory Press, Cold Spring Harbor, New York.

Parker, L.H., Schmidt, M., Jin, S.W., Gray, A.M., Beis, D., Pham, T., Frantz, G., Palmieri, S., Hillan, K., Stainier, D.Y., De Sauvage, F.J., Ye, W., 2004. The endothelial-cell-derived secreted factor Egfl7 regulates vascular tube formation. Nature 428, 754–758.

Sassoon, D., Rosenthal, N., 1993. Detection of messenger RNA by in situ hybridization. Methods Enzymol. 225, 384–404.

Schmidt, M., Paes, K., De Mazière, A., Smyczek, T., Yang, S., Gray, A., French, D., Kasman, I., Klumperman, J., Rice, DS.D.S., Ye, W., 2007. EGFL7 regulates the collective migration of endothelial cells by restricting their spatial distribution. Development 134, 2913–2923.

Schultz, R.M., 1993. Regulation of zygotic gene activation in the mouse. Bioassay 15, 531–538.

Sette, C., Bevilacqua, A., Bianchini, A., Mangia, F., Geremia, R., Rossi, P., 1997. Parthenogenetic activation of mouse eggs by microinjection of a truncated c-kit tyrosine kinase present in spermatozoa. Development 124, 2267–2274.

Sette, C., Barchi, M., Bianchini, A., Conti, M., Rossi, P., Geremia, R., 1999. Activation of the mitogen-activated protein kinase ERK1 during meiotic progression of mouse pachytene spermatocytes. J. Biol. Chem. 274, 33571–33579.

Soncin, F., Mattot, V., Lionneton, F., Spruyt, N., Lepretre, F., Begue, A., Stehelin, D., 2003. VE-statin, an endothelial repressor of smooth muscle cell migration. EMBO J. 22, 5700–5711.

Electrospun Poly(ε-caprolactone)/Ca-deficient Hydroxyapatite Nanohybrids: Microstructure, Mechanical Properties and Cell Response by Murine Embryonic Stem Cells

Alessandra Bianco[a,*], Erica Di Federico[a,d], Ilana Moscatelli[b,d], Antonella Camaioni[b], Ilaria Armentano[c], Luisa Campagnolo[b], Mariaserena Dottori[c], Josè Maria Kenny[c], Gregorio Siracusa[b], and Gualtiero Gusmano[a]

[a]Department of Chemical Sciences and Technologies, Research Unit INSTM Tor Vergata, University of Rome Tor Vergata, via Ricerca Scientifica, 00133 Rome, Italy

[b]Department of Public Health and Cell Biology, University of Rome Tor Vergata, via Montpellier, 00133 Rome, Italy

[c]Material Science and Technology Center, Research Unit INSTM, NIPLAB, University of Perugia, Terni, Italy

[d]These authors contributed equally to this work

*Corresponding author: Fax number:+39-0672594328, E-mail address: bianco@stc.uniroma2.it

Keywords: Biocompatibility, Electrospun fibers, Murine embryonic stem cells, Nanohydroxyapatite, Poly(ε-caprolactone)

Abstract

Nanohybrid scaffolds able to mimic extracellular matrix might be very promising experimental models to study stem cell behaviour, in terms of adhesion and proliferation. In the present study, the structural characterization of a novel electrospun nanohybrid and the analysis of cell response by a highly sensitive cell type, embryonic stem (ES) cells, are investigated. Ca-deficient hydroxyapatite nanocrystals (d-HAp) were synthesized by precipitation. Fibrous PCL/d-HAp nanohybrids were obtained by electrospinning, the d-HAp content ranging between 2 and 55 wt.%. Electrospun mats showed a non-woven architecture, the average fiber size was 1.5 ± 0.5 μm, porosity 80-90 %, and specific surface area 16 m^2g^{-1}. Up to 6.4 wt.% d-HAp content, the nanohybrids displayed comparable microstructural**,** mechanical and dynamo-mechanical properties. Murine ES cell response to neat PCL and nanohybrid PCL/d-HAp (6.4 wt.%) mats was evaluated by analyzing

morphological, metabolic and functional markers. Cells growing on either scaffold proliferated and maintained pluripotency markers at essentially the same rate as cells growing on standard tissue culture plates, despite a lower cell adhesion at the beginning of culture, with no detectable signs of cytotoxicity.

1. Introduction

The composition and topology of the extracellular matrix (ECM) has been found to affect cell morphology, function, and physiological response [1]. Electrospun nanofibrous scaffolds aimed to mimic the architecture and biological functions of ECM, are considered as very promising substrates for tissue engineering [2,3]. Among them, scaffolds made of poly(ε-caprolactone) (PCL), a bioresorbable aliphatic polyester, have been used to provide a 3D environment for *in vitro* embryonic stem cell culture and differentiation [4]. The use of a 3D environment might make the culture system closer to the *in vivo* situation: how various 3D scaffolds might affect the differentiation potential of murine ES cells has been the object of recent research [5-7]. Electrospun hybrid scaffolds based on bioresorbable polymers and conventional hydroxyapatite allow osteoblast proliferation and differentiation, and are thus considered very promising as bone scaffolding materials [8-10]. It is well known that Ca-deficient-hydroxyapatite (d-HAp) show more similar features to biological apatites with respect to conventional stoichiometric hydroxyapatite (s-Hap) [11]. In the present study we have evaluated the biocompatibility of PCL/d-HAp nanohybrid mats by using murine ES cells. Because of their high sensitivity to toxic agents [12], their embryonic origin [13,14] and their ability to differentiate along all tissue types [15,16], ES cells are already being used in a standard cytotoxicity and embryotoxicity test for soluble compounds [17,18], and might as well provide a good model to test biocompatibility *in vitro* of novel scaffolds. In greater detail, we have analyzed how fibrous PCL/HAp affects an essential property of ES cells: their ability to proliferate without differentiating. Fibrous PCL/d-HAp mats were obtained by electrospinning, with a d-HAp content ranging from 2 to 55 wt.%. The d-HAp nanopowders was

freshly synthesized by precipitation. Microstruture, mechanical and dynamo-mechanical properties of the electrospun nanohybrid mats were extensively investigated. The biocompatibility of the mats was evaluated by culturing mouse ES cells and analyzing colony morphology and number, ES cell adhesion, viability, proliferation and preservation of pluripotency markers. To our knowledge, this is the first report in which electrospun PCL nanohybrids containing d-HAp have been described, and their biocompatibility tested by the use of ES cells.

2. Experimental

2.1. Synthesis of Ca-deficient Hydroxyapatite (d-HAp) Nanopowders

The d-HAp nanopowder was prepared in a double-walled jacket reactor at 40 °C following a precipitation route described elsewhere [19]. Stoichiometric volume of 1M calcium nitrate tetrahydrate ($Ca(NO_3)_2.4H_2O$, 99.2% *Aldrich*) was added drop-wise to diammonium hydrogen phosphate ($(NH_4)_2HPO_4$, 99.2% *Aldrich*) pH was continuously monitored and adjusted at 9.0 ± 0.1 by adding NH_4OH conc. Precipitate was aged in mother solutions for 24 h, washed with NH_4OH aqueous solution, and vacuum filtered. Chemical analysis was performed by induced coupled plasma atomic emission spectroscopy (*AES-ICP, JobinYvon JV 24R*). Morphology was examined by transmission electron microscopy in bright field mode, accelerating voltage being 100 kV (*TEM, Philips CM120*) and specific surface area measured by N_2 adsorption (*Sorptomatic 1900, Carlo Erba*) using the Brunauer–Emmett–Teller (BET) method. X-ray diffraction analysis (XRD) (*Philips X'Pert*) was performed (CuKα λ=1.5402 Å, 2θ range20°-55°) and crystallinity degree estimated by means of X-ray diffraction analysis, according to *Landi et al.* [20].

2.2. Fabrication of Electrospun PCL Membranes

PCL (Aldrich, MW 80000) was dissolved at RT under magnetic stirring in a 1:1 dichloromethane (CH_2Cl_2) and N,N-dimethylformamide (DMF) mixture, the polymer concentration being 12 % (w/v). The solution was poured in a glass syringe (*Socorex*) equipped with a 21 G needle, fixed in a digitally controlled syringe pump (*KD Scientific*) and electrospun as follows: tension 21 kV

(*Spellman, Model SL 30*), needle-target distance 10 cm, feed rate 1ml·h^{-1}. According to a previous study [21], electrospun meshes were dried under vacuum for 24 h.

2.3. Fabrication of Electrospun PCL/d-HAp Membranes

The d-HAp nanopowder was poured to a 1:1 CH_2Cl_2-DMF solution and the suspension ultrasonicated for 2 h. PCL granules were then added and the mixture stirred for 36 h. Suspensions were electrospun and the resulting mats treated as described above. All prepared PCL/d-HAp nanohybrid samples are listed in Table 1.

2.4. Viscosity and Conductivity

Viscosity of polymeric suspensions was measured at 25 °C by digital viscosimeter (*Brookfield DV-II+*) equipped with a SC4-21 spindle at 20 rpm and electrical conductivity measured at 25 °C by conductivity meter (*CDM230, Analitica De Mori*).

2.5. Scanning Electron Microscopy (SEM) and Energy Dispersion Spectroscopy (EDS)

Microstructure of electrospun fabrics was investigated by SEM (*Cambridge Stereoscan 300*). The actual d-HAp distribution was evidenced by Energy Dispersion Spectroscopy (EDS). Average fiber diameter was determined on 120 different fibers by means of CAD software.

2.6. Density, Porosity and Specific Surface Area

Density (ρ) was estimated as mass to volume ratio on 12 mm diameter disks cut out of the membranes, four samples were considered for each material. Sample thickness was measured according to ISO7198 by means of a digital micrometer equipped with a 2 kg load cell. Porosity (ε) was estimated as follows, where ρ_0 is the density of as-purchased PCL (1.145 g·cm^{-3}):

$$\varepsilon = \left(1 - \frac{\rho}{\rho_0}\right) \cdot 100 \quad (1)$$

Specific surface area was measured by N_2 adsorption (*Sorptomatic 1900, Carlo Erba*) using BET method.

2.7. Infrared Spectroscopy (ATR-IR) and Thermal Analyses

IR spectra were recorded in the 4000-400 cm^{-1} region by means of a *Jasco FTIR-615* spectrophotometer in ATR reflection method, spectral resolution 4 cm^{-1}.

Thermogravimetric analysis (TGA) was performed by means of a quartz rod microbalance (*Seiko Exstar 6000*). Measurements were performed in N_2 atmosphere between 30 and 1000 °C, heating rate 10 °C·min^{-1}. Residual mass and maximum degradation temperature (T_d) were measured. Thermal characterization was carried out using Differential Scanning Calorimeter (DSC) (*Perkin Elmer Pyris 1*), heating and cooling scans were performed in the following conditions: sample weight 10 mg, heating rate 10 °C·min^{-1}, temperature range from -25 °C to 100 °C, N_2 atmosphere. Melting temperature(T_m), melting enthalpy (ΔH_m), and crystallinity degree (X_c) were determined from the heating scan. Crystallization temperature (T_c) and enthalpy (ΔH_c) were measured from the cooling run. X_c of the PCL component in the nanocomposites was calculated according to (2):

$$Xc\ (\%) = \Delta H_m/\Delta H_0 \qquad (2)$$

where ΔH_m is derived from the DSC curves, with respect to the actual PCL content [22], ΔH_0 is the theoretical enthalpy of the fully crystalline polymer, for PCL the considered value was 136 J·g^{-1} [23].

2.8. Mechanical Characterization

Uniaxial tensile tests were carried out on dog-bone specimens, gauge width 4.8 mm and gauge length 22.3 mm. Mechanical tests were performed at 1.2 mm·min^{-1} to rupture by an electromechanical machine equipped with a 5 kg load cell (*TA-HDi, Stable Micro Systems*). Four specimens were considered for each electrospun matrix. The tensile modulus (E) was evaluated between 0 and 5 % strain [24]. The yield stress was determined from the intersection of the stress-strain curve with a line parallel to the linear region and offset by 2 % strain. The ultimate stress (σ_{max}) and ultimate percent deformation (ε_f) were calculated considering the nominal cross-sectional area of the tensile specimen. Dynamic-Mechanical Analysis (DMA) was performed using a *Reometric Scientific-ARES* sample size was 10 mm width, 30 mm length, 0.3 mm thick. Shear

modulus was measured at RT in the dynamic time sweep test, fixed frequency 1 Hz and shear strain 0.3 %.

2.9. Mouse ES Cell Culture

Mouse ES cell line R1 was a kind gift of Dr. Heidi Stuhlmann. Following standard procedures, ES cells were cultured on a feeder layer of mitotically-inactivated primary mouse embryonic fibroblasts (MEFs) from CD-1 mouse embryos, in tissue culture polystyrene plates (TCPS) that had been gelatin-coated to facilitate cell adhesion (a 0.7 % denatured collagen solution, Sigma, MO, USA, for 10 min at 37 °C). The same procedure was used when testing experimental scaffolds. ES cells were expanded and maintained undifferentiated by culture in Dulbecco's Modified Eagle's Medium (DMEM with 4,5 $g \cdot L^{-1}$ D-glucose) supplemented with 15 % heat-inactivated fetal calf serum (ES cell tested), 20 mM Hepes, 2 mM L-glutamine, 100 μM β-mercaptoethanol, 100 μM non-essential amino acids, 50 $U \cdot ml^{-1}$ penicillin and 50 $\mu g \cdot ml^{-1}$ streptomycin (all from *Lonza*, *Switzerland*), and 10^3 $U \cdot ml^{-1}$ Leukemia Inhibitory Factor (*LIFES, Immunological Sciences*). The cells were cultured at 37 °C in a humidified atmosphere of 5 % CO_2 in air. To obtain highly enriched ES cell populations, cultures reaching 80 % confluency and forming round colonies were trypsinized and gently disaggregated by pipetting. After centrifugation, single cell suspensions were plated onto TCPS and kept for 20–40 min in the incubator. During this time, MEFs attach to the plate while ES cells, that require longer adhesion times, remain in the supernatant and can be harvested for subsequent use. Before each experiment, scaffolds were sterilized in 70 % ethanol overnight, air dried, and secured by stainless steel rings to the bottom of the wells of 24-well plates (*Multiwell™, Falcon, Becton Dickinson Labware*). MEFs were then seeded on the scaffolds and on standard TCPS and incubated overnight. The next day, ES cells were seeded in each well in 1 ml of medium, at the concentrations specified in the text, and allowed to attach for 6 h before measuring their adhesion rate to the substrates (see below). When proliferation was to be measured, after adhesion, the ES cells were allowed to grow for approximately 3 days. During such time, each adhered ES cell forms a round colony made of closely packed cells. In the proliferation experiments, the medium was changed

every 24 h until the ES colonies in the standard cultures were approximately 80 % confluent (about 3 days).

2.10. Staining Procedures

For morphological analysis, at the end of the culture cells were washed with Dulbecco's phosphate buffered saline (*PBS, Lonza*) and fixed with methanol for 5 min at -20 °C. To stain nuclei, a solution of 0.5 μg·ml^{-1} Hoechst 33258 (*Sigma*) in PBS was added for 30 min. After three PBS washes, cells were mounted with Möwiol (*Polysciences Inc.*). Fluorescent images were taken with Axioplan 2 microscope (*Zeiss*). Pluripotency of the ES cell colonies was evaluated by alkaline phosphatase assay [13,25]. Enzyme activity was detected by incubating the fixed cells for 15 min in a solution made by mixing 960 μl Fast Red TR salt (1 mg·ml^{-1}) with 40 μl Naphthol AS-BI (4 mg·ml^{-1}) (all from *Sigma*). Cells were washed with PBS and observed using a Leitz Diavert microscope. Pluripotent colonies expressing alkaline phosphatase appeared red, while the differentiated ones were colourless. Cell viability was determined by staining with a 0.4 % trypan blue solution (*Sigma*). The dead/blue cells were counted with a hemocytometer and the data were expressed as percentages of the total cell number (±SD).

2.11. Western Blot Analysis

For protein immunodetection by Western blot, cells were homogenized in lysis buffer (50 mM HEPES, pH 7.4, 15 mM $MgCl_2$, 150 mM NaCl, 15 mM EGTA, 20 mM β-glycerophosphate, 1 % Triton X-100, 10 % glycerol, 0.5 mM sodium orthovanadate, 1 mM dithiothreitol) with Protease Inhibitor Cocktail (Roche). Homogenates were sonicated, centrifuged at 4 °C for 15 min at 15000 g, supernatants were collected and protein concentration was determined. Extracts were solubilized in NuPAGE LDS sample buffer with the addition of 50 mM dithiothreitol, separated by electrophoresis on a 4–12 % NuPAGE Bis–Tris Gel System (*Invitrogen*), and transferred to PVDF Transfer Membrane Hybond™-P (*Amersham*). Membranes were saturated with 5 % nonfat dry milk in PBS containing 0.1 % Tween 20 (PBS/T), for 1 h at room temperature and incubated overnight at 4 °C with the following primary antibodies, diluted 1:1000 in PBS/T with 5 % BSA: rabbit anti-

Nanog (*Cosmo Bio*) and mouse anti-αTubulin (*Sigma*). Secondary anti-rabbit or anti-mouse antibodies conjugated to horseradish peroxidase (*Amersham*) were incubated with the membranes for 1 h at room temperature at 1:10000 dilution in PBS/T with 5 % nonfat dry milk. Immunoreactive bands were detected by SuperSignal West Pico chemiluminescent reagent (*Pierce*) and densitometric analysis of the bands was performed using ImageQuant 5.0 (*Molecular Dynamics*).

2.12. MTT Assays

Cell adhesion was evaluated 6 h after seeding $8x10^4$ ES cells on scaffolds and on TCPS by a modification of the methylthiazolyldiphenyl-tetrazolium bromide (MTT; *Sigma*) assay [26]. Parallel cultures without ES cells (MEFs only) were analyzed in order to subtract the background due to the feeder layer. Briefly, each sample was rinsed with PBS to remove unattached cells and then incubated with 0.5 $mg \cdot ml^{-1}$ MTT (250 µl/well, 1 h, 37 °C).. The MTT solution was then removed and dimethylsulfoxide (*Sigma*) (900 µl/well) and glycine buffer (pH 10.5, 125 µl/well) were added to each well. After 10 min of agitation, the absorbance at 540 nm was measured with a SmartSpec 3000 spectrophotometer (*Bio-Rad*) and recorded as optical density (OD).

2.13. [^{3}H]thymidine Incorporation

Cell proliferation was evaluated 3 days after seeding 10^4 ES cells on scaffolds and TCPS, by measuring incorporation of radioactive DNA precursor [methyl-^{3}H]thymidine, Amersham, (^{3}HTdR) in the acid-insoluble fraction. Parallel MEF-only cultures were also run as above (see MTT assay). For radiolabeling, cells were washed with PBS and incubated with fresh serum-free DMEM containing all the supplements and 1 µCi/well of ^{3}HTdR for 2 h at 37 °C. After incubation, cells were treated with 5 % trichloroacetic acid (TCA) on ice for 20 min, and then washed twice with ice-cold distilled water. The acid-insoluble material was dissolved with 1 N NaOH for 20 min at room temperature, and an equal volume of 1 N HCl was added. Each sample was mixed 1:10 with scintillation liquid (*OptiPhase 'HiSafe'3, Perkin Elmer*) and the radioactivity, expressed as counts per minute, was measured by a scintillation counter (*LS 6500, Beckman Instruments*).

2.14. Statistical Analysis

Data from the MTT and [^{3}H]thymidine incorporation assays are shown as means ± standard error of three replicates from three independent experiments. Radioactivity counts were normalized to take into account the differences in the number of adhered cells, 6 h after seeding. Statistical analysis was performed by one-way analysis of variance (ANOVA) and Tukey test for pairwise multiple comparisons.

3. Results and Discussion

3.1. Characterisation of d-HAp Nanopowder

TEM analysis show that as-precipitated d-HAp powder is made up of needle-like particles, width between 10 nm and 30 nm and length between 50 nm and 100 nm (Figure 1). The specific surface area was 100 $m^2 \cdot g^{-1}$. The composition in term of Ca/P ratio was 1.57, as expected for a calcium-deficient hydroxyapatite, and estimated cristallinity degree around 40 %.

3.2. Characterisation of PCL/d-HAp Suspensions

Viscosity and conductivity of PCL/d-HAp suspensions prepared for electrospinning are summarized in Table 2. Particularly, viscosity of P solution and 2HAp suspension were comparable, the value being around 470 mPa·s. In the case of 4HAp and 6HAp suspensions, viscosity decreased down to 414 mPa·s and 427 mPa·s, respectively. This anomalous effect is typical of fine dispersed nanocomposite systems, in which interphase characteristics predominate on bulk properties. Suspensions containing higher d-HAp amounts showed progressively increased viscosity, the maximum value being 1432 mPa·s for 55HAp suspension. In agreement with *Wutticharoenmongkol et al.* [9], the highest conductivity was registered for the neat PCL solution. The presence of d-HAp nanophase induced conductivity changes, leading to progressively higher values with increased nanofiller amounts. The conductivity increased from 1.55 $\mu S \cdot cm^{-1}$ to 4.12 $\mu S \cdot cm^{-1}$ for 2HAp and 55HAp, respectively, due to the presence of calcium and phosphate ions.

3.3. Characterization of Nanohybrid PCL/d-HAp Mats

In Figure 2A-D SEM micrographs and EDS mapping of different PCL/d-HAp nanohybrids are presented. Electrospun mats consisted of randomly oriented fibers of fairly uniform diameter. Large interconnected voids were present within the fibers, resulting in a 3D porous network. Fiber size and morphology were not significantly influenced by the presence of d-HAp, the average fiber size being 1.5 ± 0.5 μm, for both neat PCL and PCL/d-HAp nanohybrids. In sample 2HAp, the d-HAp was homogeneously distributed through the fibrous matrix (Figure 2B). As the filler content was raised up to 6.4 wt.%, a few submicronic and micronic (2-5 μm) agglomerates rich in Ca and P appeared within the fibers (Figure 2C). At higher d-HAp contents, due to suspension heterogeneity, clusters increased progressively in number and size (Figure 2D). According to the literature, density of electrospun membranes was around 0.2-0.3 $g \cdot cm^{-3}$, porosity 80-90 % and specific surface area around 16 $m^2 \cdot g^{-1}$, without significant difference among samples [9,10].

The actual d-HAp content was accurately determined by TGA measurements (Table 1), considering that by 600 °C the polymer is completely burned out. Thermogravimetric data reported in Table 3 also evidenced that electrospun meshes containing up to 6.4 wt.% d-HAp nanoparticles showed only a degradation temperature around 400 °C associated to the thermal decomposition of the polymer. The thermal stability of these nanocomposites seemed thus not remarkably influenced by low amounts of nanofiller. Further increasing the d-HAp content, the polymer matrix destabilized and the temperature decomposition onset decreased, probably due to the pseudo-catalytic and disruptive effect of oxydril groups on hydroxyapatite nanoparticles [27,28]

In order to investigate the effect of d-Hap content on the properties of nanocomposites, IR spectra were recorded (Figure 3). It mainly resulted that (*i*) the peak around 1030 cm^{-1}, associated to d-HAp, increased progressively with ceramic loading; (*ii*) absorption bands most sensitive to crystallinity changes (e.g. 1170 cm^{-1} (C=O-C, strong) and 1185 cm^{-1} (C=O, shoulder) changed in shape and intensity, the shoulder at 1185 cm^{-1} decreasing with increasing the d-HAp content [29,30].

In order to establish the structure-property correlations of the nanocomposites, DSC analyses were also performed, results are presented in Table 3. The value of T_m was not significantly affected by the presence of d-HAp. On the other side, DSC curves related to the cooling scan showed that the crystallization of nanohybrids occurred at higher temperature with respect to neat PCL, clearly evidencing that d-HAp nanoparticles act as nucleant agent (Figure 4). Moreover, the presence of low d-HAp contents (e.g. up to 6.4 wt.%) did not significantly affect X_c (~ 50 %), the effect of the fiber-forming process being predominant. The X_c value progressively decreased down to 29 % for 55HAp, possibly due to poor dispersion of d-HAp within the polymeric solution and to spatial inhibition of crystal growth (Table 3) [31]. Crystal growth was thus discouraged in high-loaded electrospun systems resulting in lower X_c, in good agreement with IR results.

3.4 Nanohybrid PCL/d-HAp Mats: Mechanical and Dynamo-Mechanical Properties

The analysis of the mechanical behaviour of nanocomposite fibrous meshes is relevant to understand their performance. Stress-strain curves of electrospun mats are shown in Figure 5. Mechanical properties are presented in Table 4**.** It should be considered that high porosity and the random oriented nature of the non-woven fabrics are responsible for their lower mechanical properties, as compared to PCL sheet/film [32]. Mechanical behaviour of electrospun polymeric mats is extensively discussed by *Li et al.* [33]. As a general trend, we found that mechanical properties of nanohybrids were not strongly affected by the incorporation of d-HAp up to 6.4 wt.% (Table 4). In more detail, tensile modulus remained substantially unchanged around 12-14 MPa. Samples 25HAp, 40HAp and 55HAp showed progressively decreased mechanical properties, due to microstructural heterogeneity (Figure 2D) and incomplete wettability of filler nanoparticles [34]. Yield stress (σ_s), ultimate tensile stress (σ_{max}), and strain at failure (ε_f) showed similar trends. In particular, σ_s remained stable around 1 MPa up to 25HAp. In the case of samples 40HAp and 55HAp, the effect due to the presence of agglomerates became predominant and σ_s decrease to 0.4 and 0.2 MPa, respectively. Up to sample 6HAp, σ_{max} values ranged between 2 and 3 MPa. For sample 40HAp, σ_{max} decreased to 0.5 MPa, again due to the presence of increasing amounts of

micrometric d-HAp clusters. In the proximity of these defects, stress concentration occurs, resulting in lower ultimate tensile strength. Strain at failure (ε_f) did not significantly change for nanohybrids containing up to 6.4 wt.% d-HAp, except for the most homogeneous sample 2HAp (Fig.2B) whose value was doubled with respect to the neat PCL mat. This latter result suggests that an interaction at the d-HAp nanocrystals/poly-caprolactone interphase occurred. Further increasing the nanofiller amount resulted in ε_f decreasing , progressively leading to a quasi-brittle behavior (Table 3). These results are in agreement with recent studies on PCL-based electrospun nanohybrids [10,35].

Furthermore, the effect of d-HAp content on dynamo-mechanical properties of neat PCL and low-loaded PCL/d-HAp membranes (up to 6.4 wt.%) was also investigated. All samples showed a constant storage modulus during the experimental time, the presence of d-HAp improving the performance in non disruptive cyclic load. In particular, electrospun nanocomposite mats showed higher shear modulus values as compared to neat PCL membranes (140 MPa), the highest value (640 MPa) being recorded for the most homogeneous sample 2HAp (Fig. 2B). This distinct behaviour of sample 2HAp suggests that d-HAp nanoparticles inhibit the sliding of PCL chains, providing the main reinforcing mechanism.

3.5. Embryonic Stem Cell Morphological Analysis

The 6HAp scaffold was chosen for biocompatibility testing, and compared with neat PCL mats and standard cultures on TCPS, as it had been shown to contain the maximum amount of d-HAp nanoparticles associated with suitable microstructural and mechanical features (see previous sections).

The ability of the three substrates to support formation of ES colonies was evaluated after 3 days of culture, as described in Experimental. Very similar numbers of colonies were obtained on PCL (330 ± 10/cm^2) and 6HAp (320 ± 20/cm^2) scaffolds, suggesting that the presence of d-HAp was not affecting the ability of ES cells to adhere and form colonies. Both values were lower than those obtained on standard TCPS (800 ± 60/cm^2), proportionally reflecting the lower rates of initial cell adhesion on the scaffolds (see below). After the 3-day culture, the size and shape of ES colonies,

that appeared round and made of closely packed cells, were similar in all experimental conditions (Figure 6A-C). Nuclear morphology, as analyzed by Hoechst staining, showed no appreciable signs of apoptosis, such as nuclear condensation, in any of the cultures examined (Fig 6A-C).

3.6. Embryonic Stem Cell Pluripotency Markers

As all cultures were carried out in conditions aimed to maintain pluripotency, cell colonies were cytochemically stained for alkaline phosphatase (AP), a marker for undifferentiated ES cells (see Experimental*)*. As shown in Figure 6D-F, all colonies grown on either scaffold were AP positive, as they were in standard TCPS cultures. In addition, the colonies were analyzed by Western blot for the presence of Nanog, a transcription factor that plays a crucial role in maintaining the pluripotent state of ES cells [36]. Figure 7 shows (upper panel) the immunodetection of Nanog and α-Tubulin, a housekeeping protein used as reference to correct for differences in gel loading and (lower panel) the densitometric analysis of the bands. The results, showing similar levels of Nanog in standard, neat PCL and 6HAp cultures, indicate that culture on the scaffolds does not hinder the maintenance of cell pluripotency, thus confirming the AP data. Interestingly, in a study in which murine ES cells were grown in the absence of a MEF feeder layer, a condition that promotes ES cell differentiation, the presence of a 3D nanofibrillar polyamide scaffold was found to help preventing loss of pluripotency [37].

3.7. Embryonic Stem Cell Adhesion and Viability

Since morphological analysis had shown that fewer ES colonies were growing on scaffolds than on TCPS, we tested whether this might be was due to some of the seeded cells simply failing to adhere to the mats. The number of attached cells was therefore evaluated by MTT assay 6 h after seeding, when ES cells should have adhered but proliferation would still be minimal or absent. As shown in Figure 8, the OD values generated by cells present on either scaffold (± d-HAp) were about 45 % those by cells in standard TCPS cultures. Since the absorbance values measured by MTT assay are proportional to the cell number, the results indicate that in our culture system PCL mats, with or without d-HAp, allow the adhesion of approximately one half of the cells that do so in standard

cultures. These results are in agreement with a previous study in which PCL scaffolds (±1 wt.% HAp) were tested for biocompatibility with mouse pre-osteoblastic MC3T3-E1 cells and the same difference in cell adhesion was found in comparison with TCPS culture [9]. Cell adhesion is a crucial step when testing synthetic scaffolds, that can be improved by immobilizing adhesive proteins or peptides on the material [38,39]. To exclude the possibility of scaffold cytotoxicity, unattached cells present in the medium withdrawn at 6 h of culture were stained with trypan blue, a dye that stains dead cells. The percentages of blue/dead cells from PCL (60±8 %) and 6HAp cultures (63±9 %) were very similar, and not significantly different from TCPS cultures (60±9%), indicating that neither PCL nor 6HAp affect cell viability.

3.8. Embryonic Stem Cell Proliferation

We finally evaluated ES cell proliferation by measuring ^{3}HTdR incorporation by cells that had been cultured for 3 days. The results show that, when the incorporation data are normalized for differences in cell adhesion at 6 h, ES cells cultured on TCPS or on scaffolds (with or without 6.4 wt.-% d-Hap) show essentially the same levels of ^{3}HTdR incorporation (Figure 9). The data indicate that the adhered cells proliferate on either scaffold at a similar rate as on TCPS.

4. Conclusions

Nanohybrids based on poly(ε-caprolactone) and Ca-deficient nanohydroxyapatite (d-HAp) were obtained by means of electrospinning technique. A relevant feature of these scaffolds is the presence of freshly synthesized d-HAp whose composition and morphology is similar to biological apatites. The content of d-HAp ranged between 2 and 55 wt.-%. Viscosity and electrical conductivity of PCL/d-HAp suspensions were appreciably affected by the nanofiller content. Nanohybrid fibers formed a randomly oriented non-woven fabric, average fiber size being 1.5 ± 0.5 μm, porosity 80-90 % and specific surface area 16 $m^2 \cdot g^{-1}$. Fibrous mats containing 2 wt.-% d-HAp showed uniform and homogeneous morphology. In the case of composites loaded with 4 or 6.4 wt.-% d-HAp few Ca, P-rich sub-micrometric and micrometric (2-5 μm) agglomerates were observed.

Generally, the incorporation of low amounts of d-HAp nanoparticles (i.e. up to 6.4 wt.-%) did not remarkably affect the mechanical properties of the nanocomposites, the tensile modulus was 12-13 MPa, the tensile strength 2-3 MPa and the elongation at break over 130 %. Only sample loaded with 2% HAp showed a doubled strain at failure. For higher d-HAp contents, mechanical properties significantly decayed, onset decomposition temperature and crystallinity considerably decreased as well.

The biocompatibility of 6HAp nanohybrids was evaluated by culturing on the scaffolds ES cells, in conditions aimed to allow their proliferation in the undifferentiated, pluripotent state. It is known that ES cell lines are highly susceptible to culture environment: if cultured in sub-standard conditions, the cells tend to lose their pluripotency and to differentiate in a random fashion. In doing this, ES cell colonies change morphology: each clone of packed stem cells starts to flatten, modifying their shape from round to polygonal, and looses ES markers. The results were compared with those obtained with neat PCL scaffolds and with standard TCPS cultures. Six hours after seeding, ES cell adhesion on either scaffold was about 45 % that found on TCPS. At this time, the viability of non-adhered cells was very similar in all experimental conditions. The cells that attached on mats proliferated, formed round colonies of packed cells and maintained pluripotency markers at very similar rates as cells growing on TCPS. Moreover, ES cell behaviour was not affected by the presence within PCL fibers of 6.4 wt.-% d-HAp. In conclusion, the data reported in the present paper show that a cell population as demanding as ES cells is able to expand in the undifferentiated, pluripotent state on a d-Hap nanohybrid scaffold as they do in standard culture conditions. These results now prompt us to evaluate if the proposed nanohybrid may become a particularly valuable substrate for studying the early steps of ES cell differentiation along the osteoblastic lineage [40] and if the presence of d-HAp and the 3D structure of the scaffold, in comparison with the standard 2D culture settings, enhances the efficiency of the process.

Acknowledgements

This work was supported by a grant (PRIN 2006) from the Italian Ministry of University and Research, for a project titled “Design and Realization of Organic, Inorganic and Hybrid Nanostructured Scaffolds as Substrates for the Differentiation of Stem Cells in Regenerative Medicine” to A.Bianco and G.Siracusa. I.Armentano and M.Dottori gratefully acknowledge the Italian Interuniversity Consortium on Materials Science and Technology (INSTM) for the financial support. The Authors wish to thank Prof. E. Bemporad and Dr. D. De Felicis of the University of Rome 3 for TEM analysis.

References

[1] F. Causa, P.A. Netti, L. Ambrosio, Biomaterials 28 (2007) 5093.

[2] S. Ramakrishna, K. Fujihara, W.E. Teo, T.C. Lim, Z. Ma, An introduction to electrospinning and nanofibers, World Scientific Publishing, Singapore, 2005.

[3] A. Greiner, J.H. Wendorff, Angew. Chem. Int. Ed. 46 (2007) 5670.

[4] X. Kang, Y. Xie, H.M. Powell, L. James Lee, M.A. Belury, J.J. Lannutti, D.A. Kniss, Biomaterials 28 (2007) 450.

[5] E. Garreta, E. Genové, S. Borrós, C.E. Semino, Tissue Eng. 12 (2006) 2215.

[6] N.S. Hwang, M.S. Kim, S. Sampattavanich, J.H. Baek, Z. Zhang, J. Elisseeff , Stem Cells 24 (2006) 284.

[7] W.L. Randle, J.M. Cha, Y-S Hwang, K.L.A. Chan, S.G. Kazarian, J.M. Polak, A. Mandalaris, Tissue Eng. 13 (2007) 2957.

[8] J. Venugopal, S. Low, A.T. Choon, A.B. Kumar, S. Ramakrishna, J. Biomed. Mater. Res. 85A (2008) 408.

[9] P. Wutticharoenmongkol, P. Pavasant, P. Supaphol, Biomacromolecules 8 (2007) 2602.

[10] H.-W. Kim, H.-H. Lee, J.C. Knowles, J. Biomed. Mater. Res. 79A (2006) 643.

[11] R.Z. LeGeros, S. Lin, R. Rohanizadeh, D. Mijares, J.P. LeGeros, J.Mat.Sc.:Mat.Med.,14 (2003) 201.

[12] G. Laschinski, R. Vogel, H. Spielmann, Reprod. Toxicol. 5 (1991) 57.

[13] A.M. Wobus, H. Holzhausen, P. Jäkel, J. Schöneich, Exp. Cell. Res. 152 (1984) 212.

[14] J. A. Thomson, J. Itskovitz-Eldor, S.S. Shapiro, M.A. Waknitz, J.J. Swiergiel, V.S. Marshall, J.M. Jones, Science 282 (1998) 1145.

[15] B.E. Reubinoff, M.F. Pera, C.Y. Fong, A. Trounson, A. Bongso, Nat. Biotechnol. 18 (2000) 399.

[16] J.S. Odorico, D.S. Kaufman, J.A. Thomson, Stem Cells 19 (2001) 193.

[17] H. Spielmann, I. Pohl, B. Döring, F. Moldenhauer, In Vitro Toxicol. 10 (1997) 119.

[18] A. Seiler, A. Visan, R.Buesen, E. Genschow, H. Spielmann, Reprod. Toxicol. 18 (2004) 231.

[19] A. Bianco, I. Cacciotti, M. Lombardi, L. Montanaro, G. Gusmano, J. Therm. Anal. Cal. 88 (2007) 237.

[20] Landi E., Tampieri A., Celotti G., Sprio S., J. Europ. Ceram. Soc. 20 (2000) 2377.

[21] Del Gaudio C, Bianco A, Folin M, Baiguera S, Grigioni M. J Biomed Mater Res A. (2008) [Epub ahead of print] DOI: 10.1002/jbm.a.32048

[22] W.Y. Yam, J. Ismail, H.W. Kammer, M.D. Lechner, C. Kummerlowe, Polymer 41 (2000) 9073.

[23] A. Arbelaiz, B. Fernández, A. Valea, I. Mondragon, Carbohydrate Polymers 64 (2006) 224.

[24] C.M. Vaz, S. van Tuijl, C.V. Bouten, F.P. Baaijens, Acta Biomat. 1 (2005) 575.

[25] J. Cai, M.L. Weiss, M.S. Rao, Exp. Hemat. 32 (2004) 585.

[26] T. Mosmann, J. Immunol. Methods 65 (1983) 55.

[27] D. Choi, K.G. Marra, P.N. Kumta, Mat. Res. Bull. 39 (2004) 417.

[28] M. Zanetti, G. Camino, P. Reichert, R. Mulhaupt, Macromol. Rapid. Commun. 22 (2001) 176.

[29] T. Elzein, M. Nasser-Eddine, C. Delaite, S. Bistac, P. Dumas, J. Coll. Interf. Sci. 273 (2004) 381.

[30] Z.G. Tang, R.A. Black, J.M. Curran, J.A. Hunt, N.P. Rhodes, D.F. Williams, Biomaterials 25 (2004) 4741.

[31] B. Lepoittevin, M. Devalckenaere, N. Pantoustier, M. Alexandre, D. Kubies, C. Calberg, R. Jerome, P. Dubois, Polymer 43 (2002) 4017.

[32] M.C. Azevedo, R.L. Reis, M.B. Claase, D.W. Grijpma, J. Feijen, J. Mater. Sc. Mater. Med. 14 (2003) 103.

[33] W.J. Li, J.A. Cooper, R.L. Mauck, R.S. Tuan, Acta Biomat. 2 (2006) 377.

[34] S.G.C. Leeuwenburgh, M.C. Heine, J.C.G. Wolke, S.E. Pratsinis, J. Schoonman, J.A. Jansen, Thin Solid Films 503 (2006) 69.

[35] K. Fujihara, M. Kotaki, S. Ramakrishna, Biomaterials 26 (2005) 4139.

[36] I. Chambers, D. Colby, M. Robertson, J. Nichols, S. Lee, S. Tweedie, A. Smith, Cell 113 (2003) 643.

[37] A. Nur-E-Kamal, I. Ahmed, J. Kamal, M. Schindler, S. Meiners, Stem Cells 24 (2006) 426.

[38] T. Boontheekul, D.J. Mooney, Curr. Opin. Biotechnol. 14 (2003) 559.

[39] U. Hersel, C. Dahmen, H. Kessler, Biomaterials 24 (2003) 4385.

[40] L. Duplomb, M. Dagouassat, P. Jourdon, D. Heymann, Stem Cells 25 (2007) 544.

Figure Captions

Figure 1

TEM image of as-precipitated d-HAp nanocrystals.

Figure 2

SEM micrographs and EDS mapping of electrospun mats neat PCL (A), PCL/d-HAp 2.0 wt.% (B), PCL/d-HAp 6.4 wt.% (C), PCL/d-HAp 24.9 wt.% (D).

Figure 3

IR spectra of neat PCL (P) and PCL/d-HAp (2.0 wt.% = 2HAp; 24.9 wt.% = 25HAp; 42.5 wt.% = 40HAp; 55.1 wt.% = 55HAp) mats.

Figure 4

DSC curves of neat PCL (P) and PCL/d-HAp (2.0 wt.% = 2HAp; 3.6 wt.% = 4HAp; 6.4 wt.% = 6HAp) membranes recorded during the the cooling scan.

Figure 5

Stress-strain curves of electrospun PCL (P) and PCL/d-HAp (6.4 wt.% = 6HAp; 24.9 wt.% = 25HAp; 42.5 wt.% = 40HAp; 55.1 wt.% = 55HAp) mats.

Figure 6

Micrographs of ES cell colonies after 3 days of growth in standard cultures conditions (A, D), in cultures on PCL scaffolds (B, E) and on PCL scaffolds containing 6.4 wt.% d-HAp (C, F). A-C: Fluorescence analysis of ES cell colonies after nuclear staining with Hoechst 33258; D-F:

Cytochemical analysis of the same colonies for alkaline phosphatase (red), an ES cell marker of pluripotency.

Figure 7

Immunodetection of Nanog and α-Tubulin proteins by Western blot (upper panel) and densitometric analysis of the bands (lower panel). Protein extracts were obtained from ES cells grown for 3 days in standard cultures (TCPS), in culture on PCL scaffolds and on PCL scaffolds containing 6.4 wt.% d-HAp (6HAp). The second lane contains the protein extract of a control culture without ES cells (MEF only). Representative immunodetection from three independent experiments.

Figure 8

ES cell adhesion, measured by MTT assay 6 h after seeding the cells in standard cultures (TCPS), in cultures on PCL scaffolds and on PCL scaffolds containing 6.4 wt.% d-HAp (6HAp). Results are expressed as percentage of the standard culture (TCPS = 100%). Different superscript letters indicate a statistically significant difference (p value < 0.01).

Figure 9

ES cell proliferation, measured by ^{3}H-thymidine (^{3}HTdR) incorporation after 3 days of growth in standard cultures (TCPS), in cultures on PCL scaffolds and on PCL scaffolds containing 6.4 wt.% d-HAp (6HAp). Results are expressed as percentage of the standard culture (TCPS = 100%). Data are normalized to take into account the differences in the number of cells after the 6 h adhesion time. Data are not significantly different (p value > 0.05).

Table 1

Designation and composition of PCL/d-HAp nanohybrid electrospun mats.

Sample	PCL/d-HAp wt.% [a]	PCL/d-HAp vol.-% [b]
PCL	-	-
2HAp	2.0	5
4HAp	3.6	9
6HAp	6.4	16
25HAp	24.9	48
40HAp	42.5	67
55HAp	55.1	77

a) values referred to residual mass (T=600°C), as calculated by TGA measurements.
b) Volume fraction of the ceramic filler (ϕ_c) was derived from the weight percentage (W_c) as follows, where ρ_p e ρ_c are, respectively the density of PCL (ρ_{PCL} 1.145 g/cm^3) and d-HAp ($\rho_{d\text{-}HAp}$ 3.156 g·cm^{-3}):

$$\frac{1}{\phi_c} = 1 + \frac{\rho_p}{\rho_c}\left(\frac{100}{P_c} - 1\right)$$

Table 2

Viscosity and conductivity
of PCL/d-HAp suspensions at different d-HAp contents.

Sample	Viscosity (mPa·s)	Conductivity ($\mu S \cdot cm^{-1}$)
PCL	468	4.74±0.03
2HAp	471	1.55±0.03
4HAp	414	1.84±0.03
6HAp	427	2.55±0.04
25HAp	574	3.34±0.05
40HAp	697	3.83±0.05
55HAp	1432	4.12±0.08

Table 3

Thermal properties of PCL and nanohybrid PCL/d-HAp mats derived from TG and DSC thermograms.

Sample	T_m [°C]	T_c [°C]	ΔH_m ($J \cdot g^{-1}$)	ΔH_c ($J \cdot g^{-1}$)	X_c (%)	T_d [°C]
PCL pellets	58.7 ± 0.3	17.8 ± 0.7	57.1 ± 0.7	46.0± 0.5	42.0 ± 0.5	404
PCL	57.7 ± 0.1	24.6 ± 0.1	68.5 ± 0.9	55 ± 1	50 ± 1	404
2HAp	57.5 ± 0.1	28.0 ± 0.1	67.3 ± 0.1	56.4 ± 0.2	49.5 ± 0.1	404
4HAp	57.3± 0.1	28.3 ± 0.1	67.8 ± 0.7	55.8± 0.3	49.9 ± 0.5	404
6HAp	56.6 ± 0.1	28.6 ± 0.1	64.8 ± 0.4	55.6± 0.2	47.7 ± 0.3	404
25HAp	61.3 ± 0.4	31.0 ± 0.1	60.8 ± 0.8	43 ± 1	44.7 ± 0.6	390
40HAp	60.0 ± 0.2	29.6 ± 0.1	40 ± 3	33± 1	29 ± 2	365
55HAp	58.6 ± 0.3	28.1 ± 0.1	40 ± 2	22± 1	29 ±1	353

Table 4

Tensile modulus (E), yield stress (σ_s), ultimate tensile stress (σ_{max}), and strain at failure (ε_f) of PCL/d-HAp nanohybrids.

Sample	E (MPa)	σ_s (MPa)	σ_{max} (MPa)	ε_f (%)
PCL	13 ± 2	0.9 ± 0.1	3.0 ± 0.5	150 ± 15
2HAp	14 ± 3	1.1 ± 0.1	3.4 ± 0.5	280 ± 20
4HAp	13 ± 5	1.1 ± 0.2	2.3 ± 0.6	130 ± 50
6HAp	12 ± 1	0.9 ± 0.1	2.4 ± 0.3	130 ± 10
25HAp	10 ± 3	0.8 ± 0.2	1.4 ± 0.4	80 ± 40
40HAp	6 ± 1	0.4 ± 0.1	0.5 ± 0.2	30 ± 10
55HAp	6 ± 4	0.2 ± 0.1	0.8 ± 0.6	15 ± 10

Figure 1

Click here to download high resolution image

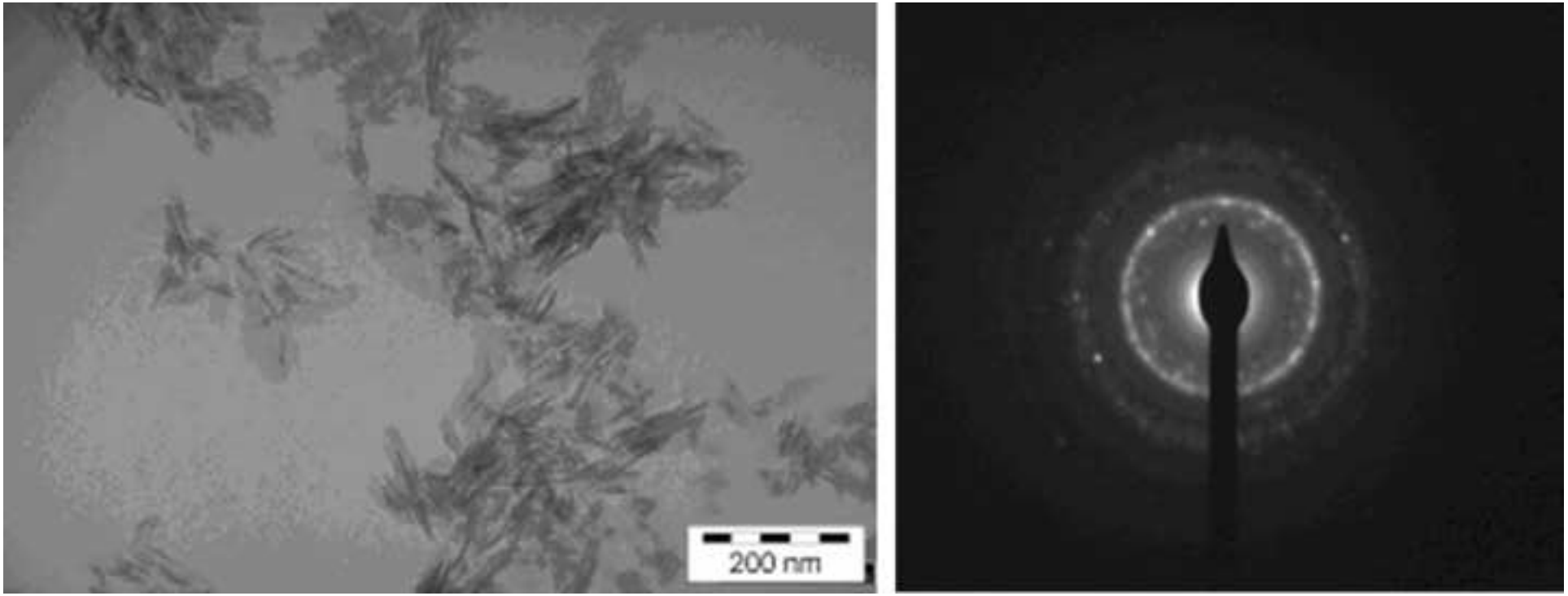

Figure 2a

Click here to download high resolution image

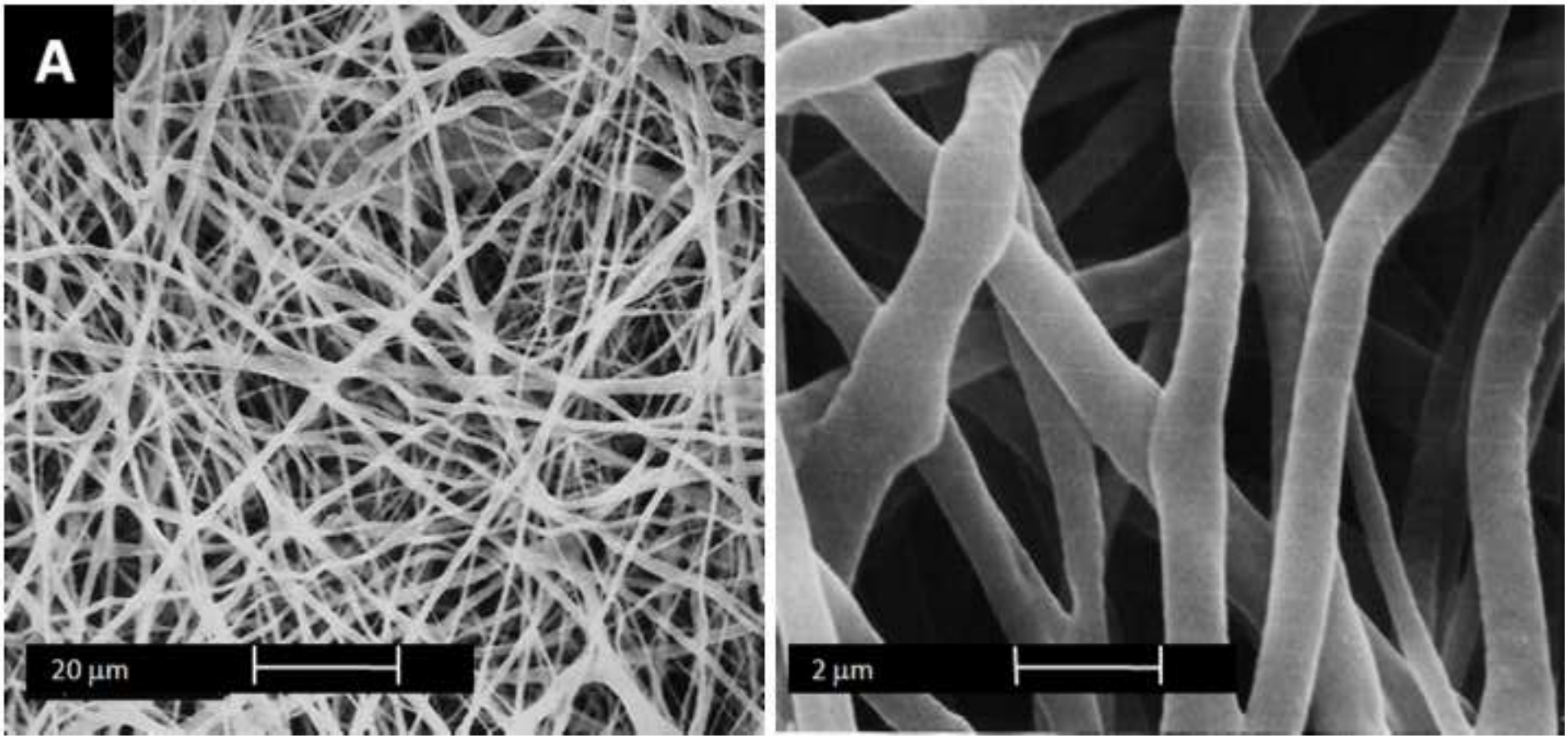

Figure 2b

Click here to download high resolution image

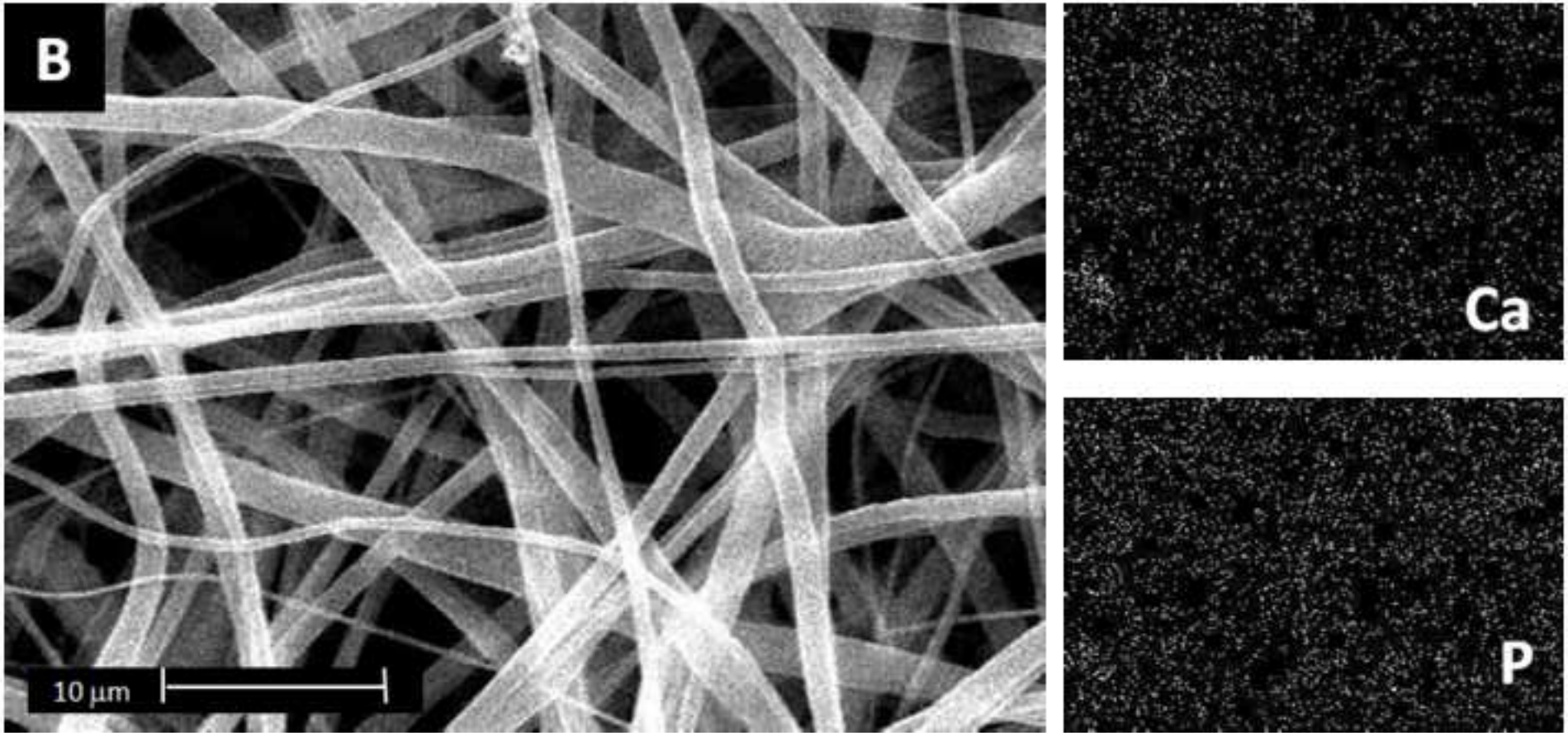

Figure 2c

Click here to download high resolution image

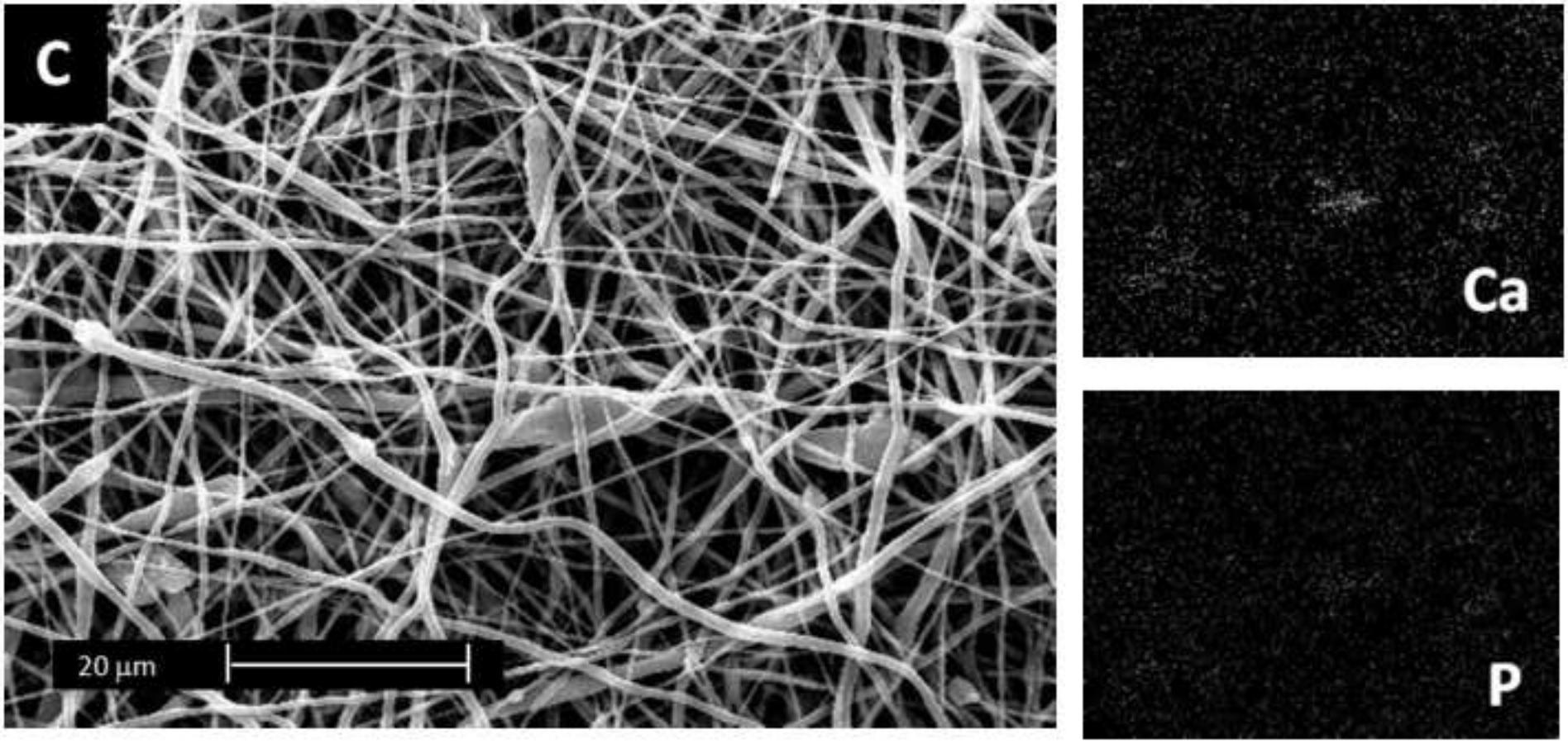

Figure 2d

Click here to download high resolution image

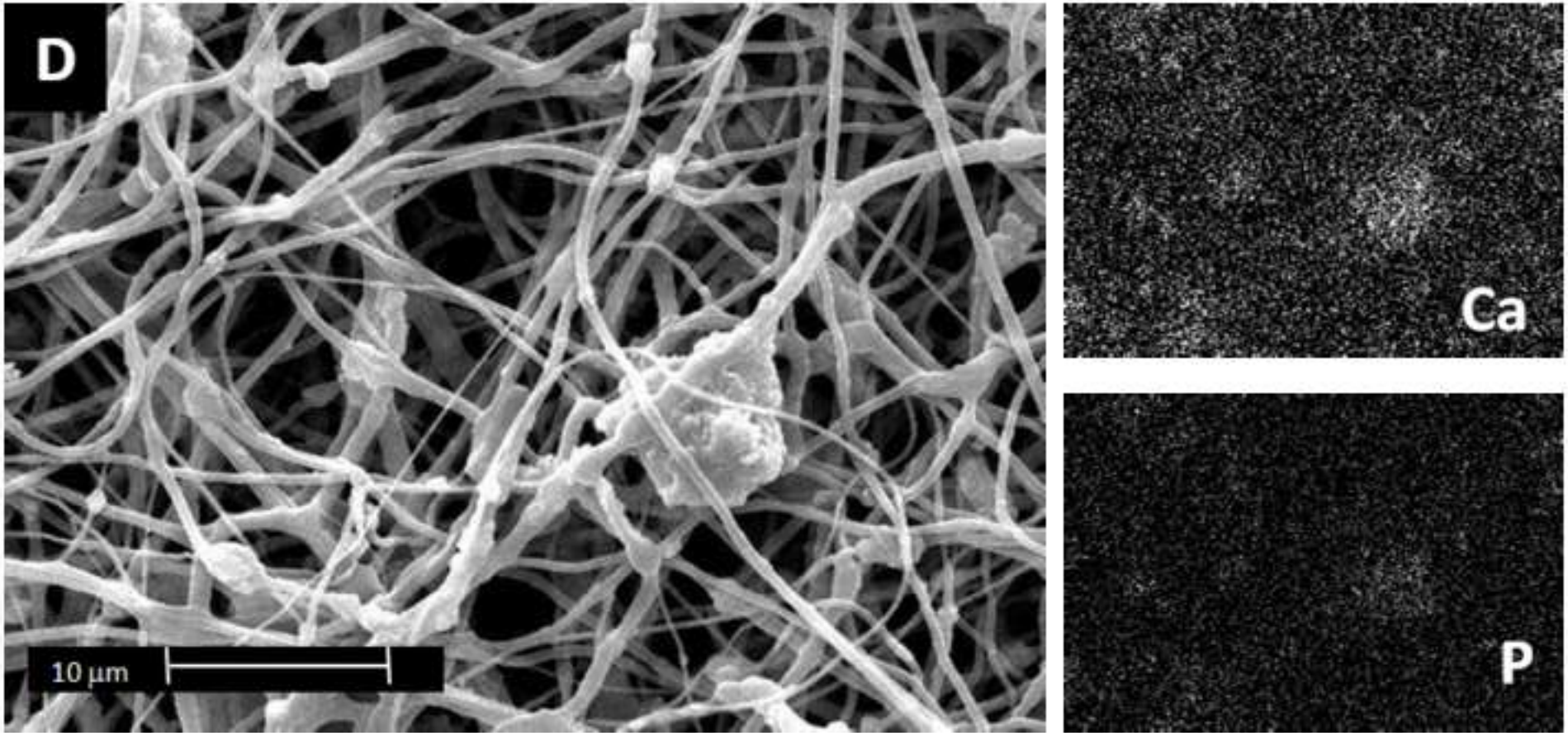

Figure 3 (revised)
Click here to download high resolution image

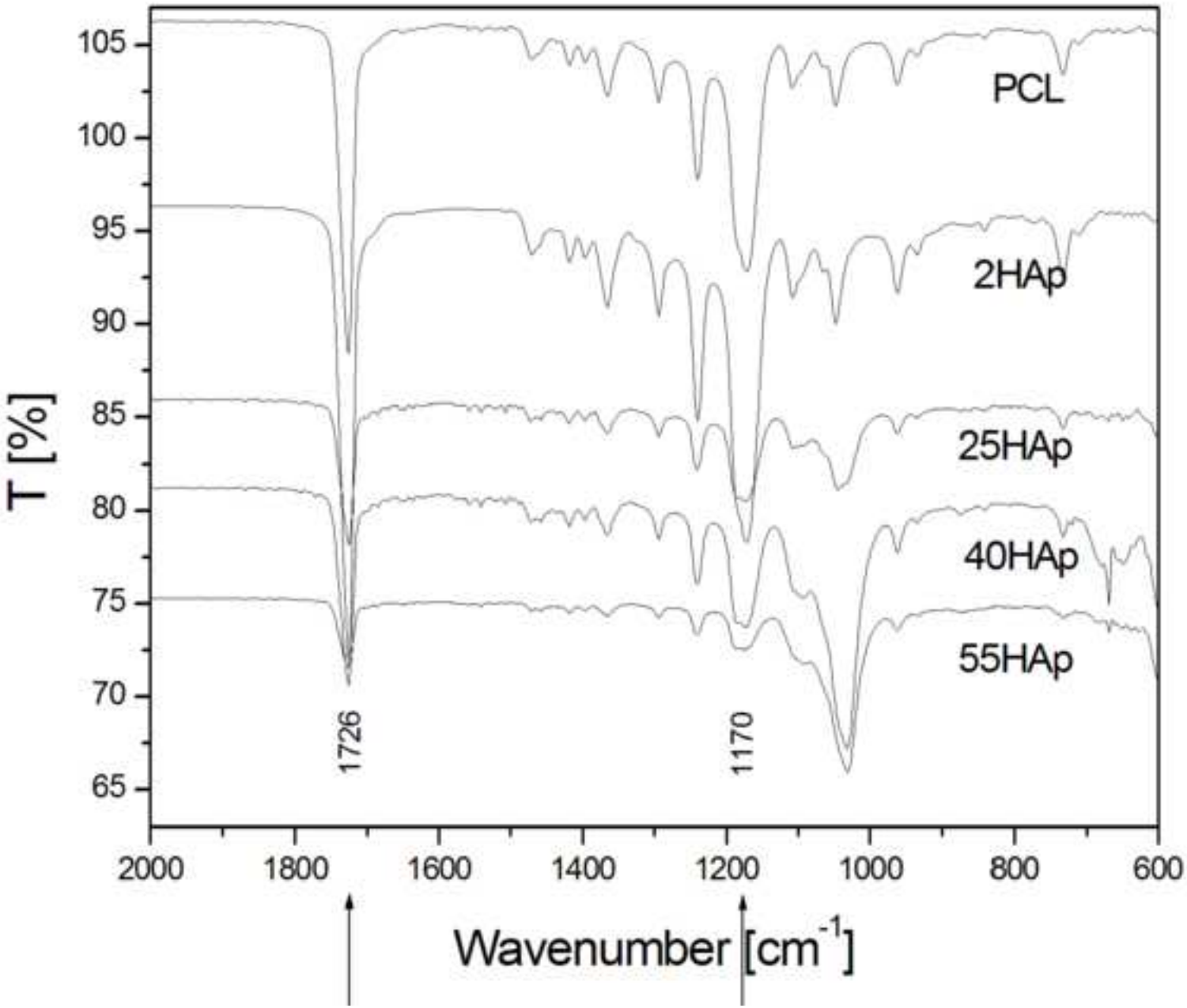

Figure 4(revised)
Click here to download high resolution image

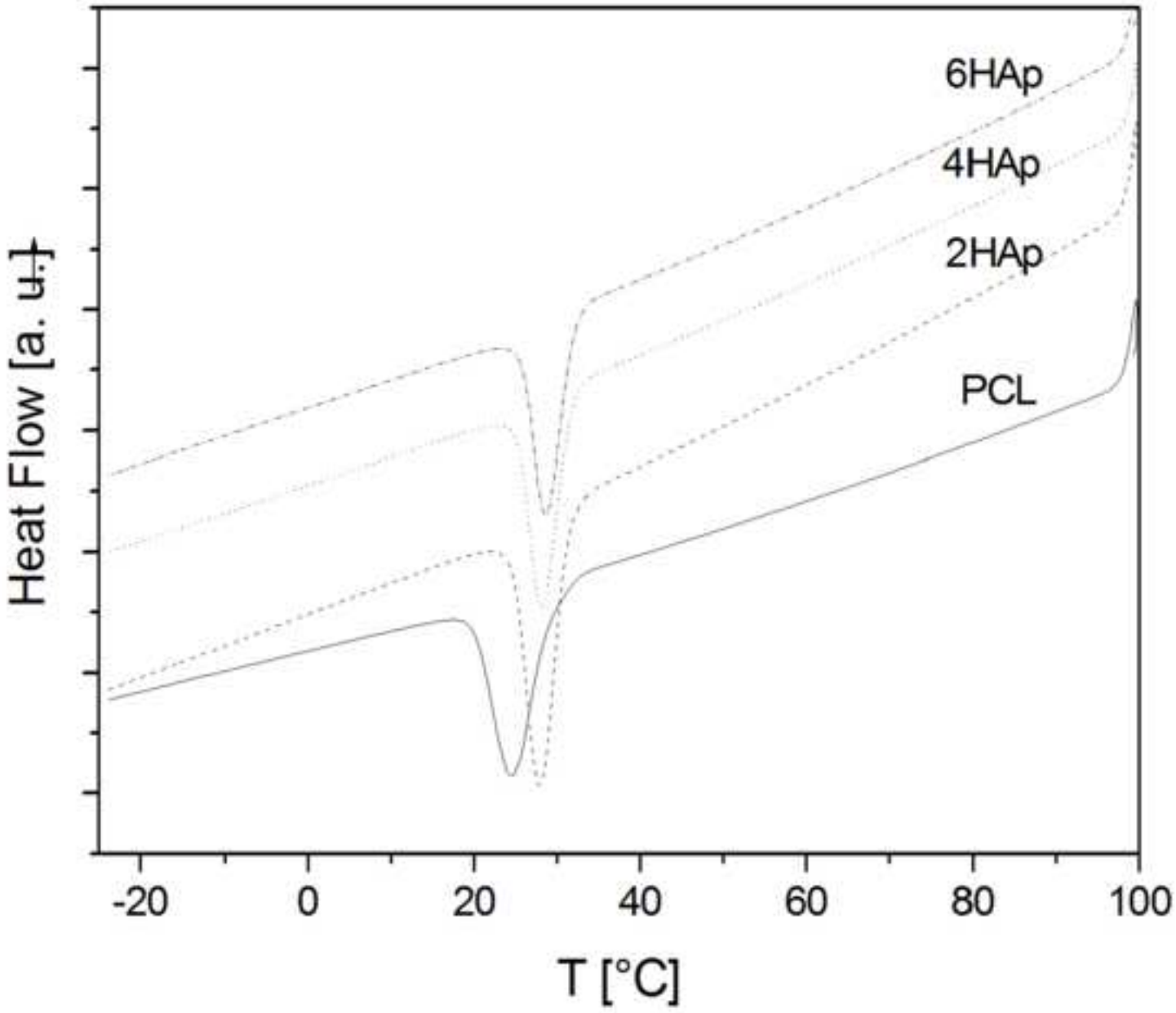

Figure 5 (revised)
Click here to download high resolution image

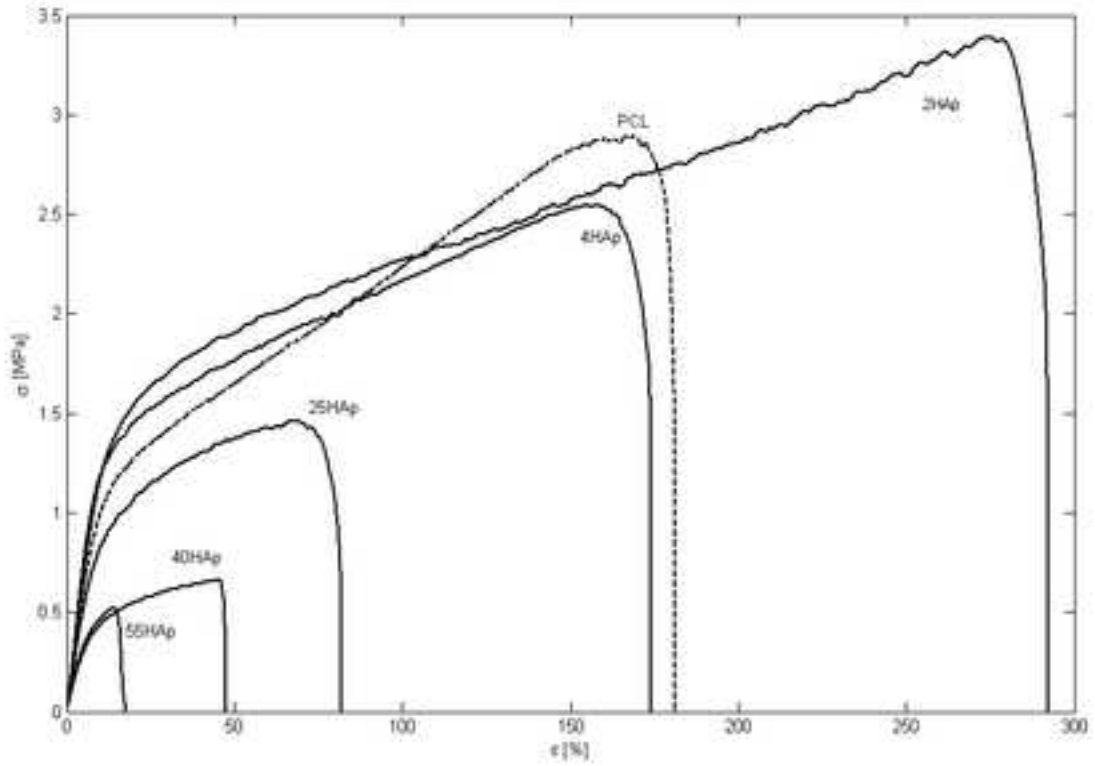

Figure 6 (revised)
Click here to download high resolution image

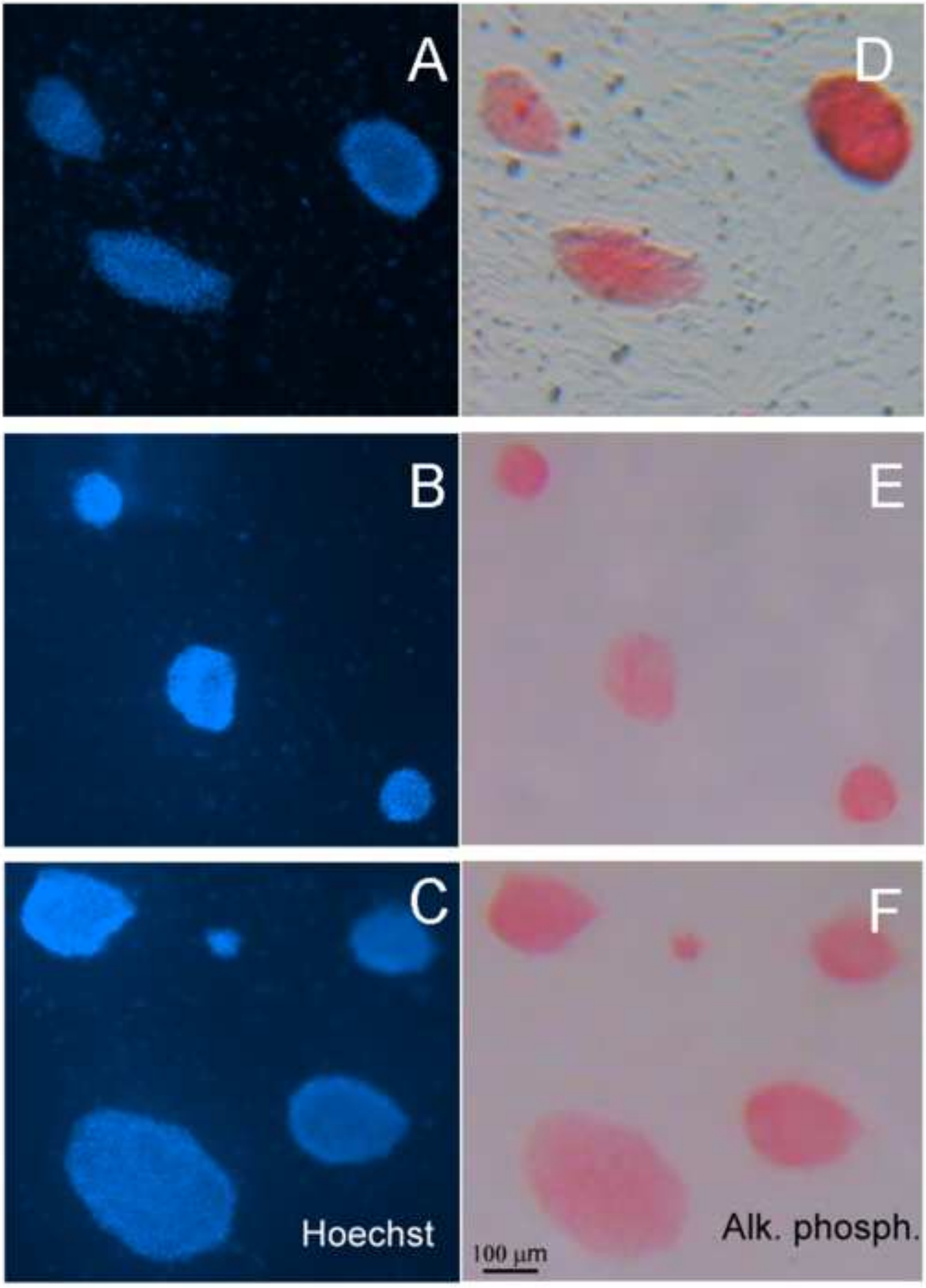

Figure 7 (revised)
Click here to download high resolution image

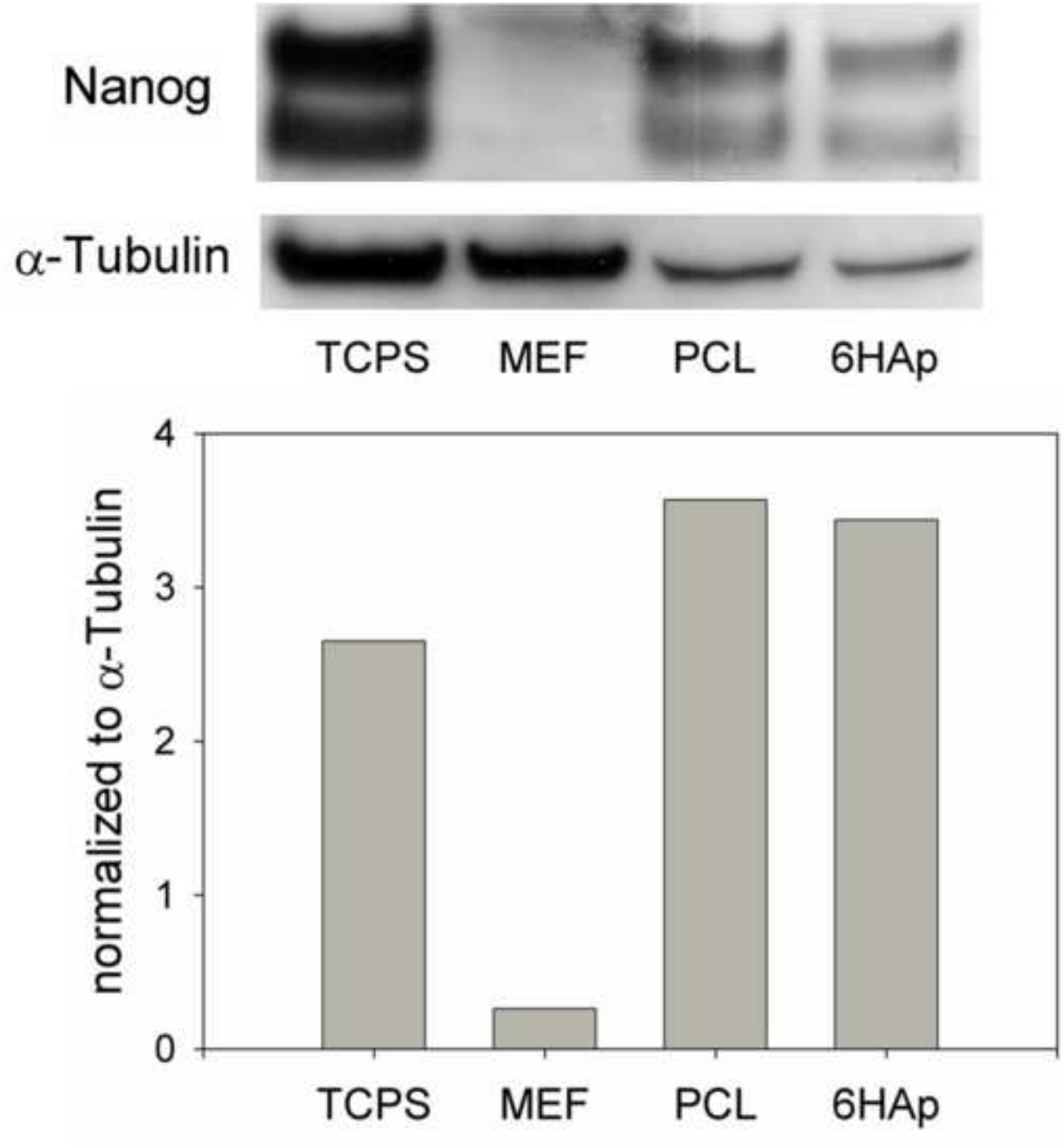

Figure 8 (revised)
Click here to download high resolution image

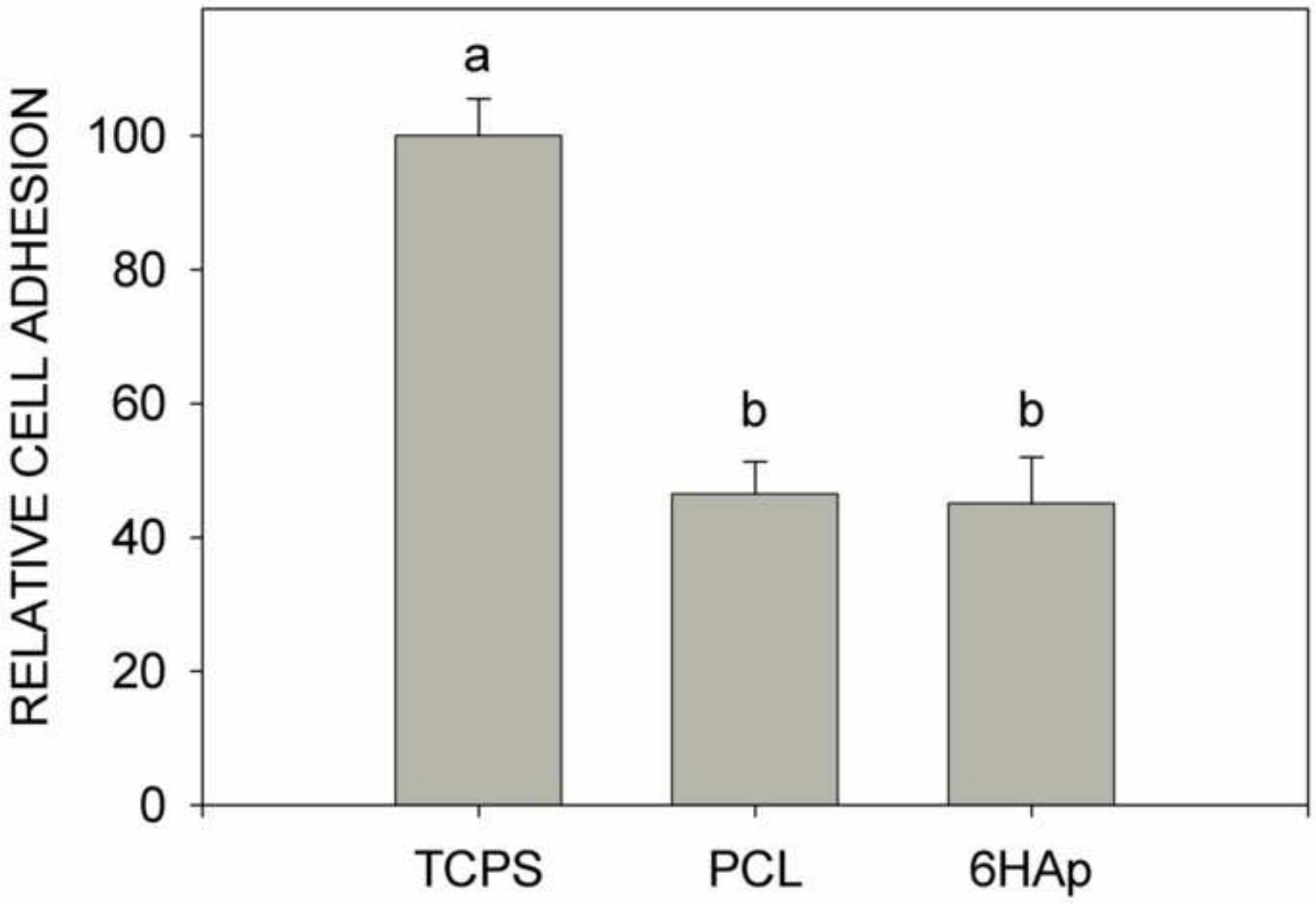

Figure 9 (revised)
Click here to download high resolution image